Applying electron microscopy analysis to assess neural tissue engineering outcomes

Georgina Elizabeth Lindop

Keele University

Master of Philosophy in Neuroscience

August 2024

Abstract:

Spinal cord injury (SCI) has a major socio-economic impact with treatments providing little to no functional recovery due to the SCI environment hindering regeneration through chemical and physical barriers. Novel approaches to alter the injury environment are needed for repair. Biomaterial implants can potentially alter the physical and chemical properties of injury environments to promote regeneration and functional recovery. Evaluation of biomaterial influence over neural cells, in sites of pathology, are reliant on fluorescence microscopy techniques. Whilst useful for providing an overview, biomaterials are difficult to observe and their influence on ultrastructural cellular properties is missed when using fluorescence microscopy. Electron microscopy (EM) is an important tool within research due to its high resolution. However, EM processes require optimisation for novel tissue engineering applications.

In this thesis, we tested two new biomaterial-based neural tissue engineering strategies (magnetoelectric hydrogels and PODS, protein-based crystals, slow-release growth factor crystals) and established EM processes for ultrastructural analysis alongside standard imaging procedures. We demonstrated that a magnetoelectric hydrogel can support the neural transplant population of neural stem cells (NSCs). Further, NSCs could differentiate into their daughter cells – astrocytes, neurons, and
oligodendrocytes. Applying an oscillating magnetic field to the constructs during NSC differentiation appeared to enhance neurite length without affecting overall cell proportions. Using Scanning EM (SEM), we could identify differentiated cell types and showed features of membranes such as pits, filopodia and circular ruffles could be observed and quantified. Subsequently, we investigated PODS delivery to a novel NSC derived injury model. We demonstrated observations made in phase and fluorescence microscopy are supported in EM, including identification of neurite protrusion, proliferation and invading immune cells. Further, we showed PODS–cell interactions are observable under SEM and membrane features were identifiable. Lastly, we showed for the first time that Transmission EM methods could be applied to a 2D multicellular and pathological in vitro model for testing biomaterials, with a key point of witnessing the internalisation of PODs into the cell. Here, we identified key cellular features such as mitochondria, endoplasmic reticulum, and microtubules, important when considering axonal function and growth.

Taken together, we believe the work demonstrates EM can be incorporated into the workflow for developing neuro-regenerative biomaterials and provide additional insights compared to standard imaging. Methodology needs to be developed to improve throughput. For hydrogels this could be adopting methods such as freeze drying to reduce the shrinkage of samples. For the multicellular

injury model adopting and adapting serial block face imaging (SBF) volume EM offers advantages of a larger overview of ultrastructure and the lesion region at high magnification. Alongside, TEM embedding and sectioning could be improved for ultrastructural analysis.

Introduction

Spinal cord injury

1.1 A brief overview of spinal cord injury (SCI) and it's socioeconomic impact

Spinal cord injury (SCI) is characterised as permanent damage to any location(s) along the spinal cord. Injury can occur in a myriad of ways including traumatic: compressive forces, blast forces, lacerations, hyperextension, and non-traumatic: infection, tumours, and haemorrhage. To add to the complexity, size of injury, number of lesions, whether it is complete or incomplete, and location are also large contributing factors to prognosis, quality of life and life expectancy. Military personnel have higher severity scores with poorer prognosis potentially as blast SCI is the most common on the battlefield (Alizadeh et al., 2019 and Quandri et al., 2018). Currently treatments can only provide supportive relief to the lifetime disability patients will face and do not offer any type of cure. Life expectancy is reduced compared to someone without a SCI, which varies depending on the level of injury. In addition, the medical care required is expensive from surgery, nursing, physiotherapy, psychotherapy to pharmaceutical dependency (Anjum et al., 2019). This means a large SCI lifetime cost to the patient and healthcare system, estimated at £2.5 million in lifetime costs per patient (McDaid, et al., 2019). With a global rate of SCI estimated between 250,00-500,00 a year, demand and treatment are only increasing. Hence, an effective treatment is a major requirement (Anjum et al., 2020).

1.2 Spinal cord anatomy: a complex highly organised structure

The spinal cord is a part of the central nervous system (CNS). It is a tubular like structure that tapers from the medulla oblongata to a length between the thoracic 12 and lumbar 1-2 vertebrae, along the dorsal part of the body. The spinal cord can be split into sections corresponding to the 31 pairs of spinal nerves, as follows from top to bottom of spine: 8 cervical (C1-8), 12 thoracic (T1-12), 5 lumbar (L1-5), 5 sacral (S1-5), and 1 coccygeal. The spinal nerves leave the cord through the vertebrae via the intervertebral foramina (Diaz and Morales, 2016), these spinal nerve pairs branch off when entering or leaving the spinal cord into anterior (motor) and posterior (sensory) roots (Snell, 2010). A cross section of the spinal cord shows the white matter to be the outer portion and the grey matter in a 'H' shape in the centre (Diaz and Morales, 2016). On the anterior end the anterior medium fissure and at the posterior the posterior medium sulcus are visible (Snell, 2010). At the core is the central canal that is an extension of the fourth ventricle. In addition to this, the meninges layers and cerebrospinal fluid surround the cord (Diaz and Morales, 2016). Figure 1.1 below shows an overview of the segments of the spinal cord in an MRI taken as a sagittal section of the human body (E.Diaz and H.Morales, 2016).

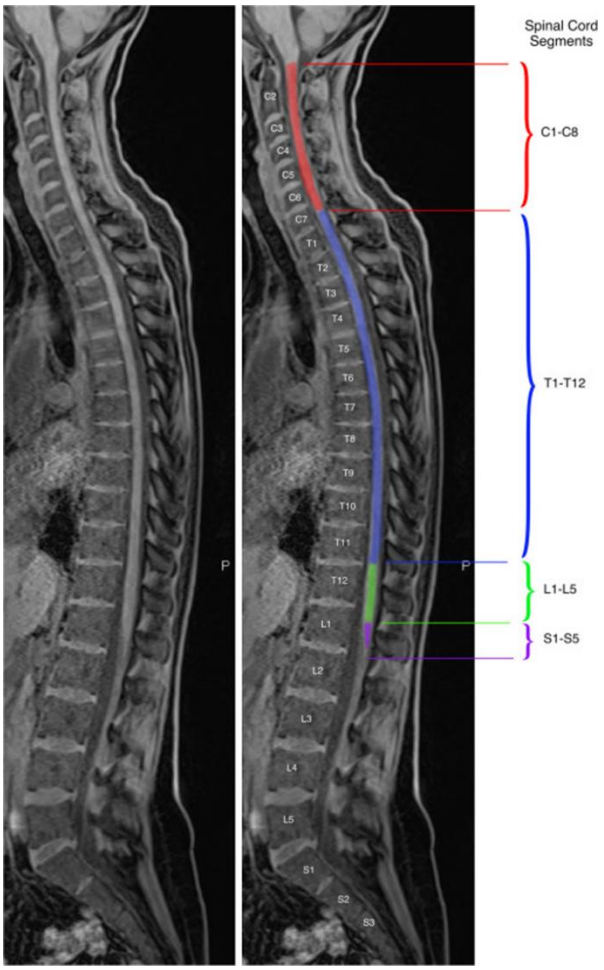

Figure 1.1: sagittal section of a human spinal cord with corresponding labels of the segmented areas. C1-8, cervical, T1-12 thoracic, L1-5 lumbar and s1-5 sacral along with corresponding vertebrae. This figure was taken from E.Diaz and H.Morales, 2016.

Within a cross section of the spinal cord, you can split the spinal cord into areas based on function and morphology, an overview is given in figure 1.2. The grey matter is made up of a grey commissure containing the central canal and on either side ventral and dorsal horns (Snell, 2010). In some areas (T2 to L2), a lateral horn is present. These horns have functional roles: the anterior for motor function, posterior for sensory information relay/interpretation and the lateral for sympathetic function. These grey matter regions contain nuclei/layers of neurones which are the cells which send and receive electrical signals throughout the body. There are many different neuronal subtypes which reside in the spinal cord including motor neurons (which excite peripheral muscle cells), sensory projection neurons (which receive sensorimotor information from the periphery and project to the brain) and interneurons (which modulate electrical signals that flow through the spinal cord). Neurons in the spinal cord then send and receive projections through the white matter tracts. The connections and relay systems vary amongst the tracts and depend on the information they are

sending (Antal Nógrádi and Gerta Vrbová, 2013). A cross section of a spinal cord is depicted in figure 1.2 from Britannica, 2019)

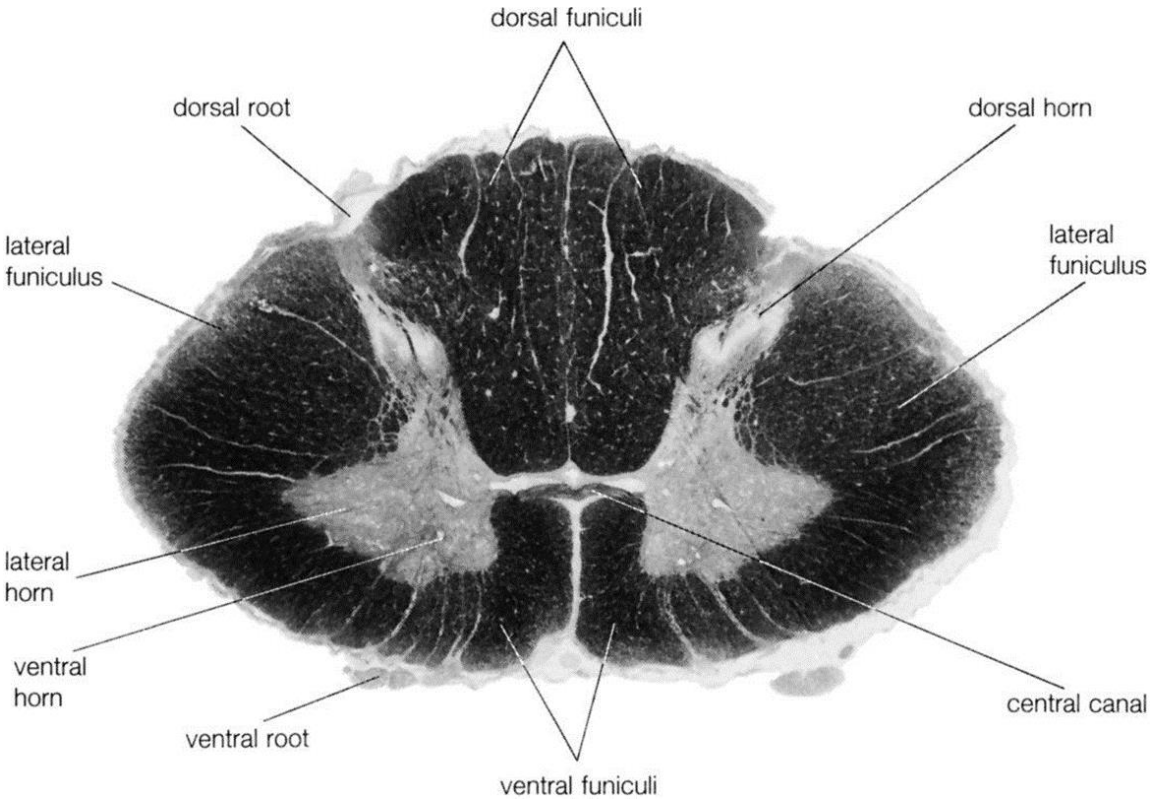

Figure 1.2: cross section of a human spinal cord. Regions have been labelled along with the image being taken from (Britannica, 2019).

The white matter can be grouped into anterior, posterior, and lateral funiculi, and anterior and posterior commissures. These commissures contain neuronal fibres grouped into ascending, descending and fasciculi proprii tracts. Ascending pathways are made up of sensory pathways such as: spinothalamic, spinoreticular and spinocerebellar, these pathways send sensory information to specific region of the brain for higher order processing. Descending tracts are made up of motor pathways including: Aminergic, Corticospinal, Tectospinal and Vestibulospinal. This information is sent from regions of the brain and helps coordinate responses to effect motor function such as muscle contractions (Mtui, Gruener and Dockery., 2016). The Proprii tracts are local connections within the cord. Some functions are believed to be localised to the spinal cord such as the reflex arc and locomotion, making the spinal cord not only a relay of information but also a coordinator and developer of responses (England and Wakely, 1991). Thus, the spinal cord is a place of integration of neuronal networks that process sensory and motor inputs and outputs, being a centre of convergence and divergence that results in the activation of motor neurones leading to a bodily response (Osseward and Pfaff, 2019).

Furthermore, the spinal cord is topographically organised with segments representing areas of the body with sensory inputs to each segment being represented as dermatomes, sensory inputs from the skin. Motor outputs can be determined in the same way in the form of myotomes, and these do not completely align with the sensory dermatomes. In addition, pathways either remain ipsilateral or contralateral. This information can be used to determine location and possible effect of SCI. For example, SCI in the cervical region will lead to a greater effect in paralysis as more connections are affected that are passing to and from the brain to the spinal cord region.

Apart from the neurones, other specialised neural cells reside in the spinal cord. Glial cells match neurones in a 1:1 ratio. One glial cell type are astrocytes a heterogeneous population varying in morphology, protein expression, varying developmental state, and distribution depending on the region of the CNS. However, all have some main functions which are vital for proper neuronal function including in the spinal cord. Mature astrocytes modulate synaptic transmission and neurone calcium levels, a constant influx of calcium or stimulation from neurotransmitters like glutamate can result in excitotoxicity. Astrocytes are vital components in preventing such effects. In addition, they also modulate action potentials via buffering excess potassium ions. Astrocytes are also involved in the ATP production and metabolism and transporting of glucose but also converting carbon dioxide into water and protons. These protons are then used to maintain the pH levels. Astrocytes maintain homeostasis within the CNS via buffering potassium ions and protons. They are also major components of the blood brain barrier (White and Jakeman, 2008).

Oligodendrocytes are generated though a highly orchestrated lineage. Within the embryonic spinal cord, the ventral ventricular zone and dorsal spinal cord generate oligodendrocyte precursor/progenitor cells (OPCs). OPCs migrate throughout the spinal cord is influenced by extracellular matrixs and growth factors (Kuhn et al. 2019). Some persist into adulthood and others differentiate into mature oligodendrocytes which produce myelin. One oligodendrocyte ensheathes multiple axons with myelin. This process is vital to provide insultation and redistributes ion channels to form nodes of Ranvier resulting in the fast action potential transmission of neurones called saltatory conduction (Bradi and Lassmann, 2009). Oligodendrocytes also provide trophic and metabolic support to axons with oligodendrocyte dysfunction resulting in a cascade effect that results in neurodegeneration as seen in multiple system atrophy disorders and multiple sclerosis (Han et al., 2022).

Microglia are another cell within the CNS but have a mesodermal origin and infiltrate the CNS at an early embryonic stage. Microglia are immune effector cells and remain in a ramified state within the CNS unless a stimulus affects them. Microglia are not dormant and have projections that sense the

microenvironment around them. If exposed to a pathogen, inflammation or anything that could trigger an immune response microglia migrate and extend processed towards the site of injury/pathogen releasing cytokines and neurotrophic factors such as nurotrophin-3 and brain derived neurotrophic factor. Microglia remove pathogens and injured cells via phagocytosis removing harmful substances from the CNS (Wake, Moorhouse and Kebekura, 2011). The reactive state of microglia can be inferred from its morphological state at a homeostatic level microglia have projections extending from the cell body, with branches forming off these extensions. In a reactive state from injury these extensions lesson but are still present. At this stage microglia are active and produce chemokines and inflammatory responses. In the fully active stage, they form an amoeboid shape looking more rounded and with no cell extensions (Reddaway, et al., 2023).

Surrounding the spinal cord is the blood-spinal cord barrier (BSCB), meninges, blood vessels and vertebrae. The vertebrae are bony structures that protect the spinal cord. Between the vertebrae and the spinal cord are the meninges layers made up of the dura mater (outer) arachnoid mater (middle) and pia mater (inner) which also taper into the cauda equina at the end of the spinal cord. The sub arachnoid space stores the cerebral spinal fluid which is located between the arachnoid matter. Within the spinal cord is an intricate network of blood vessels. What separates the spinal cord from blood vessels is a tightly controlled border the BSCB which is made up of a basal lamina, pericytes and astrocyte foot processes. The BSCB allows for tight control of what can enter the spinal cord, maintaining homeostasis and preventing unwanted bodies such as red blood cell, bacteria, large proteins, hormones etc from effecting spinal cord function (Bartanusz et al., 2011).

1.3 The complex pathophysiology of SCI – A barrier to regeneration

The spinal cord is thus a highly ordered and complicated structure in which regeneration, as we know it, is not present in its mature state. SCI can be broken down into stages. Firstly, there is the primary injury that involves the initial impact/trigger of the injury. The mechanisms of impact alter depending on the injury type: compressions, distractions, and transections (Alizadeh et al., 2019). At this stage to limit further damage decompression surgeries are performed, if decompression occurs early this could decrease SCI by two grades on the ASIA (American Spinal Cord Injury Association) impairment scale, offering a better prognosis (Venkatesh et al., 2019). Secondary injury follows minutes after primary and it also can be broken down into phases: acute, sub-acute and chronic, Figure 1.3. Secondary injury involves molecular and cellular changes to the region of SCI that remain at some level for the rest of a patient's life. Mechanisms of secondary injury response are thought to lead to the inhibition of regeneration within the SCI. Yet, these mechanisms may also offer a protective effect for remaining healthy tissue and can prevent lesion size expansion. Therefore, the

secondary injury phase is a double-edged sword (Hu et al,. 2023). Understanding how these mechanisms can be regulated or directed to a more regenerative effect may be key to treatments of SCI (Anjum, et al., 2020)

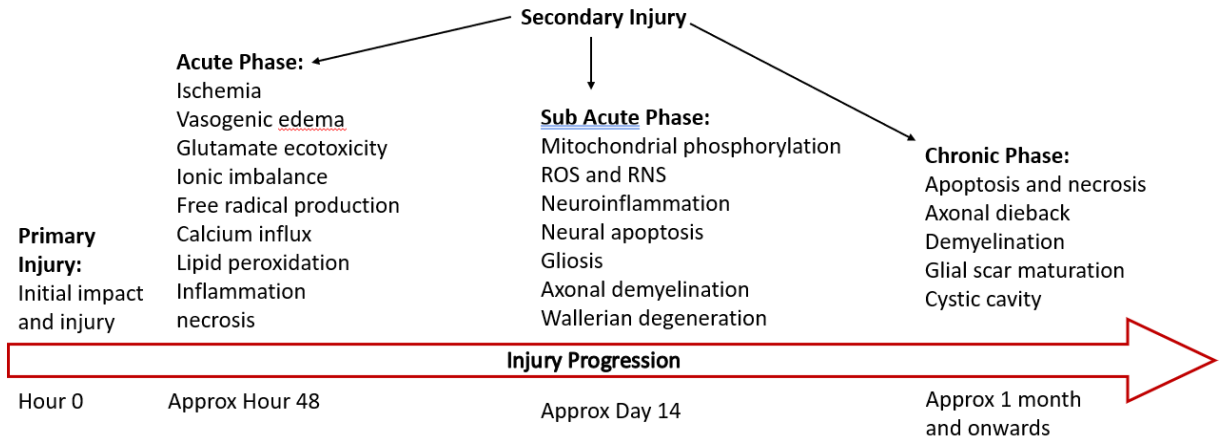

Figure 1.3: A overview of spinal cord injury progression. *Indicating the primary injury, then into the secondary injury which can be divided into three stages the acute, sub-acute and chronic. With the phases are listed the associated pathophysiology.*

1.3.1 Haemorrhage and Ischaemia

Haemorrhage is said to result directly from the primary injury with disruption to intramedullary vessels and capillaries – resulting mostly in bleeding at the grey matter level. Haemorrhage leads to the disruption of the BSCB, causing leukocytes and red blood cells to infiltrate the spinal cord tissue (Alizadeh et al., 2019). Molecules within the plasma leads to the activation of macrophages, microglia, and astrocytes; releasing cytokines and chemokines such as: TNFα and IL-β, adding to inflammation and increasing permeability of the BSCB (Montague-Cardoso and Malcangio 2021, and Venkatesh, et al., 2019). Furthermore, the iron within the red blood cells become a source of free radicals and ferroptosis. Bleeding results in oedema and high interstitial pressure compressing surrounding vessels leading to Ischaemia and vasospasm (Hao et al., 2017).

BSCB permeability and ischemia results in water and solute imbalances intracellularly, leading to swelling of cells and a decrease of cytoskeleton integrity. This potentially causes necrotic death, which causes the release of cellular glutamate that may lead to excitotoxicity, resulting in apoptosis and necrosis (Du et al., 2007). Increased permeability at the cellular and blood vessel level, overall, results in ionic imbalances, which effects the homeostasis of the environment and cells within it, disrupting their normal functions. Inflammation from haemorrhage and ischaemia results in

endothelial injury increasing cellular membrane pore size, allowing large plasma-derived molecules to pass through cell membranes causing vasogenic oedema (Amar and Levy, 1999). Ischaemia also results in cellular deprivation of oxygen supplies, leading to reduced adenosine triphosphate (ATP) production (Anjum et al., 2020). Ultimately, ischaemia and haemorrhage are the main initiators of the secondary effects that follow via initiation of ionic imbalances, oxygen deprivation, free radical production, and inflammation (Ahuja et al., 2017). However, re-establishing blood flow in Ischaemic areas can result in further damage via the production of more free radicals and eliciting another immune response. Therefore, for treatment, other areas of the injury cascade may be better targets of therapy (Fan, et al., 2018).

1.3.2 Ion imbalance/ oxidative damage/ free radical production

Damaged neurons and astrocytes end up releasing glutamate, which binds to NMDA receptors – leading to an influx of calcium into cells (Regan and Choi, 1991). High intracellular calcium overloads mitochondria, effecting respiration, ATP production, and reversing Na^+/K^+ ATPase function - increasing intracellular levels of Na^+. In turn, high Na^+ exacerbates Ca^{2+} influx by affecting the function of Na^+/Ca^{2+} exchanger (Stys et al., 1992). Glutamate activating AMPA receptors which in turn also result in an influx of Ca2+ (W. Chen et al., 2024). Leading to worsening ionic imbalance and cellular dysfunction (Stys et al., 1992). High Ca^{2+} perpetuates oxidative damage through its activation of kinases and phospholipases. High Ca^{2+} also results in apoptosis, necrosis, cellular enzyme activation, acidosis, and free radical production (Anjum, et al., 2020). In addition, mitochondrial Ca^{2+} activates nicotinamide adenine dinucleotide (NAD)H oxidase, generating superoxide formation via the electron transport chain (ETC). Radicals are also produced from iron, as Ferrin and transferrin spontaneously oxidises Fe^{2+} and Fe^{3+} into superoxide radicals. Fe^{3+} also produces hydroxyl radicals in reactions with H_2O_2 (produced from dysregulated respiration) (Huang et al., 2022). Free radicals cause damage to cellular integrity and function and, ultimately, in high levels lead to cellular death (Anjum, et al., 2020).

Reactive oxygen species (ROS) and reactive nitrogen species (RNS) produced from oxidative damage produce Poly (ADP-ribose) polymerases (PARP) via NADPH oxidases (NOX). PARP depletes NAD+, inhibiting gliosis, and thus ATP formation. Furthermore, it releases Adipose induction factor that promotes apoptosis (Venkatesh et al., 2018). ROS results in lipid peroxidation as it reacts with polyunsaturated fatty acids, producing reactive lipids that convert into lipid peroxyl radicals. These radicals result in a chain reaction with other fatty acids and only stop when quenched with another radical. The effects are loss of mitochondrial, endoplasmic reticulum and cell membrane integrity, respiratory and metabolic failure, and DNA alterations (Huang et al., 2022). In addition, the products

of radical quenching are 4-Hydroxy-2-nonenal and 2-propenal – both of which are highly toxic to cells (Alizadeh et al., 2019).

Ionic imbalances last into the chronic phases effecting the patient for the rest of their life of SCI and treatment is difficult. One potential way is the blocking of receptors such as with the inhibition of voltage Na+ channel receptors which resulted in a neuronal protective effect – yet such inhibitors include tetrodotoxin that is highly toxic therefore, making any clinical translation difficult as efficacy, administration routes and the concentrations would have to be investigated (Fan et al., 2018).

1.3.3 Inflammation/ Immune response

Inflammation is a complex process involving several chemokines and cytokines with various parts of the inflammation process being shown to be a help or hinder regeneration. Coverage of the whole of neuroinflammation is not in the scope of this introduction, but this section aims to summarise some of the factors involved. The inflammatory and immune response is conducted by, astrocytes, neutrophils, microglia, macrophages, B and T lymphocytes (Liu et al., 2021). Damage-associated molecular patterns (DAMP)s are released from damaged and necrotic cells that activate native microglia and recruit blood born monocytes that once entering the region of injury become activated into macrophages, which proliferate (Tran, Warren and Silver, 2018). It is suggested that macrophages undergo polarization into either M1 or M2 phenotypes, these phenotypes are broad and help offer a more simplistic view for the scope of this thesis, depending on DAMP exposure (Fan et al., 2018). Within SCI, an M1 phenotype is dominant and is linked to a poorer prognosis due to the reduced ability to phagocytose debris, its release of pro-inflammatory chemokines and cytokines, increased chondroitin sulphate proteoglycans (CSPG) expression, release of repulsive factors leading to axonal retraction, and higher link to tissue damage (Nakajima et al., 2020). The opposite is said for M2 phenotypes as they are anti-inflammatory and pro-regeneration. Yet, if only M2 phenotype is present this leads to a larger fibrotic scar formation that can block any regrowing axonal connections. Finding a balance in the M1:M2 ratio may be a benefit to generating a homeostatic environment beneficial to regeneration (Brennan and Popovich, 2018).

Furthermore, other factors in the immune response are a cause of a negative regenerative environment and may also lead to other SCI impairments. Active T and B lymphocytes are seen well into the chronic phase and are said to be present throughout the patient's life. Lymphocytes in SCI produce a CNS-specific autoimmune response (Ankeny et al., 2006), they can have a direct toxic effect on neurones and glia of the injury site or an indirect effect on their function by releasing proinflammatory molecules. It has also been suggested that these lymphocytes can stimulate macrophages into a M1 phenotype via releasing DAMPs. Their persistent activation can be

detrimental to the injury region and continue to create a negative environment that would result in the apoptosis of new or regenerating cells. It also has been shown to be detrimental to healthy tissue beyond the injury site. Due to its autoimmune response cardiovascular, renal, and reproductive tissue is also a target and is more likely to be dysfunctional in patients with SCI (Jones, 2014).

Astrocytes, though they are not immune cells, play a role in creating positive feedback on the inflammatory environment. Releasing their own chemokines such as (MCP)-1 to recruit neutrophils. Neutrophils release inflammatory cytokines, proteases, and free radicals, degenerating the endoplasmic reticulum membrane protein complex (EMC), causing apoptosis. They also have positive feedback on astrocytes and microglia supporting their activation and in turn neuroinflammation. Yet, removal of neutrophils leads to a decrease in growth factors and lessening of functional recovery. Astrocytes also promote the M1 proinflammatory state of macrophages and microglia. However, astrocytes also produce chemokines that promote the M2 like phenotype (IL-10). In addition, astrocytes initiate and are the main factors in scar formation, which does have negative effects on regeneration, but also restricts the expansion of inflammation and lesion size (Cekanaviciute and Buckwalter, 2016. Zamanian et al., 2012. Brambilla et al., 2005).

To remove the immune response is not viable for treating SCI as this results in an increased lesion site and worsening prognosis. Immune depression can also lead to increased risks of osteoporosis, atherosclerosis, neuropathic pain, pneumonia and sepsis. The immune response is protective to other healthy tissues and helps restore homeostasis in the injury site (Jeffries and Tom, 2021). Therefore, its modulation may be a better route. Yet, it is important to recognise the immune response varies depending on stage of injury but not every aspect is yet understood and how best to modify the immune response is still unknown (Alizadeh et al., 2019 and fan et al., 2018, Sterner and Sterner, 2023). In addition, modification of immune response may affect other immune responses in patients. Such is the case when using immunosuppressants this makes patients more vulnerable to other diseases. In addition, when used in cell transplantation of the CNS when immunosuppressants where removed most of the functional recovery is lost (Levi et al., 2019).

1.3.4 Gliosis/ glial scar formation

The glial scar is made up of three components: 1) glial components: astrocytes, NG2+ oligodendrocyte precursor cells (NG2+ OPC's), and microglia. 2)fibrotic components: macrophages, pericytes, and fibrocytes. 3)molecular component made up of a gradient of CSPG's that radiates from the lesion core (Perez-Gianmarco and Kukley, 2023). In the acute and sub-acute stages, it is recognised that the glial scar is an important component of wound healing. When the glial scar was ablated post-SCI, the lesion site expands, wound healing is reduced, and functional recovery is

negatively impacted (Alizadeh, et al., 2019 and Tran, Warren, and Silver, 2018). Yet, researchers suggest in chronic stages the glial scar is what negatively impacts regeneration. NG2+ OPC's are suggested to proliferate as a reaction to the deceased mature oligodendrocyte population from apoptosis, via signal transducer and activator of transcription 3 (STAT3) signalling, which also prevents their ability to differentiate into mature oligodendrocytes. NG2+ OPC's secretes NG2 and CSPG's helping generate a negative environment (Siebert et al., 2014). Furthermore, the NG2+ OPC's restrict axon die back and axon regrowth through entrapping and stabilising growth cones, producing dystrophic growth cones (O'Shea, Burda, and Sofroniew, 2017 and Tran, Warren, and Silver, 2018). This effect may be from the CSPG's secreted, with spot assays showing neurites will grow into CSPG's but stop as the gradient increases leading to dysphoric end bulbs (Ohtake and Li, 2015). However, whether CSPG's act via production from NG2+ OPC's or if they independently lead to the same response is unknown. What is known is these dysphoric ends remain chronically, seen in a human glial scar 40 years old. Therefore, negative effect on axonal growth is persistent (Tran, Warren and Silver, 2018).

Astrocytes are suggested to have a negative impact on regeneration in the chronic glial scar due to their upregulation of CSPG's, along with mature astrocytes increasing macrophage and fibroblast entry to the lesion and scar (Hussein et al., 2020). However, they can also have protective effects by decreasing edema of cells with aquaporin 4 expression, rebuilding and maintaining the BSCB, regulating ecotoxicity with glutamate transporters, producing glutathione to decrease oxidative stress, and increasing trophic and metabolic support. Furthermore, immature astrocytes are a benefit to regeneration as their implantation into a chronic SCI in mice resulted in axonal regrowth across the lesion core and glial scar (Chu et al., 2014). However, SCI environment favours astrocytes in the mature stage and can affect their heterogeneity to favour less regenerative forms (Tran, Warren and Silver, 2018). Fibrocytes and pericytes also have a negative effect on regeneration via producing axonal repulsive molecules such as collagen type I. Yet, fibrocyte grafts support robust axonal regeneration suggesting another factor, or lack thereof, may be leading to decreased regeneration (O'Shea, Burda and Sofroniew, 2017).

Anderson et al., 2016 shows with addition of axon-specific growth factors and activation of neurone-intrinsic growth factors, even with negative cues present axonal growth was significantly increased. Suggesting, overcoming the glial scar, and promoting axonal regeneration is more weighted on the addition of growth-stimulatory chemoattracted molecules, rather than eliminating the inhibitory molecules present (Anderson et al., 2016).

1.4 Effective repair in SCI will require combinatorial therapies

Given the above, it is likely combinational therapy targeting multiple clinical goals is needed. Such therapies may need to be capable of providing oxygen or nutrients to effected areas or promoting the rebuild of vascular architecture, balancing ionic imbalances or blocking necrotic cell death and inhibiting the reactivity of ROS. Altering the immune response may also be important to ensure the vital initial stages for wound healing and prevention of expansion of the injury site are maintained, but reducing the cytokines and chemokines produced from inhibiting new regeneration. SCI results in an injury environment that inhibits regeneration not just at the initial stages but in chronic too, with little to no functional recovery for the patient's life. An orchestrated alteration of the complex injury environment to turn it into a regenerative environment may be a key to the promotion of targeted regeneration.

SCI is a multifaceted interconnected complex signalling cascade. Targeting one area may have repercussions elsewhere. Furthermore, the complexity highlights the importance of combinatorial therapeutics to fully effect and gear the environment towards regeneration – a complex issue will need a complex response. However, to develop these treatments requires solid analytical data and research models that can provide data relating to the multiple pathological process of SCI and any therapeutic changes that may occur. This thesis will examine some of these issues and focus on conducting electron microscopy (EM) to add ultrastructural analysis of pathology, regeneration and cellular behaviour when investigating combinatorial therapies.

1.5 Stem cell transplantation offers initial basis for combinatorial therapy in SCI

Stem cell transplantation is suggested to be a possible therapeutic avenue for treating SCI. The premise is the newly transplanted cells will replace and repair neuronal connections resulting in recovery of function. Neural stem cells (NSC) are especially promising being multipotent differentiating into neurones, astrocytes and oligodendrocytes which are the major components of the CNS. Potentially allowing them to replace cells lost from injury. Furthermore, NSCs can secrete trophic factors such as glial cell line-derived neurotrophic factor (GDNF), promote differentiation into oligodendrocytes therefore promoting remyelination and have an immunomodulatory effect regulating T-cells and macrophages to reduce inflammation (Silvestro et al., 2020).

In animal models, transplantation has had positive outcomes with functional recoveries documented. Other benefits and signs of functional recovery were also noted such as: reduction in lesion size, differentiation of NCS into neurones and glia, host-to-graft synaptic connectivity, downregulation of proinflammatory cytokines, graft survival and motor function improvements. In addition, tumours, severe side effects or complications are not widely documented. The biggest variability of efficacy

can be seen in the human clinical trials that occur, shown in table 1 (Pereira et al., 2019 and Silvestro et al., 2020).

Table 1: A list of clinical trials using stem cell transplantation. *Included are identifier, Phase reached by the trial, cell types used in transplantation, safety and complications that may have occurred and the efficacy. Blank areas of the efficacy are because trials were ended prematurely.*

Clinical trials – With results

Identifier	Phase	Cell type	Saftey	Efficacy
KCT0000879	I/II	hNSPCs	safe - tolerated by patients. No tumors, futher damage, spacticity or neuropathic pain	some partial sensory motor function
NCT01321333	I/II	HuCNS-SCs	safe - no complication arised	sensory gains noticed but declined after immunosupression removal
NCT02302157	I/II	AST-OPC1	postive saftey profile	restoration of some hand fucntions
NCT01325103	I	BM-MSCs	one complication of a cerebral spinal fluid leak - was not connected to transplanation but intervention practices. No other side effects of complications occored	7/14 improved AIS score. Variably sensitivity improvements we noticed in all patients.
NCT02482194	I	BM-MSCs	no sever side effects. One patient had headaches and two others exsperanced non-sepcific tingling sensations	-
NCT01909154	I	BM-MSCs	no adverse events	significant sensitivity recovery, improvement of level of chronic pain. 7/9 showed urodynamic function
NCT00816803	I/II	BM-MSCs	mild side effect present: headaches and mild pain. Side effects were resolved.	17/50 had a ASIA conversion and improved motor functions. 2 paitnets after a year exsperianced improvments in areas of nervous tissue damage.
NCT01274975	I	BM-MSCs	19 adverse events occored but all were resolved or stabilized in a follow up	1/8 patients had an improved ASIA socre of A - C
NCT01393977	III	UC-MSCs	no side effects recorded	10/34 had improved motor fucntions and muscular tension. 5 undergoing rehabilitation therapy had similar imrpovements but not statisically significant.

Many studies do not have data available or were terminated for business and financial reasons. One clinical trial by Levi et al., 2019 highlights the predominant issues with current transplantations for SCI. HuCNS-SC were perilesional intramedullary injected into patients with C5-7 SCI 2-24months after injury. The study showed clinical safety and 7/12 patients experienced sensory improvements, yet this was decreased with the removal of immunosuppressants. After 1 year the study was terminated for not reaching the required clinical efficacy threshold set by sponsors (Levi et al., 2019).
Efficacy is currently low, inadequate, and variable among studies.

Current transplantation therapies in neurological disorders using stem cells have also shown limited success with immune system responses reducing efficacy (Rahman et al., 2022). Within rat stroke models transplanted with human embryonic stem cell derived neuronal precursors, neuronal stem

cell survival rates were at 1% after 2 months from transplantation. Differentiation only resulted in approximately 10% of surviving stem cells displaying neuronal marker MAP-2. With the majority displaying astrocyte markers GFAP. Limited control after transplantation can cause limited recovery effects with stem cells not differentiating into the desired cells. The efficacy on rat recovery compared to those with a sham operation being very limited or with no difference at all between groups (Hicks et al., 2009).

To improve efficacy, it has been suggested a combination of approaches is required, as cellular transplantation alone has not been proven to be effective enough. Such improvements can potentially be achieved through the use and modification of biomaterials and the addition of trophic factors to improve stem cell survival but also modulate differentiation (Pereira et al., 2019 and Silvestro et al., 2020).

1.6 Biomaterials could facilitate stem cell therapy and offer further platform for combinatorial therapy

Biomaterials have been designed through tissue engineering as implants or scaffolds to restore the lost CNS function by supporting cell proliferation, differentiation, adhesion, and neo-tissue genesis by creating a scaffold that can be personalised to each tissue and its needs. Biomaterials are believed to currently require several properties to achieve this goal: A) 3-Dimentional porous structure, allowing cell dispersion, oxygen and nutrient flow and potential vascularization; B) biocompatibility, prevention of immune system attack and increased inflammation and other cytotoxic events (Alaa Emad Eldeeb et al., 2022 and El-Sherbiny and Yacoub, 2013); C) be bioresorbable, as seen with photopolymerizable gels that biodegrade over time this increases the cell survival rates over those in which scaffolds do not degrade (Nguyen and West, 2002); D) have optimal physiochemical characteristics such as allowing for cell adhesion, proliferation, and differentiation; E) have mechanical properties optimal for tissue, stiffness is one factor that can alter cell differentiation; F) do not elicit any toxic effects on the cellular environment; G) have potential for multifunctionality e.g. for drug delivery or electrical stimulation. Creating and optimising such a supportive structure in implantation of new cells may result in a shift to the microenvironment and allow for cell growth and regeneration of lost connections (Chen et al., 2024 and El-Sherbiny and Yacoub, 2013).

Other biomaterials have been designed to act as drug delivery systems. For example, materials such as collagen are incorporated with drug molecules during fabrication. Thus, offering another route as to provide drug delivery via direct implantation into the injury site (Willerth and Sakijama-Elbert, 2007). If a therapeutic molecule is more susceptible to enzyme degradation or rapid kidney clearance more common drug delivery methods such as orally or intravenously would require high

concentrations of the therapeutic target for it to reach or have an impact on the injury site. Also, via the more common delivery systems drugs used may have off-target interactions that may result in adverse effects. Yet, scaffolds encapsulating therapeutics added directly to the injury site may mitigate all the current pitfalls of drug delivery (Dimetteo et al., 2018). Scaffolds can also be altered in several ways to control the rate of drug delivery through pore size, cross linking density and degradation rate (Willerth and Sakijama-Elbert, 2007). Using animal models Houweling et al., 1998 showed implantation of collagen scaffolds containing NT-3 into SCI sites, tripled the rate of axon infiltration into the injury site comparatively to just collagen scaffold transplantation. In addition, the NT-3 collagen scaffold also resulted in improved functional recovery (Demetteo et al., 2018). Unfortunately, we are unable to address the issue of regulatory approval and clinical availability within this thesis, but it is important to recognise as a barrier to biomaterial therapies. With more research this could eventually lead to improving efficacy and safety of biomaterials which is highly important for clinical translation.

There is a current drive and potential for biomaterials and the combinatorial approach of combining biomaterials and cell transplantation to elicit neurological repair. Therefore, there is a corresponding drive to investigate these scaffolds to examine how neural cells respond to these novel biomaterials. In general, new biomaterials are developed and optimised in in vitro systems as animal models of SCI are expensive, require significant expertise and are associated with ethical issues. Overwhelmingly, cellular analysis in these systems is conducted through immunocytochemistry and proteomics (normally identifying below 10 proteins). Whilst these analyses are indispensable, highly important aspects of cell health, behaviour and response to therapeutic biomaterials are overlooked. Here, we sought to develop complementary EM techniques in order to provide ultrastructural information on cellular responses to biomaterials within the neural tissue engineering field.

1.7 Electron Microscopy for ultrastructural analysis of neural tissue engineering strategies

Similar to a light microscope, electron microscopes (EM) work on the same 4 principles. 1) Illumination source. 2) condenser lens to focus illumination. 3) objective lens that magnifies the image after the illumination passes through the object. 4) magnifying lens, that magnifies the image further after the objective lens. However, the source of illumination in EM is from electrons not light.

The term electron microscope covers a family of microscopes that use a beam of electrons and electromagnetic/electrostatic lenses to produce a magnified image. Electrons act as light as both are

described as having a wave-particle duality. Electron wavelengths are determined by their speed, as acceleration increases the electron wavelength decreases. Theoretical resolution is half the wavelength of the source of illumination (Meek, 1970). The shorter wavelength of electrons in comparison to the visible light spectrum makes the resolution power exponentially higher, with EM having a 1000x better resolution than light microscopes. In addition, electrons are negatively charged offering the ability to focus them using electromagnetic/static lenses. One drawback is that due to the shortness of wavelength the electrons will interact with air particles therefore a vacuum is required, and samples must undergo expensive and specialised preparation including dehydration to be visualised optimally to the high resolution (S. Amelinckx et al., 2008, Meek 1970). Two main branches of the electron microscope family exist. The first is the Transmission electron microscope (TEM), the fist electron microscope invented back in 1932 by Knoll and Ruska. The second being the scanning electron microscope (SEM) invented in 1938 by von Ardenne (Bozzola and Russell, 1999).

SEM follows the four principles of microscopy. However, it collects imaging data via the electron beam electrons interacting with the sample generating back scattered electrons and secondary electrons, and other forms of energy information not covered in this thesis (Figure 1.4). This generates compositional distribution on the sample surface and dimensional topographical structure information respectively. The benefit of SEM is that it offers a larger depth of field than light microscopy and ultimately has a much higher resolution at around 4-10nm. Given this, cell membrane activity, cellular morphology, plus cellular interactions can be investigated in fine detail. Furthermore, SEM can be used to look at the finite structure of materials, including biomaterials, to evaluate their composition and structure – all of which can affect cellular responses. SEM is frequently used by current researchers to assess these biomaterial scaffolds in tissue engineering of bone and neuronal tissue. Within biology, SEM has allowed for the study of cell membrane activity and fine organ structure analysis, including the cochlear (Vielreicher et al., 2013).

TEM works differently to an SEM and more like light microscopy, where the electron beam passes through the sample onto the objective lens which focuses and magnifies the image onto the projector lens – which generates the final image (Figure 1.4). When the beam interacts with the sample, two types of electron interaction occur: elastic and inelastic scattering. Elastic scattering is what produces the high-resolution image. It is the event where the kinetic energy and momentum of an electron is the same as an atom before and after interaction. The difference in weight of the atom nucleus compared to the electron is the same so little kinetic energy and momentum is transferred. Therefore, kinetic energy remains constant. The closer the electron passes to the nucleus (containing positively charged protons) the more the electron path will be bent. To ensure many of these interactions are elastic scattering, staining with heavy metals is used. Typically, the resolution is

around 5nm meaning the images in magnified 50,000 times. The TEM has been vital to the study of biology contributing to the information of structure and function inside eukaryotes. In addition, within neuroscience, the use of the TEM helped develop and conclude that synapses and neurotransmitters are present a key milestone in our understanding of how the nervous system operates (Bozzola and Russell, 1999 and Meek, 1970).

The one major advantage that EM has over other forms of microscopy is its ability to have nanometre resolution. When it comes to simplicity, price, specimen preparation, live cell imaging, and maintenance the light microscope is more advantageous. Yet, the high resolution of the EM allows us to visualise the inner workings of cells and their interactions that is a valuable property in which has yet been achieved in other forms of microscopy (S. Amelinckx et al., 2008 and Meek, 1970). Without EM the ultrastructure of cells and their chemical makeup in normal and pathological states may in many ways still be elusive (Bozzola and Russell, 1999).

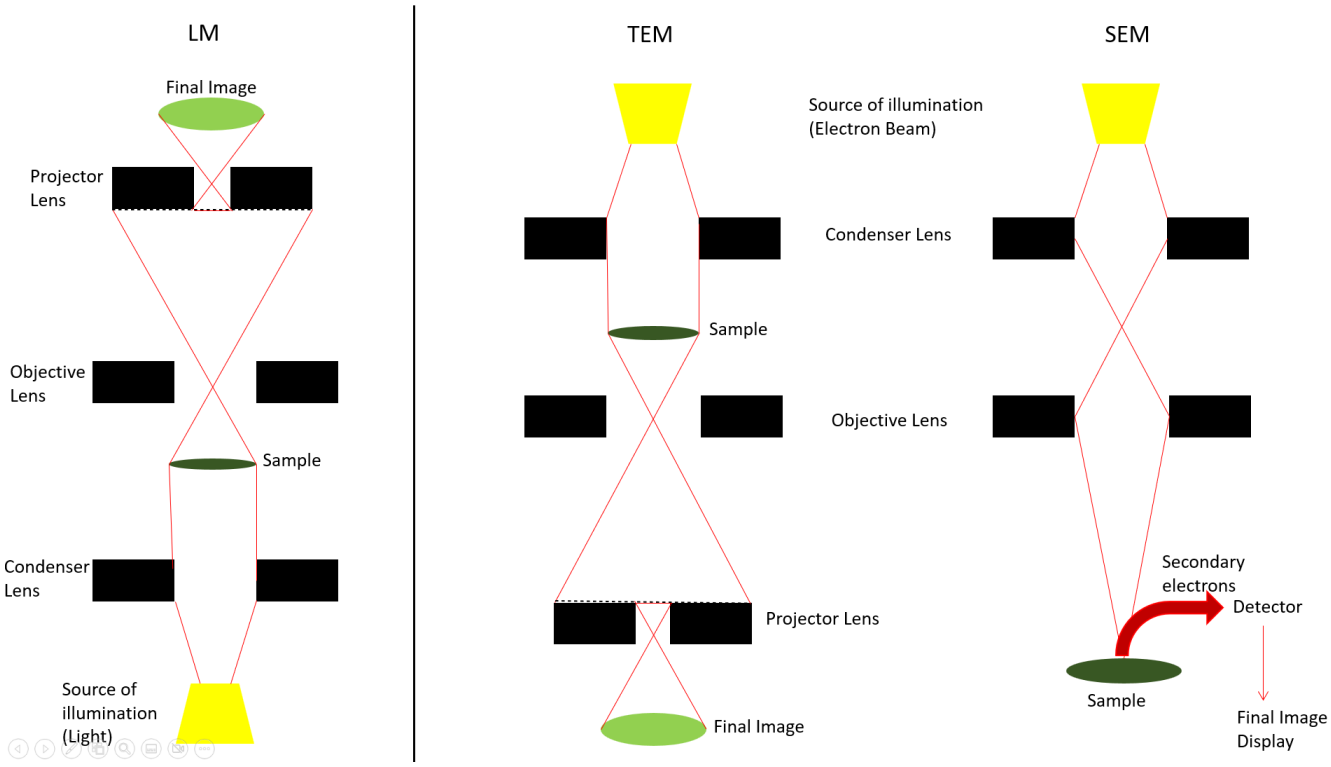

Figure 1.4: The basic principles of how Light microscopy (LM), Transmission electron microscopy (TEM), and Scanning electron microscopy (SEM) work to produce an image.

1.8 Current applications of EM in tissue engineering

Within tissue engineering EM has been used in multiple ways to aid research, predominantly in scaffold or nanofiber structural investigations and in assessing cell behaviour with scaffolds and other

added factors. Some examples using SEM for assessing scaffolds for tissue engineering include Choi, Zhang and Xia 2010, Wang et al., 2018 and Esmaeili et al., 2019. All used different EM techniques to achieve this glial including critical point drying and freeze drying. Many of the analysis involved measuring average nanofiber size, average pore size and uniformity. SEM has been effective in these experiments with images being usable in analysis and showing clear structural components of the scaffolds or fibres. In addition, SEM has been effective in experiments to evaluate stem cell cellular interaction and alterations in morphology with certain scaffolds and environmental alterations. Image analysis is focused on looking at the adherence of cells, the extensions present or their length, and comparison of cellular morphologies to controls or different environments (Choi, Zhang and Xai. 2010, Schmidt et al., 1997, Ferson, Uhil and Andrew. 2020 and Esmaeili et al., 2019). Field emission SEM a variant of the SEM has been used in one study by Fernandes et al., 2015, to evaluate membrane activity on NSCs as an indicator of cellular activity. This study was able to clearly image and show differences in unstimulated and active NSC membrane, such as membrane ruffling, filopodia, pits, nano-podia and circular ruffles. Filopodia are plasma membrane protrusions containing actin filaments usually associated with cellular behaviour involving endocytosis, viral exosome internalisation (J.L.Gallop, 2019). Circular ruffles are F-actin rich structures with two functional categories: cell motility or internalisation of substrates, receptors and membrane (J.Hoon, W.Wong and C. Koh, 2012). Pits are recognised to be clustering of receptors in specialised regions of the cell membrane that tend to occur when there is rapid internalisation, such as receptor mediated endocytosis (J. Goldstein et al., 1979). Fernandes, 2015 recognises all three of these ultrastructure's using EM techniques to investigate internalisation of nanoparticles. These structures make a good benchmark for observations of cellular activity as their structures have been observed in EM before and in internalisation of biomaterials.

It was also possible to image and compare the FESEM images to TEM imaging. TEM's apparent use in tissue engineering seems to be a supportive role. Its findings are used to compare and confirm or contrast what might be found with other imaging techniques (Esmaeili et al., 2019 and Fernandes et al., 2015). However, TEM can have its usefulness in being a predominate role in tissue analysis as seen with Wang et al., 2018 with its use to measure myelination and the degree of myelination on nerve fibres. Yet, TEM is not as widely used as SEM most likely due to its cost and time-consuming sample preparation. Even so, TEM is important as it can be used to evaluate inside the cell and may spot alterations in organelles and ultrastructure morphology to indicate the health, safety, and activity of the cell. Little research on multicellular injury models has used TEM or SEM for observation. With EM's high-resolution capabilities to see the ultrastructural view of such models it would be an advantageous avenue to explore.

1.9 What this research aims to achieve.

The overall goal of this thesis is to incorporate EM techniques into ongoing neural tissue engineering studies. Each study will be introduced in more detail in the corresponding chapter. Our specific aims are to use fluorescence and electron microscopy to:

(i) Investigate NSC regenerative responses in novel electroactive hydrogel scaffolds.

(ii) Examine ultrastructural cell features in an in vitro model of SCI.

(iii) Assess the feasibility of incorporating EM techniques into each in vitro system.

Methods

2.1 Reagents List:

Cell culturing:

Cell culturing reagents were from Invitrogen (Pailsy, Scotland, UK) and Sigma (Poole, Dorset, UK). FGF *(fibroblast growth factor)* was from Peprotech (Rocky Hill, NJ, USA). EGF *(epidermal growth factor)* was from R&D systems Ltd (Abingdon, UK). Penicillin and Streptomycin were both from Fisher (Loughborough, UK). Accutase was from Sigma, DNase was from Roche (Welwyn, UK). TrypLE, cell culturing flasks, 24 and 96 well plates and other cell culturing plastics used were purchased at Fisher Scientific, UK. FBS *(foetal bovine serum)*. Animals used from cell culture were cared for in accordance with the Animals Scientific Procedures Act of 1986 (UK) with approval by the local ethics committee.

Fluorescence:

Normal donkey serum (NDS). Primary antibodies: Rabbit anti-GFAP was from DakoCytomation (Ely, UK). Rat anti-MBP from Serotec (Kidlington, UK). Mouse anti-Tuj-1 from Biolegend (San Diego, California). Secondary antibodies: FITC and Cy-3 were from Jackson Immunoresearch Laboratories Ltd (Westgrove, PA, USA).
Cy-5. DAPI was from Vector Laboratires (Peterborough, UK). Deionised water was obtained using a Milli-Q water purification system from Millipore (Bedford MA, USA).

PODs:

POlyhedrin Delivery System (PODs)BDNF and PODs empty were purchased from Cell Guidance Systems (Cambridge, UK).

Hydrogels:

JANUS and Cobalt fibres were fabricated and characterised by The Andrew lab (University of Florida, USA; see Ferson et al., 2020) and were kindly donated free of charge.

Collagen (rat tail collagen) was obtained from scientific laboratory supplies (Nottingham, UK) produced by Sigma-Aldrich (Missouri, USA) which also produced the acetic acid used.

SEM and TEM reagents:

EM grade Glutaraldehyde, Osmium tetroxide, Sodium cacodylate, Spurs resin components, and ACLAR sheets were from TAAB (Reading, UK).

Table 2: Cell culturing mediums used in both experiments, list of their reagents and volumes used concentrations. *Mediums include Monolayer medium, stem cell medium, and differentiation medium. Reagents used include: DMEM (Dulbecco's Modified Eagle Medium), F12 (nutrient mixture f12), Heparin, B27 (B-27 supplement), N2 (N-2 supplement), Pen Strep (Penicillin-Streptomycin), EGF, FGF, and FBS.*

Reagents	Monolayer Medium	Stem cell medium	Differentiation medium
DMEM	1:1	3:1	3:1
F12	1:1	1:3	1:3
Heparin	4ng/mL	4ng/mL	4ng/mL
B27	-	2%	2%
N2	2%	-	-
Pen Strep	50µg/mL	50µg/mL	50µg/mL
EGF	20ng/mL	20ng/mL	-
FGF	20ng/mL	20ng/mL	-
FBS	-	-	50µg/mL

2.2 Material and substrate preparation:

2.2.1 Magnetoelectric fibres

Cobalt (Co) fibres and Janus (Ja) fibres were weighed into separate containers, Co at 18.8mg and Ja at 16mg. 10mL of 70% ethanol was then added to the containers. The containers were sonicated for 20

minutes then centrifuged for 5 mins at 1000rpm. The ethanol was then replaced with 10ml of sterilized water. The containers were then sonicated and centrifuged again. Sterilized water was replaced with 10xMEM at a specific concentration of each fibre type. 594µl of 10xMEM was added to Co fibres to obtain a final concentration of 12.6mg/ml. 794µl was added to Ja fibres, setting the concentration to 36.9mg/ml. The 10xMEM solutions were then used in the synthesis of hydrogels.

Control collagen gels were made up with: 332µl Acetic acid, 568µl Collagen, 30µl 1M NaOH and, 100µl 10xMEM; combined into a 50ml tube in that order. The Co hydrogels 10xMEM contained the Co fibres. Ja hydrogels used 10xMEM containing Ja fibres in the method described above. Each gel was pipetted into three 96 well plates (50µl in each well) and left to set at 37^{o}C for 3 hours before use.

2.2.1 Substrate preparation for PODS experiments

Glass coverslips and ACLAR® (thermoplastic film) sheets, cut into cover slip sizes, were both coated in laminin in accordance with the following protocol, conducted under a culture hood in sterile conditions. Initially, 70% IPA was added to disinfect the cover slips and ACLAR sheets. These were then washed 3 times in distilled water. Polyornithine 0.1 mg/ml was added, and the materials were incubated for 1hr at 370^{o}C. The cover slips and ACLAR sheets were then washed again 3 times in distilled water. Laminin was added and materials were then again incubated for 1hr at 37^{0}C. The materials were washed again in distilled water before cells were plated.

2.3 NSC collection and seeding:

All experiments involving animals were approved by the local animal welfare and ethical review body. P0-1 CD1 mice were sacrificed through Schedule 1 procedures. Subsequently, the brain was removed from the mouse via decapitating the mouse, holding the head, and making a cut in the skin from the back of the head to the nose. The skin was peeled back, and the same cut was made along the skull with 4 release cuts, exposing the brain. A spatula was used to remove the brain that was then placed into PBS on ice. This processed was repeated for 8-10 brains.

The brains along with some of the PBS were placed into a petri dish in a culture hood. A brain was lifted out with curved tweezers onto autoclaved tissue where a scalpel was used to cut 1mm posterior to the olfactory bulb on the frontal lobe – which was discarded. Next, another coronal slice from the remaining brain was cut 2mm from the previous cut – this section was collected as it contains the sub ventricular zone (SVZ). The slice was placed into a separate petri dish containing monolayer medium (see table 2). Using a dissection microscope and scalpel, the cortex of the slice was removed leaving the SVZ, this was repeated 8-10 more times. All SVZ's collected were pipetted out into a 30ml bijou containing 1ml of stem cell medium.

100µl of DNAse was added to the bijou for one minute. Using a 1ml Eppendorf pipette the SVZ pieces were mechanically dissociated to separate the cells from each other. The cells were centrifuged for 5 minutes at 1000rpm. The solution was then separated from the cell pellet, fresh stem cell medium was added, and the cells were then mechanically disturbed to mix them with the medium. The cell solution was then passed through a 70µm sieve. A cell count on the newly sieved solution was performed using a haemocytometer with trypan blue stain under a phase microscope. From the cell count, the amount of cellular solution to add to 50mL stem cell medium to make the cellular concentration up to $1x10^5$ cells/mL was derived and added to the stem cell medium. 5ml of the new solution was then added to culturing flasks, coated in poly-D-lysine, and left in an incubator at 37°C until at least 80% confluence. This was determined by if cells had stuck to the flask wall or when neurospheres. Neurospheres are NSCs that grow in suspension forming spheres. As their size increases so does their density and under phase they being to appear brown in the centre. Therefore, confluence was their size and the 'darkness' of the neurosphere centre. For feeding, 50% of the stem cell medium was exchanged every two days to ensure the cells had the nutrients required to survive. This was conducted by placing the culturing flasks upright so any neurospheres would gravitate to the bottom of the medium so half the medium at the surface could be collected without removing or damaging the cells.

To passage neurospheres and obtain a single cell solution for plating experiments, spheres of the culturing flasks were collected into 50mL falcon tubes using a transfer pipette. These were then centrifuged for 5mins and 1000rpm. The excess solution was removed from the falcon tubes leaving behind a cell pellet which was mechanically dislodged by flicking the bottom on the tube. 800µl of PBS was added to the falcon tubes and they were once again centrifuged for 5mins at 1000rpm. To each tube 900µl of accutase and 100µl of DNAse was added and left for 5-10 mins. Using a 200µl air displacement pipette, the cells were dissociated gently until no large clumps were visible and cells appeared evenly distributed. To stop enzyme activity 1ml of stem cell medium was added to each tube before centrifuging again for 5mins at 1000rpm. The stem cell medium was removed, and 500µl fresh stem cell medium was added to the pellet. The cells were mechanically dissociated again to resuspend them into the solution before it was then passed through a 70µm sieve into a new 50ml falcon tube. Another 500µl of stem cell medium was then used to pass through the walls of the old falcon tube and passed through the sieve to collect all the potential cells. Another 500µl stem cell medium was then passed through the sieve to clean it and wash any stuck cells.

Sometimes, the neurospheres attached firmly to the bottom of the culturing flasks, requiring slightly different treatment to above. Here, the medium was removed from the culturing flasks and replaced with PBS, this was then removed after a few seconds and replaced with 3ml of 1x TrypLE for 5 mins.

Then the same steps used for neurospheres were employed post accutase treatment.

With the solution and cells in the new falcon tube they were then used to perform a cell count using a haemocytometer using Trypan blue as a stain. This was used to work out the amount of cell solution to add to 50ml of new monolayer medium to make the concentration of cell to 4.5x105 cells/mL.

2.3.1 Seeding cells onto magnetoelectric fibre hydrogels

The cell count was used to work out the amount of cell solution to make the concentration of cell to $4.5x10^5$ cells/mL 150µl of the new cell solution was then added to each Hydrogel that was made in the 96 well plate, then left to incubate for 3 days before the monolayer medium was replaced with 150µl differentiation medium, see table 2 for cell medium solutions.

2.3.2 Establishing an NSC based injury model for testing PODs drug delivery

The cell count was used to work out the amount of cell solution to make the concentration of cells to $4.5x10^5$. This new cell solution was made up and 600µl of the cell solution was then added to each cover slip and ACLAR sheet in a 24well plate and incubated at 37^0C. Every 2 days, the samples underwent a 50/50 medium change with monolayer medium to ensure cell survival and the stem cells could maintain proliferation.

Day 5 after seeding, the monolayer medium was replaced with differentiation medium to differentiate the stem cells into a multicellular culture until the next phase of the experiment. Until a multicellular culture was reached on day 12.

2.3.3 Cell feeding for both experiments

In a cell culturing hood, every 2 days, 50% of the medium was exchanged for 50% fresh medium, the type of fresh medium depending on what medium the cells were in. 50% of the medium was collected from the surface of the 96 well plates in experiment one and the 24 well plates for experiment 2, to avoid disturbing the cells on the hydrogels or coverslips/ACLAR at the bottom of the wells. The medium was then replenished with equal parts of fresh medium, this was gently pipetted into the well to prevent any damage.

2.4 Stem cell stimulation in the magnetoelectric fibre experiment

Once differentiation medium was added, samples were separated into parameters of – (i) Control nostimulation, (ii) F0 - where samples were exposed to a magnetic field of 0Hz and (iii) F4 - where samples were exposed to 4Hz frequency oscillating magnetic field at a displacement of 5mm. All magnetic field conditions had samples of collagen (col), Cobalt fibres (coco) and JANUS fibres (coJa) Hydrogels. Making up to 9 different conditions as follows. No magnetic field collagen hydrogel (col nm), no magnetic field Cobalt fibres (coco nm), no magnetic field JANUS hydrogel (coja nm), 0Hz

displacement collagen hydrogel (col F0), 0Hz displacement Cobalt hydrogel (coco F0), 0Hz displacement JANUS hydrogel (coja F0), 4Hz displacement collagen hydrogel (col F4), 4Hz displacement Cobalt hydrogel (coco F4), 4Hz displacement JANUS hydrogel (coja F4). A summary of the conditions and lay out of well plates can be seen in figure 2.1. F0 and F4 stimulations happened twice daily, once in the morning and in the evening for 30 minutes each time for 5 days. Magnetic fields were applied using the magnefect nanoTM (nanoTherics Ltd., Stoke-onTrent, UK) system and a 96 magnetic array, compatible with 96 well plates.

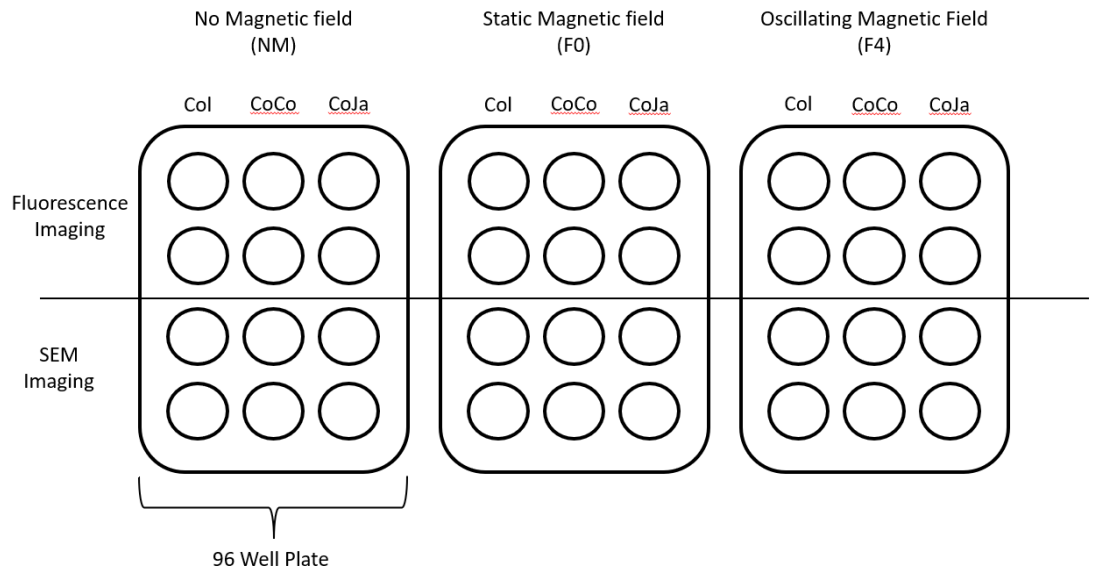

Figure 2.1: Overview of experiment 1 variables and lay out of samples in a portion of a 96 well plate. *The overview shows how 36 samples are first divided into groups of three depending on magnetic field, either no magnetic field (NM), static magnetic field (F0) or oscillating magnetic field (F4). These are then further split into three groups depending on the hydrogel components: Collagen based hydrogel (Col), collagen hydrogel and Cobalt fibres (CoCo), and collagen hydrogel with JANUS fibres (CoJa). The samples a further split in half depending on the imaging that would be conducted - either fluorescence microscopy or SEM.*

2.4.1 Lesioning, PODs drug delivery experiment

On day 12, the cell layer was scraped in a straight line using a 200µl pipette tip from top to bottom of the coverslip/ACLAR sheet, this was to induce the lesion injury to the multicellular monolayers. The tip needed to maintain contact with the cover slip with even pressure applied. Afterwards, the sample was washed in monolayer medium to remove detached cells. All medium was removed and 8µl of PODs in PBS, empty or with BDNF was added to some lesion samples, after monolayer medium

is applied. The remaining lesion models only had monolayer medium applied with no PODs to act as a control. Lesioned cultures were then incubated until fixation at the time points of 24 hours and 72 hours. Making up conditions of Control at 24hours and 72hous, PODs empty 24 Hours and 72hours, PODs BDNF at 24 hours and 72 hours. A summary of the experiment is given in figure 2.2.

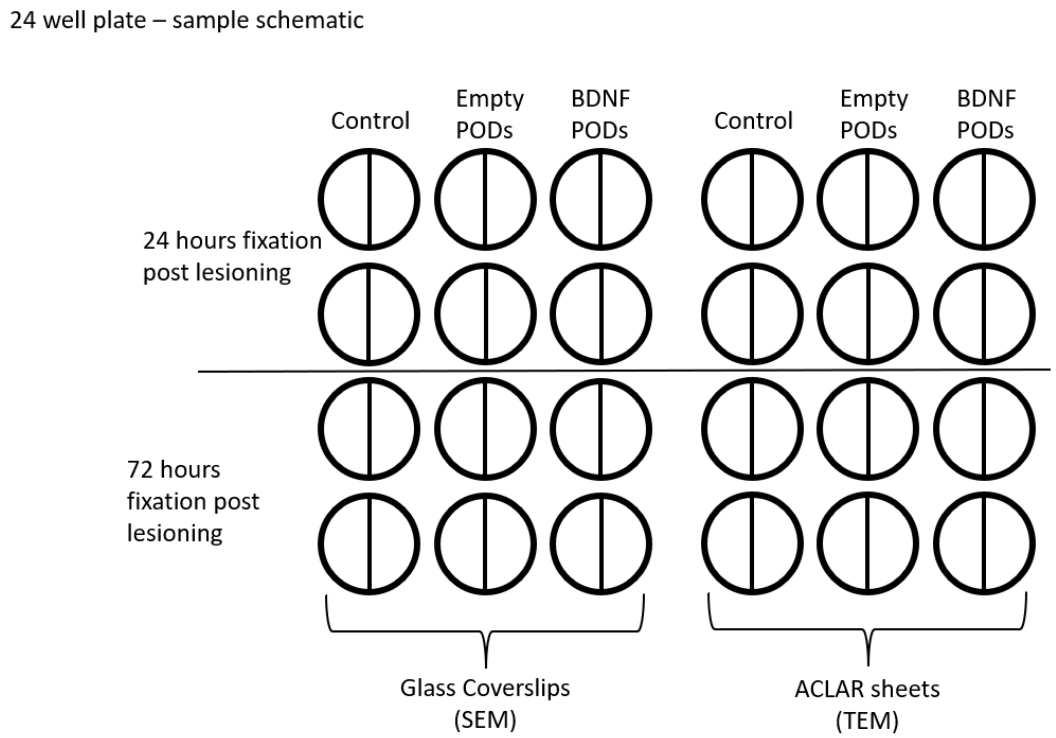

Figure 2.2: Overview of the experimental variables and outline of experiment 2. *Where 24 samples on a 24 well plate where split into three groups of, control (lesioned with no additions), PODs empty (addition of PODs after lesion with no BDNF), and addition of PODs BDNF after lesioning. Then split further into 24 hours and 72 hours depending on the time of fixation postlesion. Then both 24Hr and 72Hr groups were split further based on imaging modality of SEM where cells were cultured on glass cover slips or TEM imaging where ACLAR sheets were used for culturing. The line through the circles depicts the samples being lesioned.*

2.5 Immunohistochemistry, magnetoelectric fibre experiment

Stem cell medium was removed, and gels were washed in PBS three times. PBS was replaced with 4% paraformaldehyde for 1hr at room temperature. PBS was removed and gels washed three times with PBS. The last PBS wash was left in the well to prevent the gel from drying out.

The PBS was removed and replaced with blocking solution (5% normal donkey serum and 0.3% Triton x-100 in PBS) and incubated at room temperature for 1 hour. The primary antibody solution contained Glial fibrillary acidic protein (GFAP) rabbit, Myelin basic protein (MBP) rat, class III

betatubulin (Tuj-1) mouse, and 6000µl blocking solution. Blocking solution was removed and replaced with 500µl on primary antibody solution. Samples were then left overnight in the dark on a shaker.

Primary antibody solution was removed, and gels were washed three times with PBS, each wash was left for 5 mins. The PBS was then replaced with 500µl secondary antibody solution made up of cyanine dye 5 (Cy5) donkey anti-rabbit, Fluorescein isothiocyanate (FITC) donkey anti-rat, Cyanine dye 3 (Cy3) donkey anti-mouse, and 6000µl PBS. Samples were left for three hours in the dark on a shaker. Concentrations of antibodies and a summary of the immunostaining can be seen on the table below.

Table 3: Overview of the immunohistochemistry.

Cell type	Primary antibody	Secondary antibody	Fluorescence colour
Astrocytes	GFAP (rabbit) 1:500	Donkey anti-rabbit 1:200	CY5 (far red)
Oligodendrocytes	MBP (rat) 1:200	Donkey anti-rat 1:200	FITC (green)
Neurones	Tuj-1 (mouse) 1:1000	Donkey anti-mouse 1:200	CY3 (red)

Gels were mounted onto slides using tweezers and were covered in Vectashield mounting medium with 4,6-diamidino-2-phenylindole (DAPI) before the cover slip was then applied. Mounted samples were left overnight in a 4°C fridge to dry. Gels were removed from well plates using tweezers and a dark background to make the gels more visible and pinching one outer section of the gel with the tweezers, to reduce damage, and lifting it out onto the slide. Then nail varnish was used to seal the coverslips to prevent movement. Coverslips were stored in 4°C fridge in darkness until imaging.

2.6 SEM Sample preparation

Samples on glass cover slips were fixed at 24hr and 72hr time points with cell medium being removed and samples washed with PBS. PBS was replaced with 2.5% Glutaraldehyde in 0.1M Sodium cacodylate/ 2nM $CaCl_2$ and incubated for 2 hours. This was replaced with 0.25% Glutaraldehyde in 0.1M Sodium cacodylate/ 2nM $CaCl_2$, which was left overnight in the fridge at 4°C.

A major part of the staining step involves Osmium, Thiocarbohydrazide, Osmium, Thocarbohydrazide and Osmium (OTOTO) method to build up contrast for imaging. Samples were washed in distilled water that was then replaced with 1M Osmium in 0.1M Sodium cacodylate/ 2nM CaCl2 (O) which

was left to incubate for 1 hour. Osmium solution was then removed, and samples were washed five times with distilled water. One drop of Thiocarbohydrazide in distilled water was placed onto the sample, if the drop remained clear the samples were submerged into the thiocarbohydrazide (T) and left for 15 minutes. If the drop turned brown, the samples were washed again in distilled water until they were clear (this process was used for each distilled water wash). After 15 minutes the Thiocarbohydrazide was removed, samples were washed in distilled water and Osmium was added and left to incubate for 15 minutes (O). the osmium was removed, and samples washed again with distilled water. After Thiocarbohydrazide was added for 15 minutes (T). Samples were washed again, and Osmium was added for 15 minutes (O). Osmium was removed and samples were washed again 5 times in distilled water which was then replaced with 70% ethanol. Samples were left overnight in a fridge at 50C.

Samples then went through a series of ethanol solutions (90%, 100%, and 100% dry). Samples were then placed into a holder and submerged in 100% dry ethanol, which was placed into the Critical point dryer. The chamber was filled with liquid $C0_2$ and kept at 13^0C. Samples were left for 15 minutes after the $C0_2$ was dropped below the samples then back up to submerge them, this was repeated 2 times before the $C0_2$ level was left with samples submerged for 15 minutes. This was repeated 3 times then the CO_2 was heated to 35^oC, so it returned to its gaseous state. The $C0_2$ was then let out via a vent before the chamber was opened and the samples removed. Samples were mounted onto the aluminium stubs using carbon stickers. A microscope was used to determine the cell side up before the sample was placed onto the carbon sticker. In Experiment 2, Silver DAG paint was used on the samples, avoiding the region of interest, to reduce charging of samples in imaging. Charging occurs when electrons from the beam cannot be conducted away from the sample so instead remain on the sample making it difficult to image, some examples of this have been noted in this thesis as the samples from were still affected, how this could be further mitigated is discussed in the discussion of experiment 2.

2.7 TEM Sample preparation

Samples with ACLAR sheets were processed for TEM. 24hrs or 72hrs post lesioning, samples were fixed in 2.5% Glutaraldehyde in 0.1M Sodium cacodylate/ 2nM $CaCl_2$ for 2 hours. This was then washed in 0.1 M sodium Cacodylate/ 2mM CaCl2, then postfixed in 1% OsO4 for 1 Hour. Before being washed again in the buffer solution. Samples were then stored in 70% ethanol prior to dehydration and embedding.

Samples were then dehydrated in an ethanol series 70% to 90% to 100% then 100% dry with the samples being left in each ethanol series for 15 minutes. Samples were placed in a 1:1 ratio of Spurr's resin and 100% dry ethanol for 1hour. Then into a 3:1 ratio of Spurr's resin to 100% dry ethanol overnight at room temperature.

Once left overnight, samples were infiltrated with pure Spurr's resin 4 times, before samples were placed into moulds with fresh pure Spurr's resin for 16 hours, or until set, in an oven at 600C.

Spurr's resin was made up out of the following:

- Nonenyl Succinic Anhydride (NSA), 26g
- ERL – 4221, 10g
- Diglycidyl ether of polypropylene glycol (DER), 6g
- S-1 dimethylaminoethanol, 0.4g

Samples were cut into 80nm thin sections using a Reichert-Jung Ultracut-E ultramicrotome (Buffalo, NY, USA) and a glass knife made using a LKB Knife maker Type 7801B. Sections were placed onto a copper grid and left to dry before staining.

For staining, 4g of Lead citrate was added to 10ml distilled water and 500µl NaOH into a glass vial. In addition, 0.04g Uranyl acetate was added to 2ml of 70% ethanol into a glass vial. Both solutions are sonicated for 5 minutes and then centrifuged at high speed for 5 minutes. Two Petri dishes with a strip of dental plastic was set up, one petri dish also contained hydroxide pellets. The dish without the pellets had 4 drops of the Uranyl acetate solution placed onto the dental wax, a copper grid with samples was added to each drop of Uranyl acetate solution and was left for 20 minutes. Each grid was then rinsed in distilled water three times, each rinse involved dipping the grid into the distilled water 10 times. The grids had excess water removed by blotting on filter paper. Then, within the second petri dish, 4 drops of the Lead citrate solution were placed onto the dental wax and the grids were submerged into the drops for 5 minutes, before being washed in distilled water again in the same process and being blotted on filter paper and left to dry within a grid case overnight before imaging.

2.8 Fluorescence imaging and analysis of magnetoelectric fibre experiment

Fluorescent images of samples were taken with a Zeiss Axio Observer using ZEISS Zen 3.3 blue edition software. At least three images were taken randomly from each sample and were then analysed using Image-J.

2.9 SEM Imaging:

SEM samples were Imaged using a Hitachi S4500 SEM at 5.0 kV with pictures collated into a .tif format. Images were then analysed using image-J.

Magnetoelectric fibre experiment

Morphological investigation was conducted, comparing the cellular morphologies to what was seen in the fluorescence images and if any cellular membrane activity was visible. Along with visualising the nanofibers used and the cellular interactions with the hydrogels. Images were taken of each modality. Some lower magnification images were taken for comparison with fluorescence whilst; to observe membrane activity, images of cellular bodies were taken for analysis to avoid confusion between cells and because they provided easier visualisation of cell membrane structures. Whole cell images were taken to try and identify cellular morphology (Fernades et al, 2015). Biocompatibility is evaluated by observations in any cell death or apoptosis and necrosis morphologies like blebbing. Furthermore, if cell type morphologies appear as expected in experimental conditions compared with conditions, then biocompatibility can be assumed on the morphological level. With neurones expecting to have long projections and astrocytes to have more broader projections. Along with observation of cell adherence to hydrogels.

PODs drug delivery experiment

Observational investigation was conducted to visualise lesions under SEM, looking for signs of POD interactions, growth into the lesion and how the imaging modality compares to TEM images.

2.10 TEM Imaging of PODs drug delivery experiment:

Samples were imaged using a Joel 1230 TEM (JEOL ltd, Japan) at 80kV. Images were analysed using Image-J. Images of Figure 4.8 were taken using a FEI Techni G2 (Thermo Fisher scientific, USA). Images collected were used to observe any signs of internalisation of PODs or any ultrastructural changes visible, such as signs for cell death or regeneration along the lesion.

2.11 Statistical analysis

Magnetoelectric fibre experiment:

Cell counts were performed on cells stained for MBP, GFAP, Tuj-1 and DAPI to investigate proportions of differentiation. Cell counts occurred on three different experimental repeats stemming from different SVZ cultures, n = experimental repeats from different SVZ collections (n=3). DAPI staining was counted for total cell counts, cell bodies of MBP were collected for oligodendrocyte counts and Tuj-1 stained cell bodies were collected for neurone cell counts. The GFAP image was superimposed

on Image-J of the counters for DAPI, Tuj-1 and MBP. And DAPI counts that fell outside of GFAP staining was counted as unstained. The Tuj-1, MBP and unstained were then taken away from the total DAPI to generate the number of GFAP stained cells. the percentage of each staining was generated and for all three repeats of each condition. Each staining type and the unstained were inputted into separate two-way ANOVA using GraphPad Prism 9.5.0 (730). Comparing the magnetic field stimuli with the gel type as predictor variables.

Furthermore, neurite projection lengths were measured to investigate if extension length is altered based on the parameters. Data on neuronal projection length was collected by using Image-J measuring tool measuring 5 neurones in each field (three fields were taken from each hydrogel) for each experimental repeat (two repeats of the experiment, repeats were done from new SVZs) totalling to 30 neurones in each modality from the edge of the cell body to the end of the projection, n = each field image taken (6). Each measurement was in µm. Neurones were picked based on ability to measure, with neurones having no overlap with other neuronal projections. with clear visible cell bodies and projections to ensure measures taken were as accurate as possible. All measurements were imputed into a two-way ANOVA using GraphPad Prims 9.5.0 (730). Comparing gel type and magnetic field.

Data for cell membrane activity was collected from five cell bodies of each modality in three separate experimental repeats (n=3). A 'total activity score' from 0-3 was given to each individual cell if membrane structure was present 0 = unstimulated membrane (means no pits, circular ruffles or filopodia were visible) and one point was awarded for the presence of one or more structures that were pits, filopodia or, circular ruffles were present. A summary of scoring is shown in table 4 below. Cells were picked based on visibility of cell body to ensure the whole structure is visible encase ultrastructure's are missed and image resolution. Images were taken at random where cells were visible on low magnification as not all the gel was confluent. Images were collated from all experimental repeats generated from different SVZs collections for each condition.

Table 4: A summary of the requirements and scoring for cell membrane activity.

Cell Requirements	**Ultrastructure**	**Score**
Visible cell body	Pits (P)	1
Resolution reached ultrastructural level	Filopodia (Fp)	1
no artifacts visible from sample preparation	Circular ruffles (CR)	1
Cells are healthy with no signs of cell death	Unstimulated (US)	0
	Total activity score of each cell	P + Fp+ CR (if US = 0)

As the data collected was categorical including multiple comparisons, Chi squared in Excel (Microsoft 365) was decided on for statistical analysis of cell membrane activity.

Experimental

Chapter 1

3.1 Introduction

3.1.1 Application of hydrogels for NSC transplantation

Hydrogels are a category of polymeric hydrated materials of natural, synthetic or hybrid origins commonly used in neural tissue engineering due to their positive qualities. They are non-toxic, 3-D and porous allowing for cell infiltration and movement of nutrients. In addition, they mimic the structure of the extracellular matrix making them highly biocompatible. In addition, they do biodegrade in vivo which at the desired rate helps promote regeneration, the rate of biodegradation can be altered based on the origin and addition of other materials, flexibility and optimisation is vital for positive results. It has been shown that softer hydrogels promote NSC differentiation into neurones. Leipzig and Shoichet (2009) showed softer hydrogels with a stiffness of < 1 kPa promoted differentiation into neurones, compared to a stiffness of <1 and 3.5 kPa which favours astrocyte lineages. Therefore, altering the stiffness of hydrogels can help control the lineage of stem cells, potentially directing them to differentiate into neurons (Niemczyk-Soczynska et al., 2021).

Modification of hydrogels is straightforward meaning physical and chemical parameters can be tuned to mimic the nervous system. Further, additional therapeutic agents (e.g., growth factors) can be encapsulated within hydrogels for targeted drug delivery. For translational use hydrogels are easily reproduced, processed, and cheap to make, making them ideal for clinical application. To further enhance the therapeutic efficacy, studies have suggested providing electrical stimulation results in alterations to differentiation, proliferation, migration, and neurite extension. For example, Ciofani, et al., 2010 showed that neuronal like PC-12 cells experienced 30% increase in extension sprouting under electrical simulation than controls. Furthermore, NSCs seeded on nanofibrous scaffolds when exposed to 100mV/mm direct electrical stimulation underwent significantly increased proliferation (Ghasemi-Mobarakeh et al., 2009). In addition, during neuronal wound healing in normal biological environment neuronal cells experience a 140mV/mm electrical field – indicating an importance in healing and helping regenerate lost tissue (Kopyl et al., 2021).

Therefore, the incorporation of materials that provide electrical cues has shown positive outcomes, but how is it beneficial to regeneration and repair? The mechanisms of action are not yet fully understood with several hypothesis existing. It is believed that the electrical field can either influence cell differentiation, migration and proliferation via cell membrane receptor activation, generation of ion influxes such as effecting calcium channels, microfilament reorganisation and effecting cell signalling cascades. Potentially resulting in alterations to gene and protein expression and cell behaviours. (Cheng et al., 2021). Whatever the mechanism being able to understand how it works and the cellular effects it may have would help our understanding of electrical field/ biomaterial –

cellular interactions. For optimisation but also efficacy and safety-based questions before clinical trials. Part of this understanding would come from the observations of ultracellular structures to evaluate cellular changes.

However, direct electrical stimulation of implants has drawbacks for clinical application. This includes use of wired electrodes which may need to be surgically removed post-treatment. In addition, electrodes are often hard and mechanically mismatched with neural tissue so cause scarring. Electrical stimulation could be delivered externally. This can have off-target effects such as increasing inflammation and further damage. Therefore, developing novel materials to facilitate wireless electrical stimulation would provide a clinically more translational approach. One such approach is the use of magnetoelectric fibres. These are fibres in which a magnetic field induces distortion or constriction in a fibre thus resulting in the fibres emitting an electrical signal (Hermenegildo et al., 2019), as illustrated in figure 3.1. As magnetic fields are used as the stimuli it allows for wireless stimulation of fibres, potentially through equipment such as ultrasounds that are already available in clinics. Within Hermenegildo et al., 2019 the addition of CoFe2O4/PVDF magnetoelectric spheres improved cell viability by 80% when added to $CoFe_2O_4$/ Methacrylated Gellan Gum (GGMA)/poly(vinylidene fluoride) (PVDF) based hydrogels with exposure to electrical cues. Indicating electrical stimulation can result in positive outcomes that may be beneficial to regeneration. Electrical stimulation induced wirelessly is a more positive approach and such materials have been developed such as Pezioelectic fibres that can produce an electrical current through decompression/movement that could be induced by the patients themselves. In addition, Magnetoelectric materials that combine magnetorestrictive and piezoelectric components into fibres working via a magnetic field inducing compression on the fibre that results in an electrical current, Fig 3.1. Both fibres can be added to hydrogels. Producing a combinational approach of wireless electrical cues and the biocompatible and easily optimised hydrogel scaffold as a support. Potentially this can result in NSC proliferation and differentiation. With electrical cues potentially directing NSCs into neuronal differentiation and hydrogels providing a scaffold support for cell adherence and migration for the formation of connective projections. Making them viable candidates to act as supports to NSC transplantation in cases of SCI. Investigating this option for implantation is a viable avenue in research. This in turn may bridge the gap in lost connections resulting in functional recovery. However, despite the potential benefits for incorporating magnetoelectric fibres into cell carrier implants, this approach has not yet been widely tested for neural cells. Their efficacy, toxicity, biocompatibility, degradation, mechanism of action, performance in a neural environment is not fully known or researched. This thesis will look at two set of fibres and their incorporation into hydrogels. One being solely magnetic cobalt fibres (Coco) (control) and the other being JANUS (CoJa)

magnetoelectric fibres (Ferson et al., 2020). Integrating these fibres into hydrogels may shed some light onto whether, in combination, they generate favourable behaviours into NSCs that could determine if future in vivo studies are worth exploring whilst also evaluating if the JANUS fibres elicit any toxicity or biocompatibility.

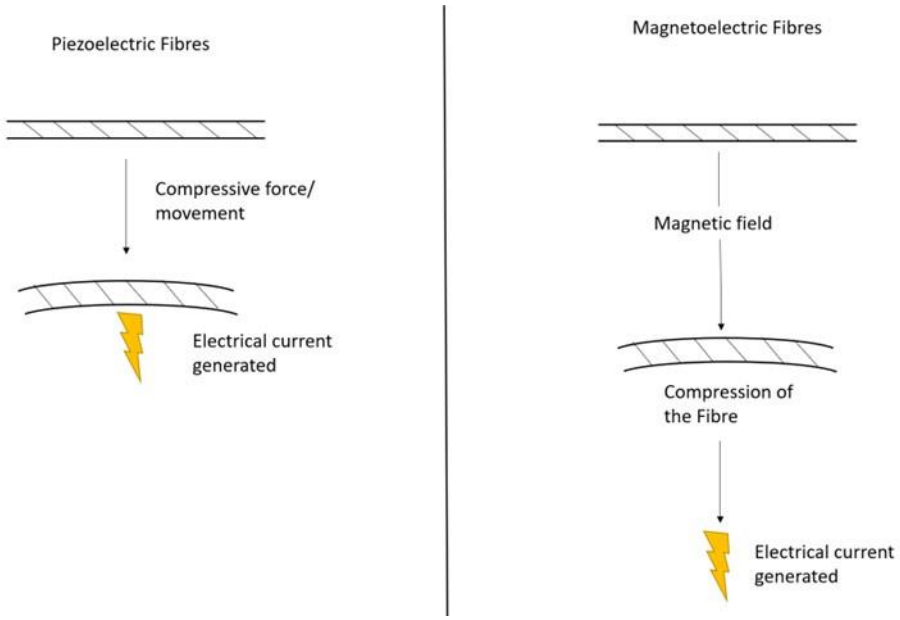

Fig 3.1. A diagram summarising the mechanisms of Piezoelectric and magnetoelectric fibres in the production of an electrical current. *Whilst Piezoelectric fibres (left) produce an electrical current from a force or movement that results in their distortion and compression. Magnetoelectric fibres (right) compress due to a magnetic field that results in the production of an electrical current.*

3.1.2 Aims

Given there is potential clinical utility in wireless electroactive implants containing magnetoelectric fibres. Investigations into the compatibility and efficacy of fibres being developed is a good avenue for research. As combinational approaches have been pointed as the better alternatives for improved functional recovery combining these fibres with biocompatible hydrogels maybe provide added improvements. In this thesis JANUS magnetoelectric fibres encapsulated in hydrogels as a combinational therapeutic approach will be investigated, our aims are to:

i) Fabricate magnetoelectric hydrogels by encapsulating JANUS nanofibers in collagen hydrogels.

ii) Assess the biocompatibility of the fabricated magnetoelectric gels.

iii) Examine whether wireless magnetic stimulation can modulate NSC behaviour on the magnetoelectric gels.

We will employ both fluorescence, to view cell types and neuronal extensions, and SEM, to assess any cell membrane activity and potential toxicity.

3.2 Results

3.2.1 Magnetoelectric hydrogel characterisation:

Fibres were visualised under SEM with collagen, cobalt and JANUS fibres being easily distinguished from each other due to the significant size difference. These JANUS fibres displayed some integration with the collagen fibres as shown in Figure 3.2 below. With the cobalt fibres it is harder to distinguish. A side-by-side comparison of each gel type and their integration is displayed in the images within Figure 3.2. Yet, these fibres may look different in reality as the shrinkage and chemicals used in EM may have led to distortion. Yet, as all conditions went through the same methods, they can be compared to one another. The JANUS and Cobalt fibres did not interact with cells – they were located at the bottom of the gel most likely due to their size.

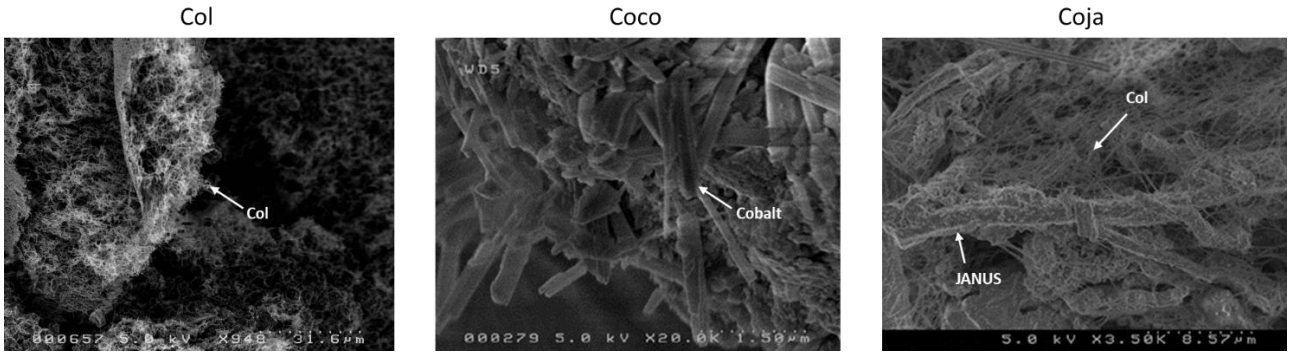

Figure 3.2. SEM images, Col displaying a hydrogel containing only collagen fibres labelled as Col. Coco, image of a hydrogel containing cobalt fibres, indicated in the image. Coja, image of a hydrogel containing JANUS fibres with collagen (Col) and JANUS fibres indicated.

3.2.2 Fluorescence analysis, proportion of cell types and neuronal projection lengths:

In fluorescence imaging, examples given in on Figure 3.3 below, Fluorescence images of one field of each example condition Col nm, Coco F0 and Coja F4 and the different fluorescence staining of DAPI, GFAP, MBP, and Tuj-1. DAPI staining showed nuclei to be rounded with very little pyknotic nuclei in each field of all variables. In all variables astrocytes appeared with GFAP staining as complex sheet like structures with cell bodies having vast projections with individual cells being hard to distinguish. Neurons (Tuj-1 stained cells) had rounded cell bodies with one – three projections in most cases in all variables. Oligodendrocytes (MBP stained cells) were varying morphologies mostly the cell body was

clearly visible. Other morphological structures that would be expected such as processes radiating from the cell body were not easy to distinguish. Images of Figure 3.5 offer examples of morphological conclusions reached.

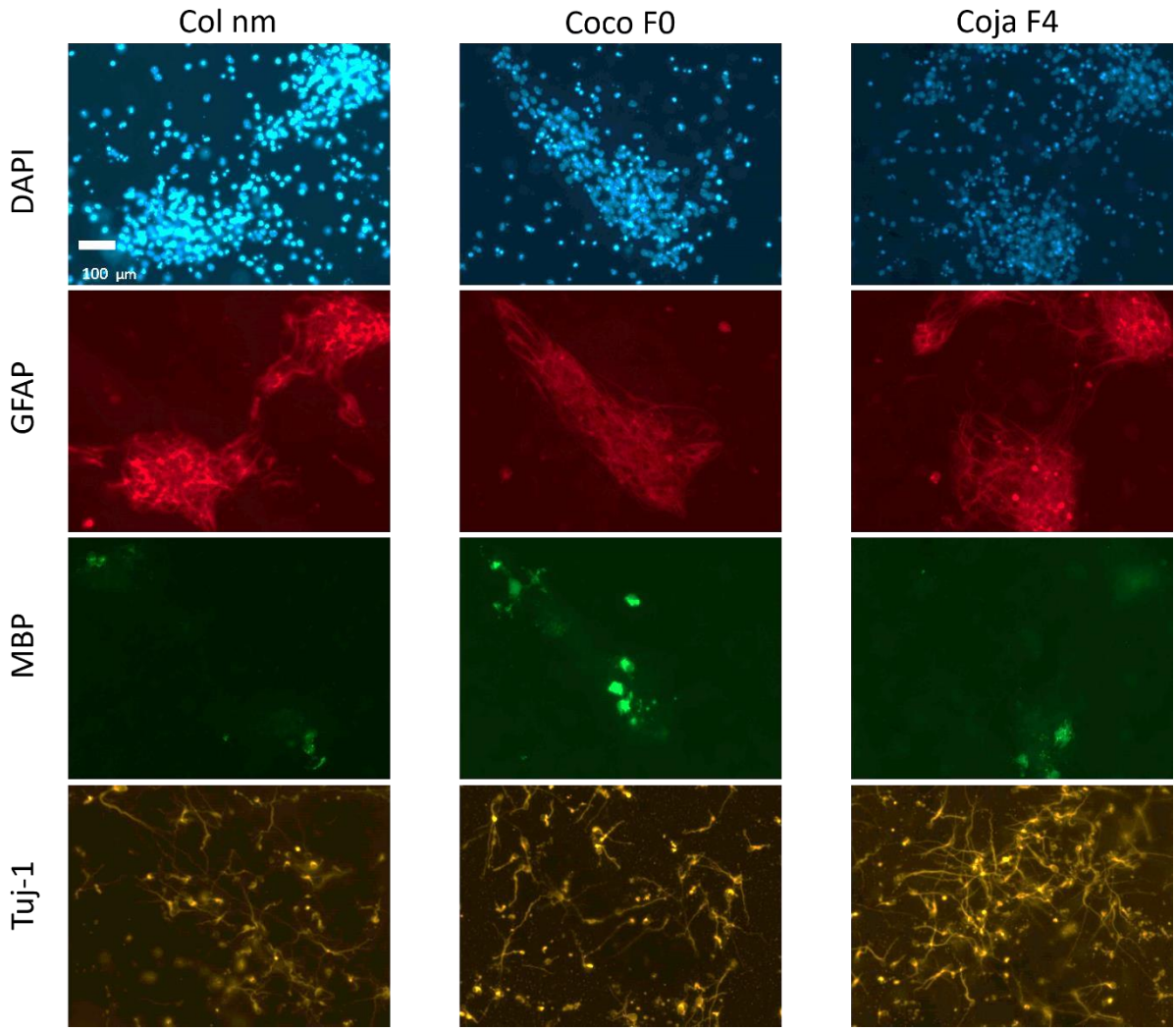

Figure 3.3. Fluorescence images taken at 20x magnification: samples Col nm, Coco F0, and Coja F4*. All fluorescence types are displayed separately for each condition as DAPI (nucleus), GFAP (astrocytes), MBP (Oligodendrocytes), and Tuj-1 (neurones) but have been taken within the same field using a Z stack. To give an example of the cell morphologies, amounts of each cell type and the fluorescence staining quality.*

No significant difference was noted between gels or magnetic field type when comparing the cell proportional rates of Tuj-1 presenting cells (neurones), GFAP presenting cells (astrocytes), MBP presenting cells (oligodendrocytes), and unstained cells, a summary of statistical analysis of each cell type is provided in the graphs within Figure 3.4 comparing the hydrogel types with the proportion of cells of each magnetic stimulation condition. Differentiation proportions for each cell type was on

average for GFAP 80.37 ± 7.16 %, Tuj-1 8.74 ± 4.62%, MBP 2.97 ± 2.09 %, Unstained 7.99 ± 5.11%. GFAP, Tuj-1 and MBP. In each stanning type no significant difference was noted when performing a two-way ANOVA. Tuj-1 (p = 0.9575, f = 0.1562, n=3, two-way ANOVA), GFAP (p = 0.9665, f = 0.1366, n=3, two-way ANOVA), MBP (p = 0.9803, f = 0.1009, n=3, two-way ANOVA), and Unstained (p = 0.9403, f = 0.1901, n=3, two-way ANOVA).

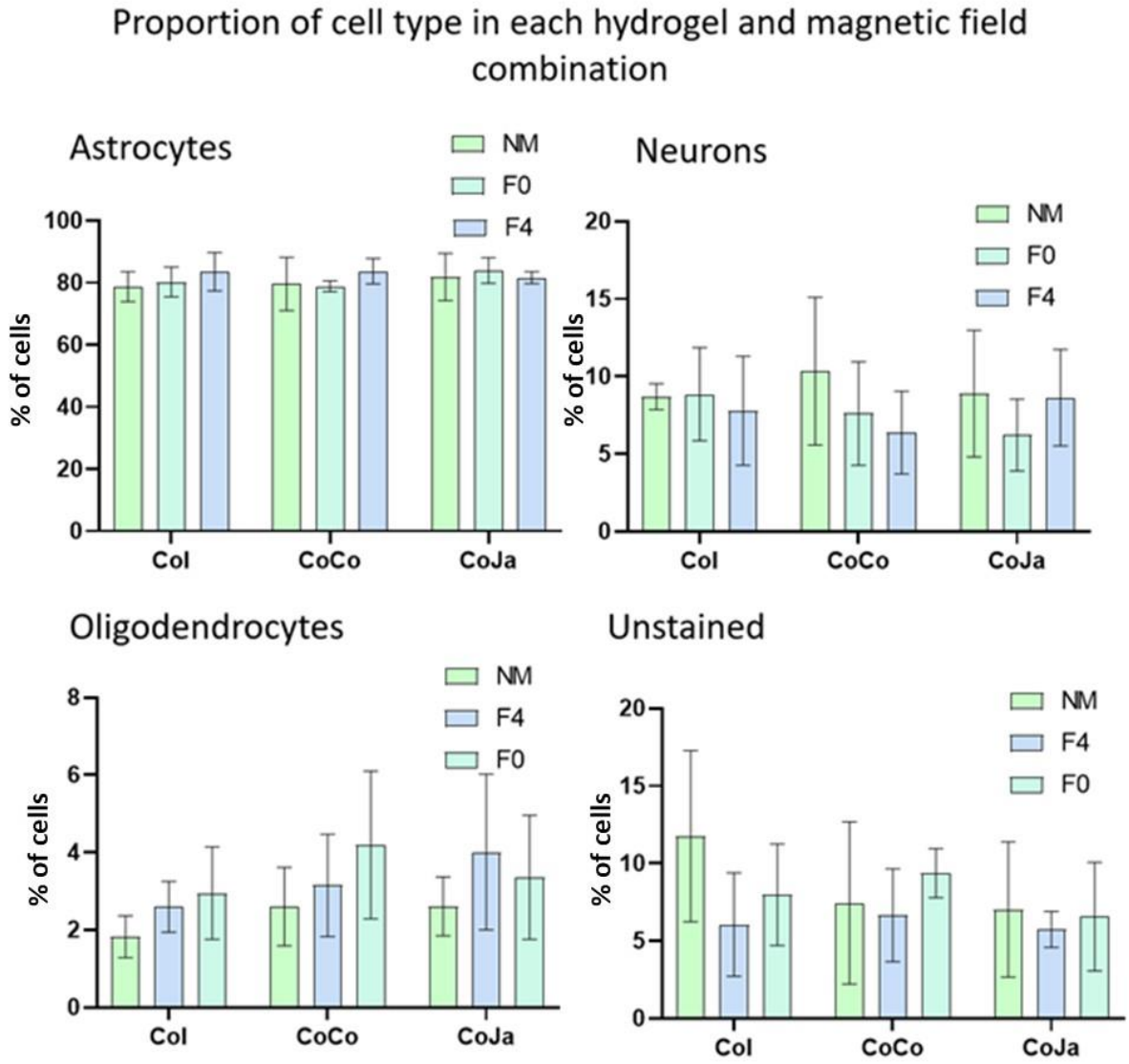

Figure 3.4. Column graphs depicting the proportion of each cell type for astrocytes, neurones, oligodendrocytes and unstained cells on each experimental substrate*. Col is collagen alone; CoCo is cobalt fibres and CoJa is JANUS fibres hydrogel. No significant differences between experimental groups were noted for any cell type.* Tuj-1 (p = 0.9575, f = 0.1562, n=3, two-way ANOVA), GFAP (p = 0.9665, f = 0.1366, n=3, two-way ANOVA), MBP (p = 0.9803, f = 0.1009, n=3, two-way ANOVA), and Unstained (p = 0.9403, f = 0.1901, n=3, two-way ANOVA.

A significant difference was witnessed between the hydrogel types regardless of magnetic field present with neuronal length. Figure 3.5 illustrates how a significant increase in neurone length can be seen based on gel type whilst the different types of magnetic field had no effect with neuronal lengths staying similar in each gel group. As in Figure 3.5, magnetic field showed no significant difference ($p = 0.3414$, $f = 1.079$, $n = 6$, two-way ANOVA) whilst comparison of substrates there was a significant difference ($p < 0.0001$, $f = 33.48$, $n=6$, two-way ANOVA). Coco compared to collagen showed a $p<0.05$ significant difference in increased neuronal length. CoJa also had a greater neuronal length compared to collagen with a $p<0.001$ significant difference as seen on the graph in Figure 3.5. There was no significant difference between the magnetic fields. Combination of hydrogel and magnetic field did not show a significant difference when comparing all conditions. For example, when looking at the F4 conditions where all gel types were exposed to magnetic field Col gels showed an average of 67.31 ± 20.49µm neurite length. This increased in Coco neurite projections to 88.79 ± 38.10µm, then again further to the longest neurite projection average in CoJa gels of 115.77 ± 32.26µm (Figure 3.5).

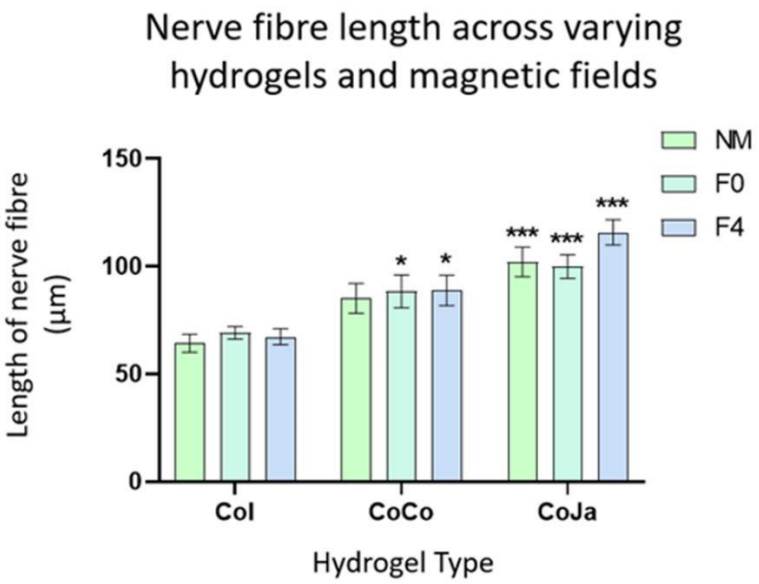

Figure 3.5. A column graph displaying nerve fibre length across all variables*. Significant differences are highlighted as *p<0.05 and ***p<0.001 versus collagen no magnetic field. When comparing ColNM: CoF0 p=0.0971, CoF4 p=0.0261, CoJaNM p<0.0001, CojaF0 p=0.0002, CojaF4 p<0.0001(n=6, two-way ANOVA, multiple comparison test).*

3.2.3 Comparison of SEM to Fluorescence imaging:

In all experimental variables imaged using SEM, cells showed adherence to the hydrogel. No cells interacted with the Cobalt or JANUS fibres. When comparing fluorescence images to SEM images, in both instances cells were clustered on all hydrogels and not evenly distributed across all gels. Within fluorescence, it appears the astrocytes are creating a sheet like structure across the gel. Sheet like cell groups were also visible with SEM imaging. However, the SEM gels experienced noticeable cracking and shrinkage so a definitive comparison cannot be drawn. Fluorescence z stack was not able to show gel-cell interactions. However, with immunohistochemistry cell types were imaged in isolation for quantitative analysis. Whilst for SEM, cell morphologies could be used to determine some cell types (Figure 3.6), this was not possible for analysis on the larger scale. With the high resolution of the SEM, quantitative analysis of membrane activity was possible. This resolution was not available with fluorescence. Fluorescence was favoured however for quantitative analysis of neuronal projections. Using SEM to measure neuronal projections was more difficult and not used as the images were too complex plus shrinkage to the samples may not reflect reality.

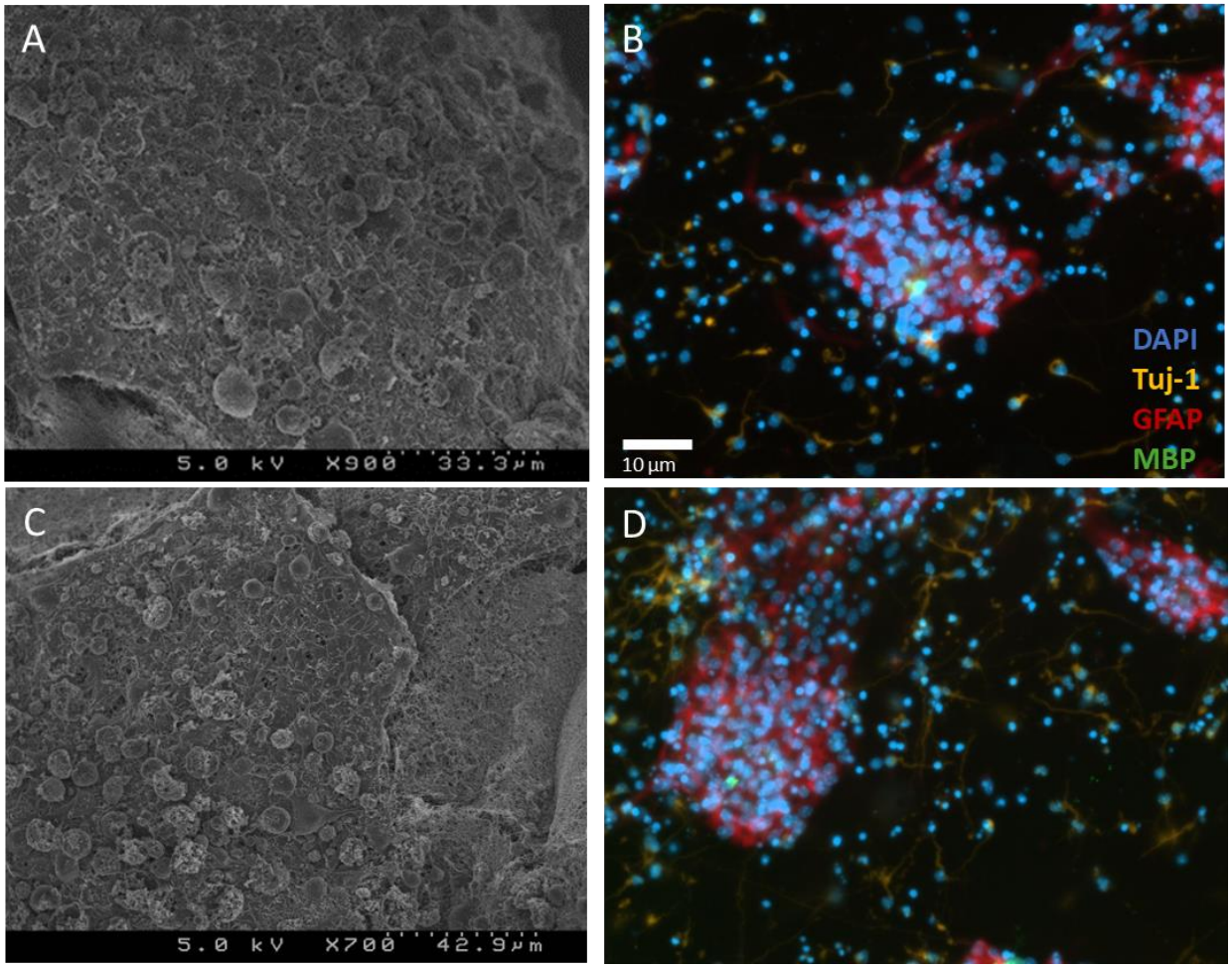

Figure 3.6 A-D. Side by side comparison of SEM and fluorescence images*. Pictures A and C are SEM imaged of col hydrogel surface with cell layer at the surface. Images B and D are fluorescence images taken of col hydrogels with all fluorescent types superimposed on each other. Fluorescence images were taken at 20x magnification.*

3.2.4 SEM analysis – ultrastructure membrane activity:

All variables had cells which presented unstimulated cell membranes (US) with no activity. Some cells in all conditions displayed cell membrane activity in the form of pits (P), filopodia (Fp) or circular ruffles (CR). Figure 3.7 displays the structures observed and quantified including circular ruffles, filopodia, and pits. When comparing total membrane activity via SEM imaging using Chi squared *overall membrane activity showed no significant difference ($p = 0.9768$, $X^2 = 0.4653$, Chi squared test with multiple variables (n=3). When comparing hydrogel materials under different stimulus no significant difference was also recorded, Col: $p = 0.3052$, $X^2 = 2.37$*, Coco: $p = 0.2780$ $X^2 = 2.56$ and CoJa: $p = 0.2671$ $X^2 = 2.64$ (n=3). No significant difference was also noted in Chi Squared analysis comparing different types of stimulation, NM: $p = 0.2216$ $X^2 = 3.01$, F0: $p = 0.3418$ $X^2 = 2.14$ and F4: $p = 0.2991$ $X^2 = 2.41$ (n=3). Therefore, no gel or magnetic field showed a significant difference in increasing membrane activity. In addition to this the predominant morphology witnessed in SEM

imaging was more astrocyte like, with broad extensive projections, forming a more sheet like appearance (example given on Figure 3.7 image D). Neuronal like morphology, Figure 3.7 image C, with less projections that were smaller than those of astrocytes were harder to find. The majority of cells did show a healthy morphology and signs of necrosis was not visible, as such structures like blebbing, large punctures in cell membranes, rounded detached cells were not observed.

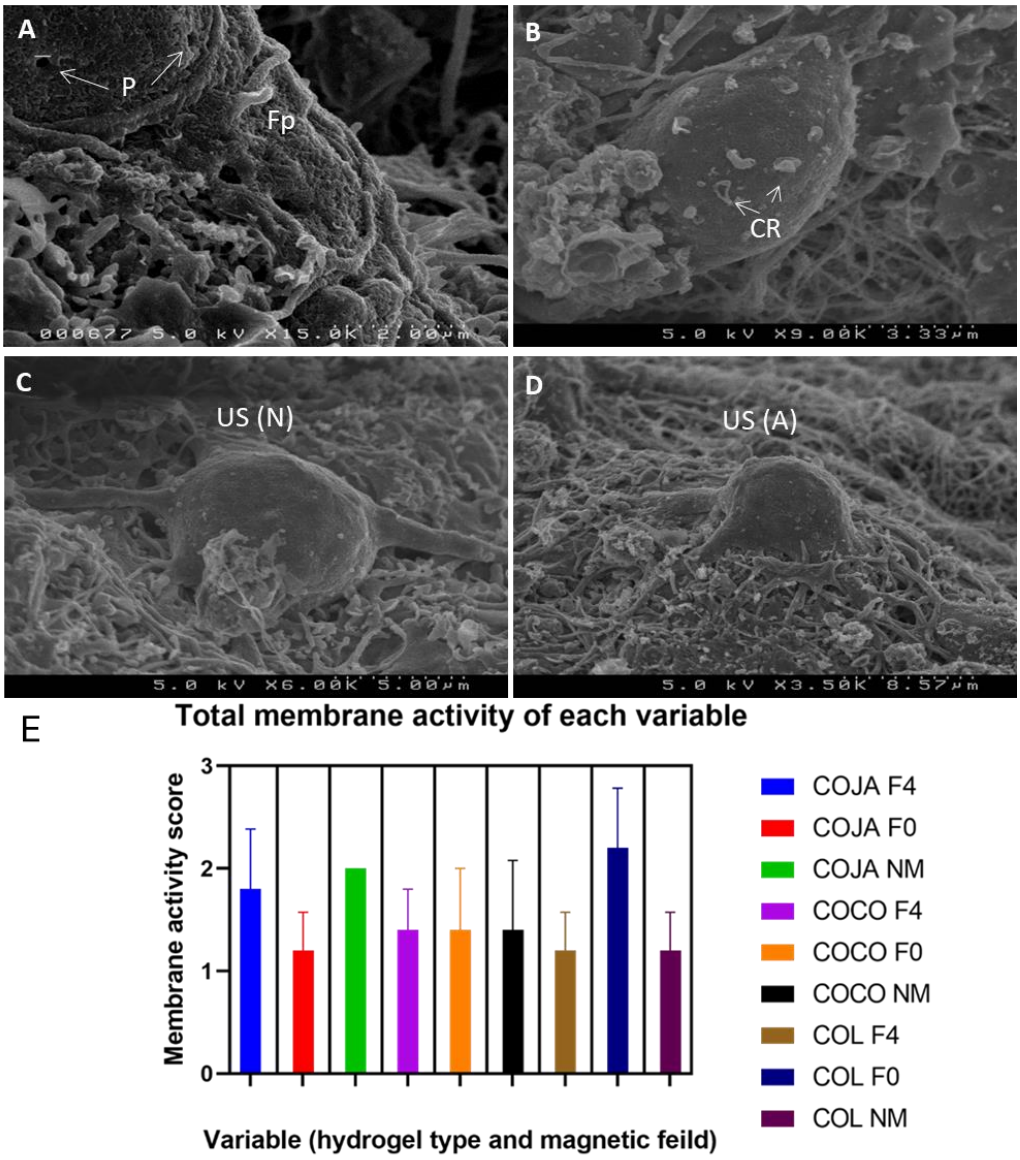

Figure 3.7 (A-D): SEM images of cells visible on hydrogel conditions*. Image A shows examples of pits (p) and filopodia (Fp) membrane ultrastructure under SEM. Image D indicates circular ruddles (CR) membrane ultrastructure under SEM imaging. Structures indicated in images A and B were classed as indicators of membrane activity. Image C offers an example of what an unstimulated cell membrane (US) and the cell in image C shows neurone like morphology with smaller bipolar projections (N). Image D also shows what unstimulated cell membrane looks like but also what astrocyte morphology looks like under SEM, with cell forming more broad and frequent projections. all cells visible are displaying a healthy morphology with no signs of necrosis. Figure 3.7 E is a graph displaying the total membrane activity of each variable. A NESTED graph comparing the total membrane activity score of each variable and the error bars with SEM (COJA F4, COJA F0, COJA NM, COCO F4, COCO F0, COCO NM, COL F4, COL F0, COL NM).*

3.3 Discussion

3.3.1 Effect of magnetoelectric fibre/collagen scaffolds on neural stem cell cultures

Cells showed good adherence to all hydrogels suggesting that the hydrogels even with the introduction of new fibres still have some level of biocompatibility with observation of cell morphology, necrosis and adherence to gels. Along with no signs of pyknosis using fluorescence (Figure 3.3) or signs of necrosis under SEM in all conditions, this implies all gel types displayed no toxicity towards cells. Thus, the hydrogels with JANUS and cobalt fibres show potential safe use for future studies. However, form SEM imaging cells did not make direct contact with JANUS fibres (Figure 3.2). The next stage of establishing toxicity would be to see if direct cell adherence may lead to any toxicity effects. Direct contact with fibres may also help improve the electrical stimulation to cells and would be interesting to explore whether this alters results.

No variation in proportions of cell types was seen in control or magnetic field/hydrogel combinations (Figure 3.4). This suggests JANUS magnetoelectric and Cobalt piezoelectric fibres did not alter the percentage of neurones present and can be assumed under static and oscillating magnetic field at 4Hz they did not alter differentiation rates of astrocytes, neurones, or oligodendrocytes. Therefore, neither gel type or magnetic stimulation hindered or altered cell differentiation under the parameters set in this experiment. From this we can deduce JANUS fibres have no effect on cell differentiation. However, it also displays no effects on differentiation that may hinder regeneration. Fibers having no effect in this manner may suggest a good level of biocompatibility ideal for future vivo studies. Yet, JANUS fibres did not directly interact with cells therefore future studies using more direct cell-fibre interactions may be required to review these findings.

Cell membrane activity in the form of pits, circular ruffles and filopodia, displayed no significant difference regardless of magnetic field or hydrogel (Figure 3.7). This suggests that cellular activity at the membrane level is not affected by alterations in the presence of JANUS fibres or 4Hz magnetic field along with any displacement mechanical force. As cells were only interacting with collagen fibres and not to that of cobalt or JANUS then it can be assumed there was no internalisation of the fibres therefore no increase in membrane activity. As Fernades 2015 witnessed the same cell membrane structures assessed in this experiment noticed an increase in cell membrane activity features with internalisation of magnetic nanoparticles at 4Hz (Fernandes, et al., 2015). However, using an ANOVA in this thesis when the data of cellular membrane activity was categorical would potentially mean that the analysis of this data may not be statistically meaningful.

Regardless of magnetic field JANUS hydrogels had a significantly longer neuronal projection length compared to collagen hydrogels. Cobalt fibre hydrogels also had a significantly longer neuronal

projection length than collagen, but JANUS hydrogels showed the greater statistical significance indicating a longer projection length. Potentially, the fibres influence the environment making it more favourable for longer neuronal projection length than collagen hydrogels alone (Figure 3.5). Electrical stimulation has been shown to increase neural projection length within other studies such as, Kotwal and Schmidt, 2000. They showed that the addition of oxidized polypyrrole (PP), that is electrically conducting to fibronectin gels increased neurite length, with the stimulated PP having a median neurite length of 99.1µm whilst the unstimulated PP only had a neurite length of 62.0µm. Yet, this would not explain how the projection length was significantly longer in the JANUS hydrogel that did not undergo any magnetic field stimulation compared to the collagen gels that underwent 4Hz. The fibres could potentially be altering the stiffness of the gel improving projection growth (NiemczykSoczynska, et al., 2021). This could be tested via a stiffness indentation test. In addition, potential outside forces of mechanical stimulation from moving the well plates from one place to another, handling the gels could have caused an electric field that may have influenced neuronal cell growth. The fibres may have acted by effecting a different environmental factor which is not yet known that may have resulted in the projection lengths observed. JANUS fibres showing a more positive impact than Cobalt fibres on neuronal projection length suggests something that may differ between the two fibres such as JANUS being stimulated by a magnetic field. More investigation would have to be done to reach a conclusion. What has been shown is that JANUS fibres within a collagen-based hydrogel have a positive effect on neuronal projection lengths. Ciofani, et al., 2010 also experienced and increase in neuronal projection lengths in PC-12 lineage cells when they experienced electrical stimulation. However, for JANUS fibres this may be the first findings of neuronal projection lengths. This has benefits in tissue engineering strategies as axonal projections are needed to extend long distances. This is in order to form connections with neurones outside the injury site, hopefully bridging the gap of communication.
Potentially this may result in functional recovery that is the ultimate goal for clinical use.

Fibres did aggregate at the bottom of the gels due to their weight and setting time of the gel. Altering the order in which reagents were added to the gel mixture was attempted to make the fibres more suspended but did not change the outcome. The fibres not being in contact with the cells or in as close proximity may have affected the reach of the electrical current generated. Thus, the fibres may have had little electrical impact on the cells. Therefore, if the effect of the magnetic field may have had no effect based on its strength, having no impact on the cells, or its reach. Making the gels thinner, turning them upside down, or rotating the gels as they set may offer a better dispersal of the fibres. In addition, exploring different frequency ranges would give more insight into if the stimulation from the fibres offers any impact onto the cells. This was not done within this experiment

as the machine used did not exceed 4Hz. Plus, mechanical movement involved in moving the well plates regardless of condition may have produced background stimulation to fibres that is not accounted for. Seeing how and if mechanical movement such as moving the well plate may produce an electrical stimulus may be of importance to mitigate background stimulation, but taking extra care and avoiding sudden movements and gentle placement can reduce such forces as was done within this thesis. Testing the different Young's modulus of the gels produced could also shed light if stiffness is a factor.

3.3.2 Comparison of SEM and fluorescence imaging techniques

SEM has proven to have beneficial analysis use for tissue engineering mostly regarding looking at the high resolution of the cell in membrane activity and potential cell death. In this thesis we were able to show the harnessing of SEM to produce quantifiable data on cell membrane activity which became useful in evaluating hydrogel effects on cellular behaviour. Furthermore, SEM can be used to look at the adherence of cells onto scaffolds but the methods regarding collagen hydrogels that experience mass shrinkage and cracking might need to be developed. One such alternative may be to freeze dry the gels this would minimise shrinkage but also means samples would have to be thinner, but this might pose as an advantage to get the cells in proximity to the fibres. Yet would make any damage from handling more of a risk. Using SEM, cell types could be distinguished but on the larger scale, fluorescence proved more favourable in being able to count cell types and gauge overview of morphology and qualitative results. A comparison of Fluorescence and SEM observed in this experiment have been summarised into Table 4.

Table 4: a summary comparing SEM and Fluorescence imaging on sample preparation and imaging analysis.

	SEM (Hitachi S4500)	**Fluorescence (Zeiss Axio Observer)**
Sample preparation time	SEM was the lengthier procedure with staining, dehydration and mounting taking weeks.	Fluorescence staining take up to three days
Distinguishing cell types	Using morphological analysis some cell types could be distinguished when imaging. However, quantitative data would be hard to acquire and apply for the whole gel. The inability to isolate cell types adds complexity to distinguishing one cell from another making measuring extensions or cell counts to complicated and unreliable.	Staining with immunohistochemistry made ease of identifying cell types. In addition, it allowed for the cell types to be isolated when imaging for more quantitative analysis. This also allowed for measuring of neurite extensions.
Cell membrane activity	Images from SEM were at high enough resolution to image and quantify cell membrane activity using morphological analysis of ultrastructure's	Fluorescence microscopy was not a high enough resolution to witness membrane activity
Identifying cell toxicity	Morphological analyse allowed for trying to identify cells undergoing cell death	Using DAPI stain to identify any pyknotic nucleus allowed to identify any cell death
Imaging 3D	SEM 2D images of sample topography was acquired.	Fluorescence imaging using a Z stack allowed for some 3D visualisation – this has a
		limited depth and relies on the sample being translucent

Hydrogel interactions with cells	Hydrogels and there interactions with the cells were witnessed and imaged. Yet, hydrogels underwent shrinkage and cracking so any analysis of the gel fibres would not be realistic to their true form.	None of the hydrogel could be imaged or the hydrogel cell interactions.
Quantitative and qualitative analysis	Ultrastructural cell membrane structures were analysed. Cell-hydrogel adherence. Any potential signs of apoptosis and necrosis. Gross morphological indicators between astrocytes and neurones	Gross morphology of astrocytes and neurones. Cell proportions of neurones, astrocytes, oligodendrocytes and unstained cells. neuronal projection length. And pyknosis of nucleases.

Z stack fluorescent imaging allowed for some 3D capabilities. However, this is dependent on size and transparency of the sample as regions of dense JANUS and cobalt fibres were hard to image through. The SEM imaging used can only show the surface of the sample but did offer a wider depth of field. Yet, there are other forms of SEM imaging that could offer a 3D rendering that is beneficial for analysing 3D biomaterials including serial block face imaging. Serial block face (SBF) imaging has a high magnification of approximately 20,000x but relies on many sections of a sample being taken and the images being stitched together this may take more time. In addition, SBF imaging relies on resin embedding and can be the same methodology used in TEM. Meaning the same sample can be used for both imaging modalities streamlining and reducing costs. Resin embedding may also help with reducing shrinkage artifacts in a sample, as seen with the hydrogels under SEM using CPD. Regardless samples undergo dehydration in an ethanol series so shrinkage would still occur but on a lesser scale. Another method would be using freeze drying, this may reduce the shrinkage of samples, but samples would be imaged at surface level, to get a cross section of the structure freeze fracturing would be the most ideal especially for observation of the fibre structure but this is also dependant on the thickness of samples. If a sample is too thick freeze fracturing will not penetrate all the way through as areas that are a higher temperature will form ice crystals and distort the sample.

Furthermore, Focused-Ion beam (FIB) SEM has the capabilities of creating 3D images, but this is limited to a small area on a sample and in addition the sample is destroyed in the process. Exploring these techniques would offer more an in-depth idea of what the optimal methodology would be to use SEM imaging for hydrogel-based scaffolds. Even though the methodology used in this experiment was not optimal, it was also dependant on the type of SEM available and the software attached. In addition, quantitative and qualitative analysis was still possible with the method and instrument used and displayed some insight into cell behaviour on the hydrogel conditions used.

Fluorescence and SEM shown in this study can be used in a complementary manner. With SEM offering higher resolution that is not possible with fluorescence and fluorescence offering that overview and ability to isolate cell types in a broad manner. Yet, modifying SEM sample preparation and imaging modality may be the key to generating the high-resolution 3D images needed to evaluate 3D tissue engineering scaffolds and their interactions with cells. Yet, this type of imaging is still not as easy or cheap and requires access to facilities that can provide as such.

3.3.3 Summary

The presence of JANUS fibres resulted in the increase of neuronal projection length independently to magnetic field stimuli when compared to collagen. Other parameters observed such as morphology, cell membrane activity and cell differentiation rates were not affected. All conditions showed no toxicity towards cells indicating a level of biocompatibility. JANUS hydrogels with more research still show promising results for regenerative properties.

Fluorescence was useful to identify cell types with ease and made gross morphological observations easy for neurones and astrocytes. Being able to fluorescently isolate cell types proved useful for quantification in the case of proportionality of cell differentiation and neuronal projection length, with SEM the same analysis would be too complex, and fields of view would be smaller maybe not offering a better picture of the whole hydrogel. However, fluorescence was unable to show the ultrastructure of cells. Fluorescence also could not be used to image the hydrogels or the interactions between cells and hydrogels. SEM showed its usefulness through being able to overcome the limitations of the fluorescence showing cell – hydrogel interactions, becoming a tool to quantify filopodia, circular ruffles and pits which are ultrastructure's presented on cells when cells membranes are active. In addition, SEM was a tool to identify differing morphologies within the culture such as differences between astrocytes and neurones. Astrocytes displaying broader and many projections from the cell bodies, whilst neurones displayed a more bipolar projections morphology that were thinner with less extensions. As fluorescence is limited to what can be stained in one given sample to

prevent overlap in wavelength of fluorescent markers used, SEM may be a more effective tool to gather morphological observations of all cell types within the culture.

SEM and fluorescence worked complementary to each other where fluorescence fell short SEM was a useful tool of analysis. Yet, SEM displayed its own set of drawbacks in the imaging of hydrogels specifically, adapting the technique via researching SBF, FIB SEM, and freeze-drying methods may prove useful in getting a better idea of the true structure of the sample.

Experimental

Chapter 2

4.1 Introduction:

4.1.1 Growth factor delivery for neuro-regeneration

Lack of axonal regeneration may be more dependent on limited trophic factors than the presence of inhibitory ones. Therefore, addition of trophic factors after SCI might have a positive effect on restoring functional recovery. The Neurotrophic family appears to have the most potential. The family includes NGF, NT-3, and BDNF. All three prevent neuronal death by inhibiting or reversing apoptotic mechanisms suggesting they will protect current cells in SCI but also could protect newly transplanted stem cells. Both NGF and BDNF promote axonal regeneration making them a potential therapy in restoring synaptic function (Fan et al., 2018). BDNF within the brain is a key factor in developing dopamine neurones and a deficiency of BDNF is linked to neurodegenerative diseases suggesting it has an impact on differentiation and survival. Studies have shown transplanted NSCs engineered to overexpress BDNF in a stroke model increased angiogenesis and had a 3x higher cell survival rate at 2- and 8-week post transplantation (compared to non-engineered cells), and behavioural recovery was observed (Lee et al., 2010). Furthermore, in a SCI rat model BDNF gene delivery resulted in less TUNEL-positive apoptotic cells and increased NG2 expression– suggesting BDNF promotes oligodendrocyte lineage which potentially benefit the need for remyelination to make axonal connections functional (Nakajima et al., 2010). Other effects noticed with exogenous BDNF administration to SCI is increased axonal outgrowth (Tom et al., 2013), myelination (Fletcher et al., 2018), decreased neuronal atrophy, NSC differentiation into neurones and glial proliferation (Yin et al., 2017). In addition, BDNF is an important modulator of synaptic plasticity, a vital component is modulation connections to aid functional recovery (Rauti et al., 2020). Thus, BDNF is an interesting neurotrophic factor and may be a component to treatment of SCI (Fan et al., 2018).

However, direct administration of neurotrophic factors is difficult due to their quick degeneration and rapid loss of bioactivity. In addition, administration would have to occur more than once as there would be no controlled steady release this may be invasive to patients as injection would have to be direct into the SCI area (Chang et al., 2020). Bergman, et al., 1997 used gelfoam soaked in neurotrophic factor (either NT-3 or BDNF) along with foetal cells transplantation over SCI induced in rat spinal cords. This required invasive surgery to place the gelfoam over the injury site, with the gel providing a continuous dosage. Both BDNF and NT-3 increased axonal elongation into the injury site by three-fold compared to controls, which used gelfoam soaked in saline. However, this strategy may not be suited to intravascular delivery. Future, simple soaking methods, whilst facile, may not provide the requisite control over temporal release of neurotrophic factors required for optimal repair. There

may also be a need to target intracellular delivery, which a scaffold will also not be able to achieve. The long-term effectiveness has also not been studied as experiments only lasted 1-2 months. Furthermore, genetic engineering of NSCs to express BDNF before transplantation by virally transfecting them with viruses encapsulating DNA that codes for BDNF or increases BDNF expression may poses issues with safety. As several viral vectors are considered risky for oncogenesis. Some viral vectors including Adenovirus vectors and Herpes viral vectors are toxic and can be immunogenic (Ghosh et al., 2020). Along with higher cost and development times plus strict clinical regulation, clinical use may be a long way off.

4.1.2 New biomaterial-based delivery strategy could facilitate effective growth factor therapy

Nanotechnology may be a useful asset in solving the hurdles present. The suggestion is compounds and structures could encapsulate, preserve and control the release of effector proteins (BDNF) into the target area. One such technology is PODs® which are 5µm across cuboid crystal structures made up of polyhedrin protein and the target protein. The structure is designed to slowly degrade over weeks and months providing a steady rate of target protein to the site. The use of BDNF with PODs has been utilised in transplantation of Otic neuronal progenitor's spheroids, with a hydrogel scaffold, into the cochlea. PODs are advertised as stable at pH of 3-10 and have an expiry date of 6 months making them stable and slower at degrading making clinical use far easier to translate into. Results showed increased cell survival, neuronal differentiation into neuronal Otic lineages and directed extension of neurites (Chang et al., 2020). Thus, PODs are compatible with hydrogels and BDNF shows similar effect as noticed in SCI such as promotion of cell survival, axonal growth, and differentiation. The potential of PODs in SCI and with NSC has not yet been tested. Yet, positive results from other administrative avenues of BDNF in SCI suggest it is a worthwhile avenue to pursue.

4.1.3 Novel multicellular model of traumatic neurological injury to test PODS delivery of BDNF

Many new nanotechnology approaches are often trialled on animal models. However, these can require ethical approvals, substantial time, resources for housing and care along with licencing. Whilst animal experiments will be necessary before clinical human trials, for initial investigations a more simplistic model would allow for better observation of individual cell interactions with nano technologies as animal tissues especially the spinal cord is highly complex. Moving initial experimentation of nanotechnologies into multicellular models would minimise the highly regulated process of animal experimentation with nanotechnology that should only be done when necessary.

To evaluate how they may potentially affect a SCI a multicellular monolayer lesion model can be used as a starting point. Here, we have used differentiated NSCs grown in a monolayer, maturing into the major neural cell types: astrocytes, neurones, and oligodendrocytes. To induce an injury, scratching the monolayers with a pipette tip can be performed to mimic a transection injury in vivo. This model is still being developed by other members of the laboratory. Some similar models have been mentioned within the literature, such as Lööv, et al. (2012) that used a scalpel to score differentiated neural cells cultures 20 times at 2mm as a traumatic brain injury model. In one article to evaluate astrocyte behaviour to engulf cellular debris and whole apoptotic cells, protecting neurones from apoptosis. As with confocal observation neurones that made cell-cell contact with cell corpses, induced by injury, resulted in increased neuronal mortality. Apoptosis was induced when neuronal cell bodies made contact with these cellular corpses. Therefore, observations of astrocyte engulfing indicates that they have a positive effect on neuronal survival (Lööv et al, 2012). Lööv, et al, 2013 again used this method to investigate molecular and cellular effects after trauma where they were able to distinguish 155 proteins specific to the injured model. Indicating that from inducing an injury within such models can have a molecular effect. However, such models have not yet demonstrated neural cell interaction with nanotechnology.

4.1.4 Our aims are to:

(i) Assess how the PODs containing BDNF may influence morphology, regrowth, regeneration, any internalisation or interactions with cells in the lesion model.

(ii) Examine the feasibility of using SEM/TEM to evaluate ultrastructural cellular morphology and interactions after PODS delivery to sites of traumatic injury in neural multicellular cultures.

4.2 Results

This part of the thesis was performed in conjunction with Anthea Mutepfa, a PhD student developing the current model. The images of phase and fluorescence microscope were kindly provided by her as a means of comparison with the EM images.

4.2.1 Injury progression observation through phase microscopy

At zero hours after injury no projections can be seen within the lesion. After 24hours some growth into the lesion could be noted with cells extending projections, with more occurring after 72 hours. In addition, lesion size appears to get smaller as time goes on, with lesions ranging at approximately

325µm for zero hour to approximately 225µm at 72 hours. Cell projections appear broader and over time cell bodies also migrate into the region indicating cells are moving to infiltrate the lesion site in all conditions, figure 4.1.

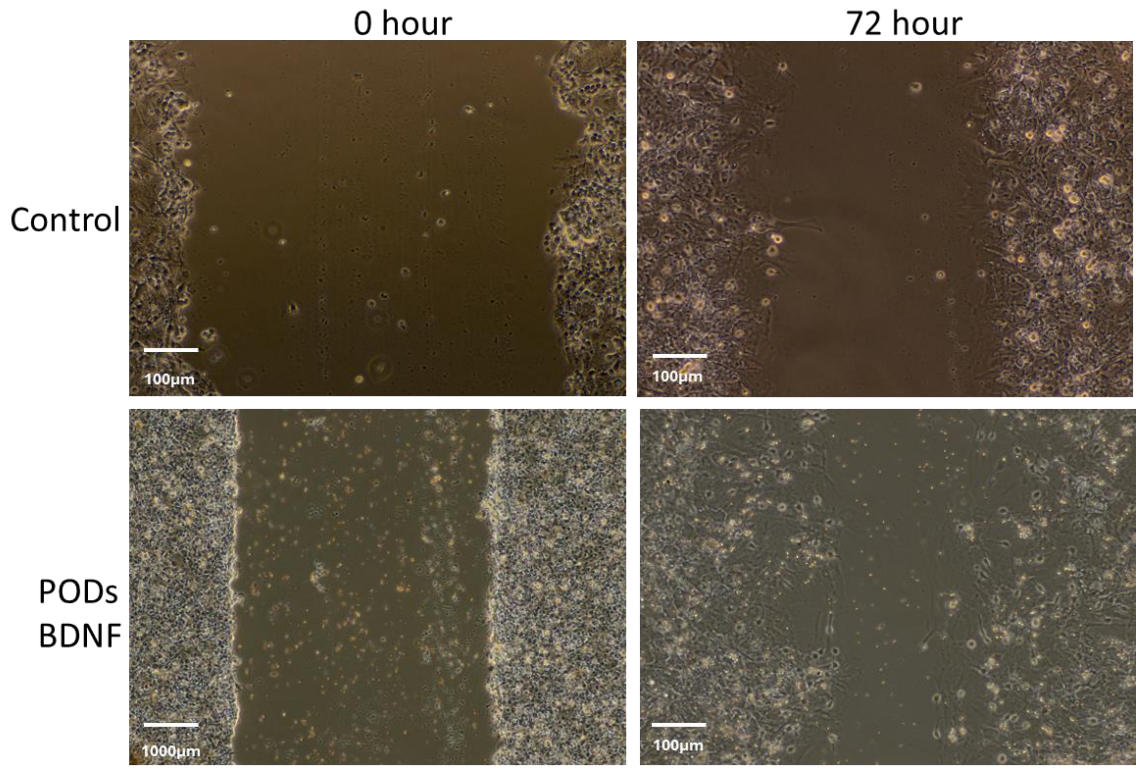

Figure 4.1. Phase microscope images showing the overall differences between zero hours and 72 hours in control and PODs BDNFconditions.

4.2.2 Comparisons between Phase, Fluorescence and SEM when observing injury conditions.

Phase indicates an overall view of the lesion site with cells showing some projection into the lesion, with cellular debris within the lesion site. Bright spots in the overview which are cuboidal in structure can be observed, likely to be the PODs added to the site. Some PODs appear in the lesion however the majority seem clumped around the cells at the lesion edge, displayed in fig 4.1.

Fluorescence offers a more in-depth view of the projections at the lesion site with GFAP presenting cells, astrocytes (green in fig 4.2.B), making up the majority of cells producing broad fibrous projections into the lesion. Tuj-1 presenting cells, neurones (red in fig 4.2.B), are at the lesion site but in lesser amounts. Only a few seem to have projections into the lesion site and the ones that do

appear to be supported by the GFAP cellular projections underneath. The TUJ-1 presenting cells projections are much smaller than that of the GFAP cells and are more uniform in shape and size rather than the splayed-out shape of the GFAP.

The low magnification, SEM overview does not provide good detail, but the lesion can be observed. Similar to phase some debris within the lesion can also be identified. At higher magnification, detailed observations of the morphological characteristics of the projections can be made. For example, in the injury site we could identify neurite projection growth cones (fig 4.2 D). Broad, likely astrocyte projections can be seen, occasionally supporting thinner, neurite type projections (Fig 4.2 E). Neurite like projections infiltrating the lesion unsupported by other cells were also observed (Fig 4.2 F). SEM imaging experienced large amounts of charging within the lesion (fig 4.2 C, D, E and F) making some analysis difficult but the projections from the cells around the lesion into the lesion site still remained clear enough to get some morphological information.

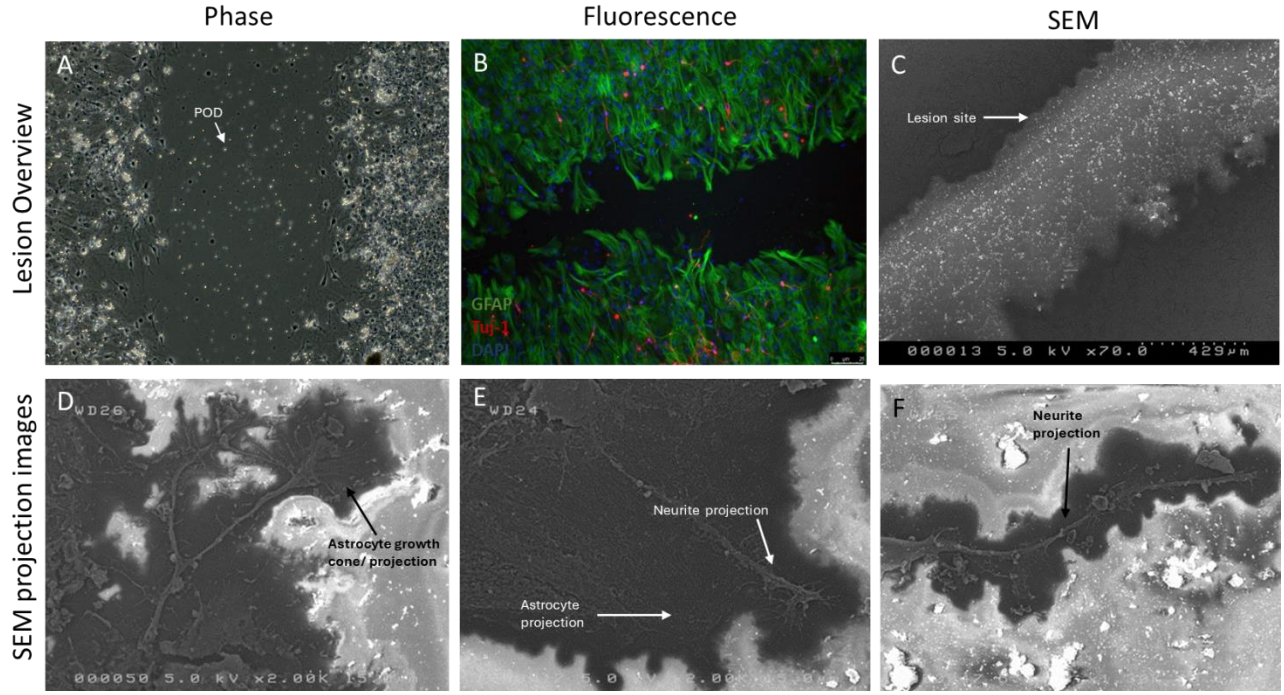

Figure 4.2. Overview of lesion sites under Phase, fluorescence, and SEM along with higher mag images of projections under SEM. Image A is a phase image of a PODs BDNF 24 hour. *Image B is a fluorescence image of PODs BDNF 24 hour using GFAP (green) Tuj-1 (red) and DAPI (blue). Image C is a low magnification image using SEM of a lesion in PODs BDNF 24 hour. images D, E and F are higher magnification SEM images of projections observed at the lesion edge.*

In addition, both Phase and SEM showed microglia in the lesion sites of injury models. Phase microglia appeared to have a reactive sate, with many projections extending from the cell bodies

(Reddaway., et al, 2023) shown in Fig 4.3.A. Under SEM similar ramified projections could be imaged and some images were generated (fig 4.3.B). However, these could only be observed infrequently due to the high amount of charging in the lesion area.

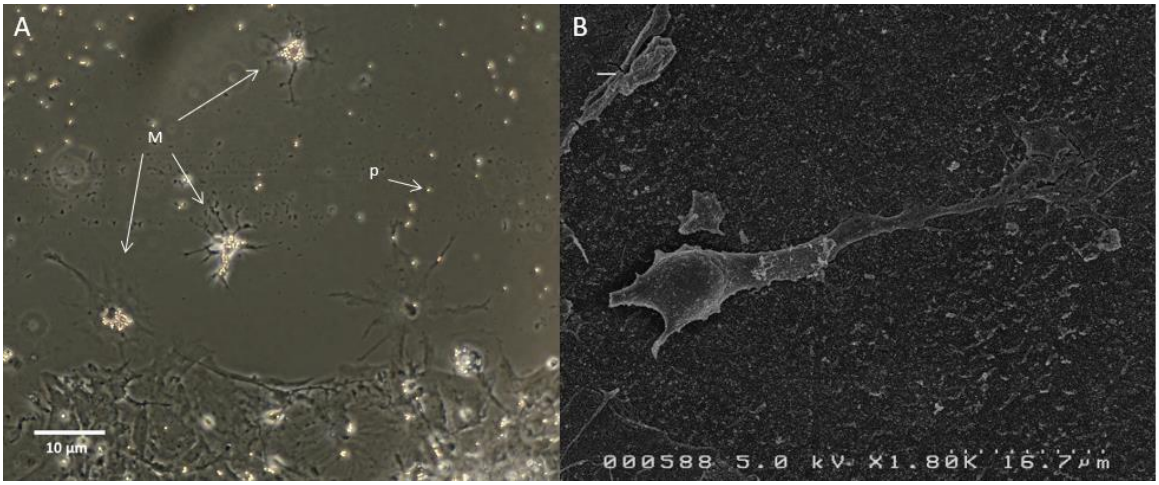

Figure 4.3 A-B. displays on the left an SEM image of a potential microglia cell withing the lesion site*. Image A is a phase microscopy image of the lesion site with microglia (M) like cells witnessed within the lesion itself. The bright cuboidal like structures within the phase images are PODs with some being witnessed at the cell bodies of the microglia like cells in the lesion site. Image B is an SEM image from the lesion site of a microglia like cell.*

Fluorescence Ki67 expression used to observe proliferation displayed a higher expression rate, when looking at the images provided, in PODs BDNF 72 hour injury models than that of Control 72hr, fig 15. Using SEM, cells expressing morphological traits of replication were witnessed via observation in PODs BDNF 72 hour and not in any other conditions, (fig 4.4 E, F and G), some of which can be visualised replicating near the lesion site (fig4.4.G) or in close proximity to PODs, fig 3.4.A. This is purely observational but is grounds for further investigation.

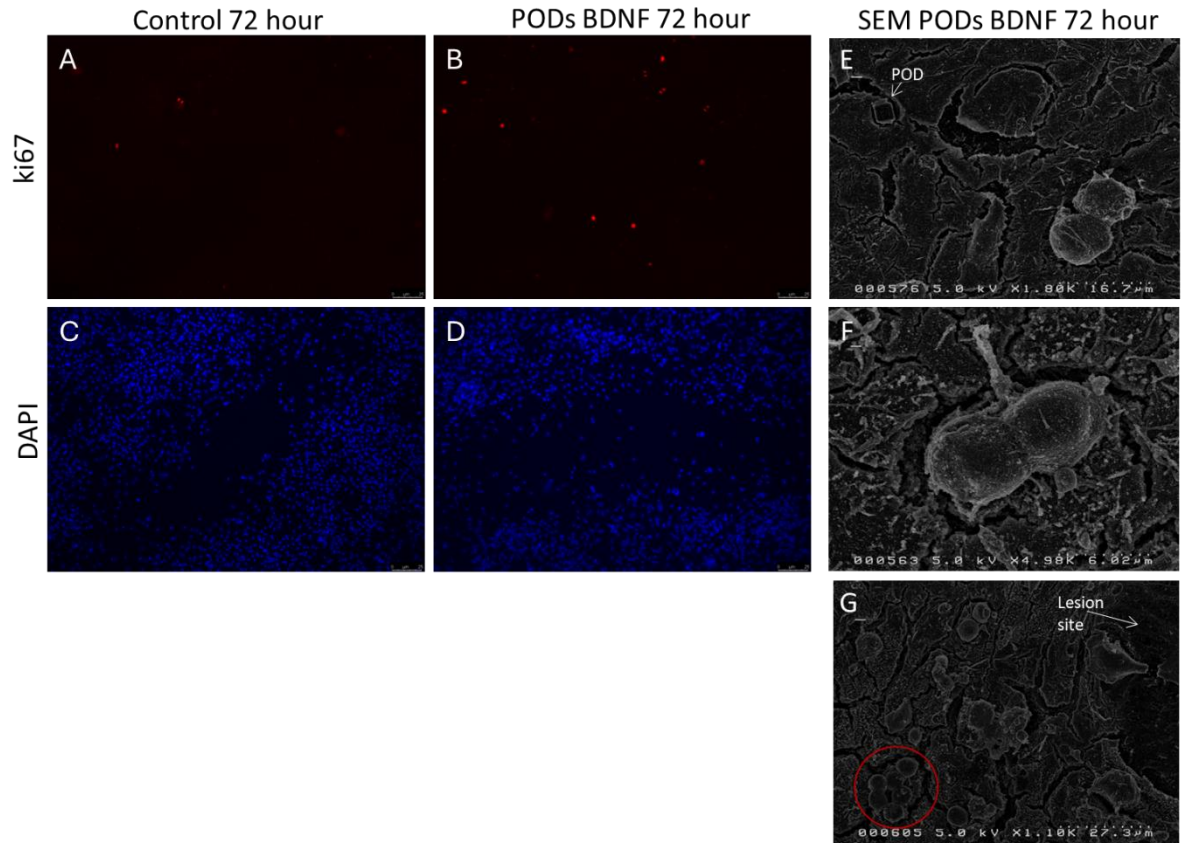

Figure 4.4 A-G. Fluorescence images of Both Control 72 hour and PODS BDNF 72 hour injury models expressing Ki67 (A and B) and DAPI (C and D)*. Image A indicates Ki67 expression in a control 72-hour condition. Image B shows ki67 expression in PODs BDNF 72-hour condition. Image C is the DAPI expression in the same field as image A. whilst image D shows the same field as image B but with DAPI expression. Image E, F and G are SEM images taken in PODs BDNF (PB) 72hr conditions. image E is an image of proliferating cells in proximity to a POD. Image F is a cell undergoing proliferation at a higher magnification. Image G is that of a group of proliferating cells near the lesion edge.*

Ultrastructural characteristics of cellular activity, linked to internalisation can be witnessed on cells close to the lesion. Such structures include circular ruffles and filopodia. This was only observed in SEM imaging as displayed in figure 4.5.

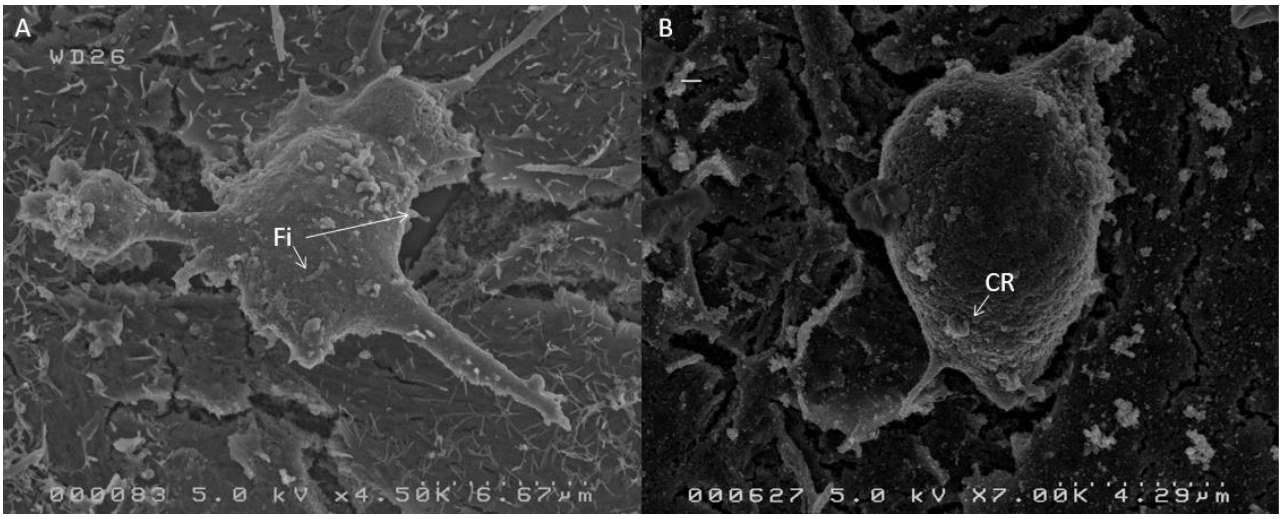

Figure 4.5 A-B. SEM images of cells from the injury model where cell membrane activity was imaged*. Membrane structures of filopodia (Fi) observed in image A. Image B shows membrane structures of circular ruffles (CR).*

4.2.3 The PODS nanocrystal delivery system could be observed with SEM

SEM did provide its own unique observations and details not witnessed with fluorescence or phase. PODs were identified in SEM imaging displaying the cuboidal structure approximately 2µm in diameter. Cell-POD interactions were observed in all conditions containing PODs either empty or with BDNF supporting the phase images that display some idea of interactions. For example, cellular projections towards PODs were noted and, in some cases, these showed the beginnings of wrapping round the PODs (fig 4.6).

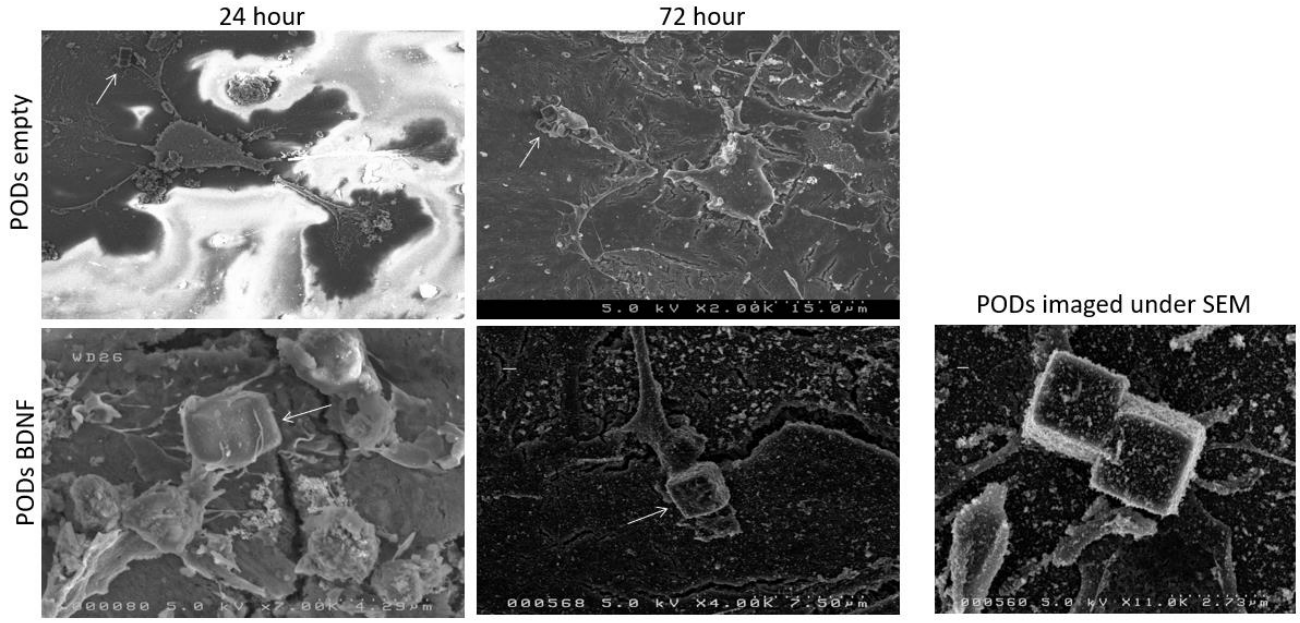

Figure 4.6. All conditions containing PODs with SEM images indicating cell-POD interactions*. Arrows indicate site of POD-cell interactions. Images depict cell projections extending and contacting PODs. Plus, SEM an image of two PODs at higher magnification as a structural reference.*

4.2.4 TEM production of high-resolution ultrastructural images on multicellular injury model

As one of the first trials of imaging multicellular injury models under EM, TEM images were gathered of the Control 24Hr condition with ultrastructural structures being observed from mitochondria to microtubules. No other TEM images were acquired for other conditions, but preliminary observation is promising. Whole sections of cells were observed, and ultrastructural structures were visualised such as microtubules (Fig 4.7 A), endoplasmic reticulum (Fig 4.7 B), nucleus (Fig 4.7 C), mitochondria (Fig 4.7 D), and their structural components.

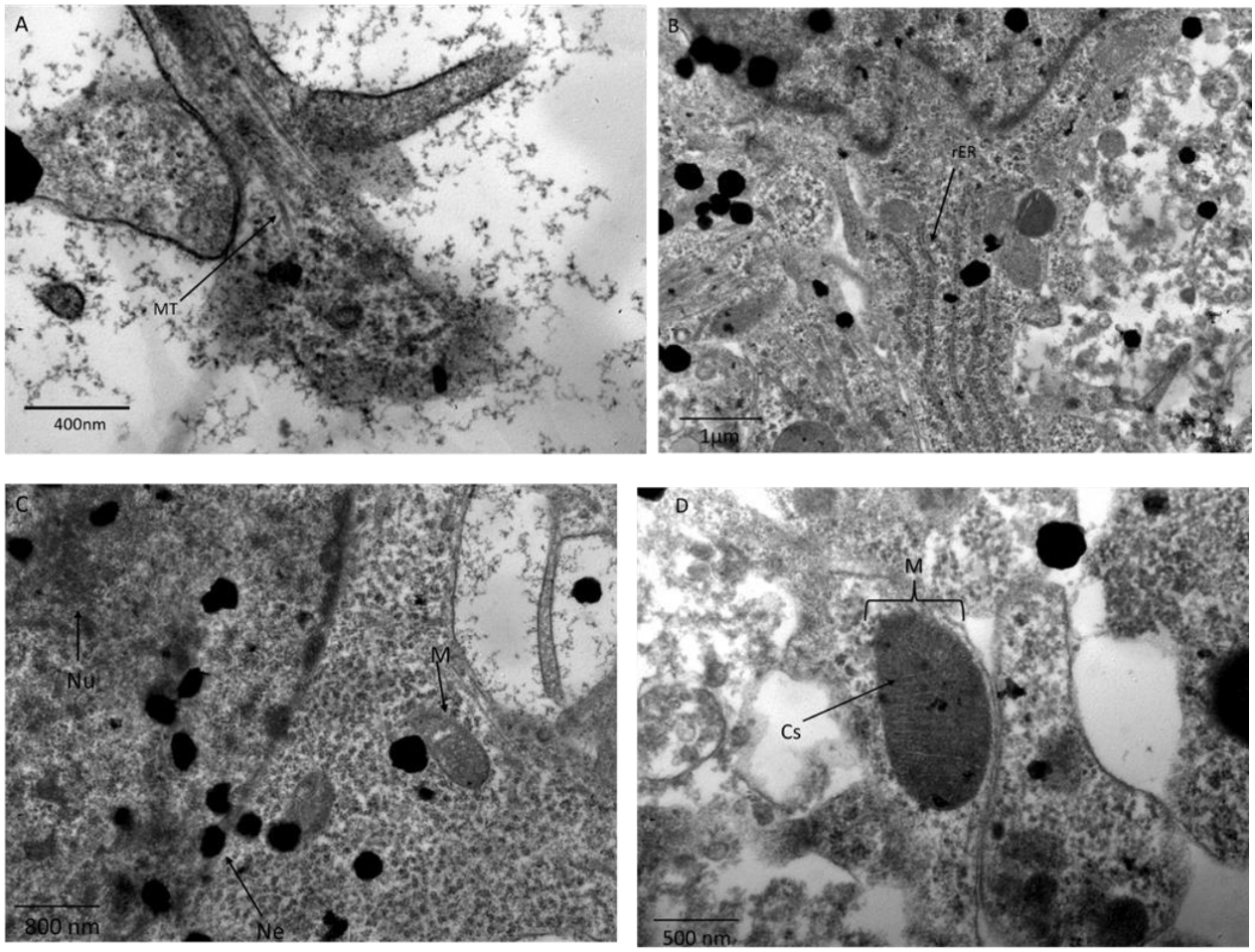

Figure 4.7 A-D. Images A, B, C, and D are of condition Control 24hr under TEM. *image A, appears to be a projection into the lesion with microtubules (MT) visualised. Image B displays the ultrastructure of a cell body specifically showing the rough endoplasmic reticulum (rER) within the cell. Image C shows the cell body of a cell indicating structures of the nucleus such as nuclear envelope (Ne) and nucleolus (Nu). In addition, the structure of a mitochondria (M). Image D is a higher magnification image of a mitochondria (M) where the structures of cisternae (Cs) can be visualised.*

As seen in Figure 4.8 PODs are fully internalised into the cells under the condition of PODs empty 72 hours. Figure 4.8 C shows the POD-Cell interface as the POD is fully integrated into the cytoplasm with no cellular membrane surrounding it. From all images in 4.8 no assumptions can be made about toxicity, but the cells imaged containing PODs did not show any obvious signs of apoptosis or necrosis.

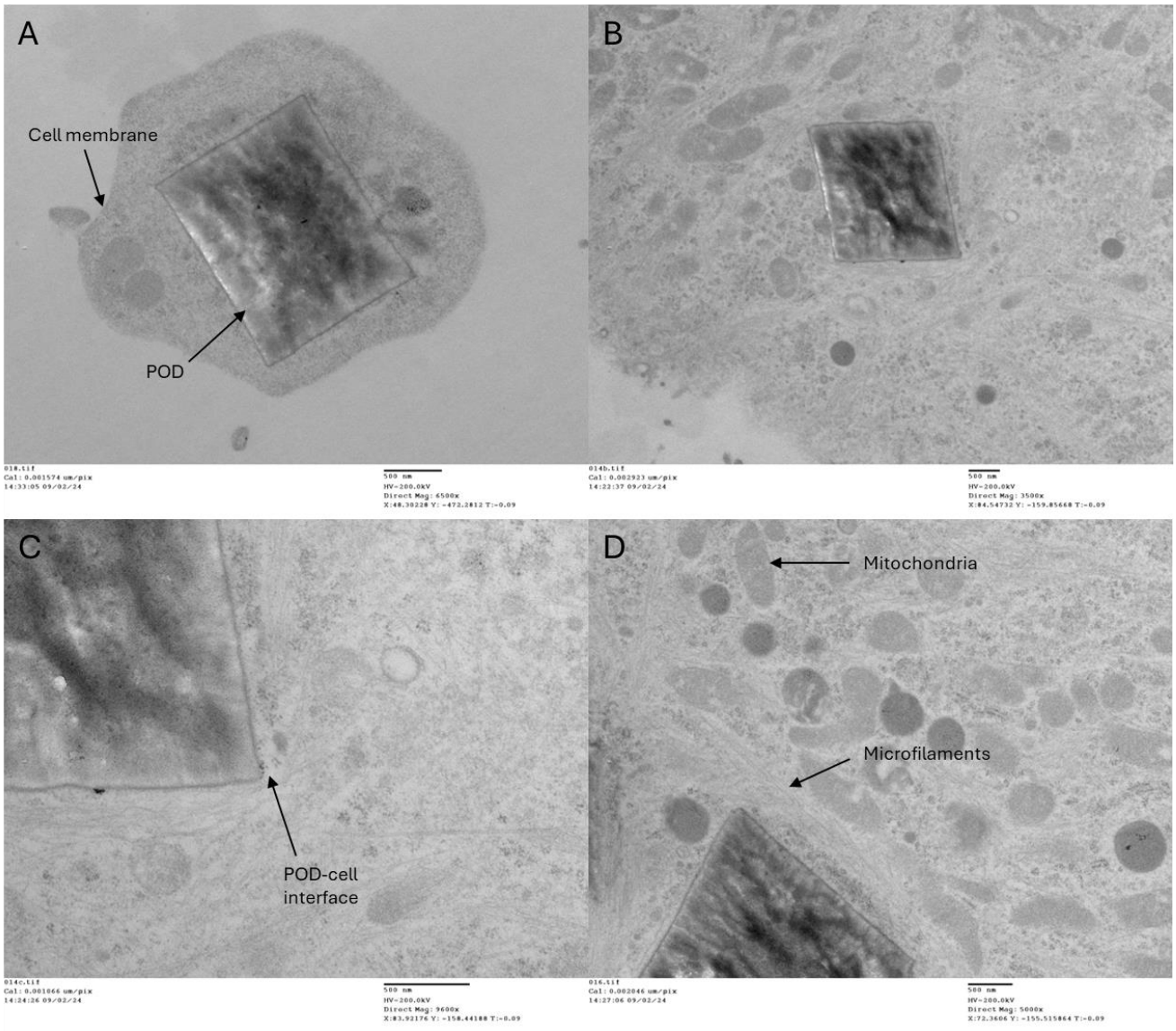

Figure 4.8: TEM images of condition PODs empty 72 hours displaying PODs inside of cells. *Images A and B show a lower magnification. Image A indicates the POD structure and the cell membrane. Whilst images C and D show a higher magnification. Image C indicates the POD-cell interface. Whist image D also shows the same interface it also indicates some of the other ultrastructure's visible like mitochondria and microfilaments.*

4.3 Discussion

4.3.1 Overview of injury model progression though using Phase, Fluorescence, and EM microscopy – an argument for multi-imaging methods with electron microscopy providing a key corner stone

We have shown that injury progression results in broad projections made up of GFAP presenting cells entering the lesion along with smaller amounts of Tuj-1 presenting cells following suit. Lesion size was smaller at 72 hour than at 0 hour in controls suggesting the lesion does undergo a level of repair regardless of interventions. In future experiments measuring the lesion size in all conditions and time

points maybe a good experiment. As it may indicate if different conditions accelerate lesion repair compared to controls. For example, if JANUS fibres show a smaller lesion size at 72 hours than controls, it could be an indicator that PODs BDNF does have a positive effect on regeneration. This would be a good avenue to explore in future research.

Microglia-like cells also could be found within the lesion itself as injury progressed, as microglia do not stem from NSCs they potentially survived cell passaging and grew in culture. Fluorescence of the cultures before lesion with markets for microglia may be able to determine the prevalence and perhaps if this is altered after an induced lesion. In addition, it is clear to see from imaging that glial cells such as astrocytes and neurones are not a 1:1 ratio seen in vivo. This may be a limitation of the model being a translational one to in vivo trials, altering the cell culture method to try and create this 1:1 ratio may be an avenue for future models to see if this effects results. However, for preliminary studies the model has been effective at producing observations of a lesion model and POD-cell interactions and ultrastructural imaging. The simplicity of the model has its advantages especially in ultrastructural imaging and would be beneficial for other electron microscopy techniques such as CLEM, which is discussed in more detail later, but a single cell could be isolated and imaged far easier than in a 3D complex model.

Cell POD interactions were visible under SEM with PODs BDNF 72Hr conditions resulting in increasing cell proliferation within the sample. Furthermore, cell membrane activity was observed under SEM along with other internal ultrastructure such as microtubules, endoplasmic reticulum, mitochondria, and other structures using TEM. TEM also allowed us to observe PODs that had been internalised into cells. This may potentially affect the PODs ability to slowly distribute BDNF across the whole injury and might potentially have issues with toxicity. It may suggest that PODs biocompatibility may not translate into an injury model as the internalisation by cells, particularly by microglia witnessed in phase indicates an immune response to PODs. No obvious signs of apoptosis or necrosis were witnessed in cells that had internalised PODs. Yet, this is a small collection of cells in one condition of empty PODs after 72 hours so more analysis will be needed. In addition, this does not rule out any metabolic issues that might be derived from POD internalisation that may benefit from proteomic analysis. As this is the first time this has been concluded more research into the potential effect this had on POD efficacy and whether they would promote functional recovery in vivo models has to be determined.

The model within this experiment showed astrocytes (GFAP presenting cells) were projecting into the lesion. The movement of astrocytes into an injury site can be seen in vivo usually in the formation of a glial scar through the process of astrogliosis (Alizadeh et al., 2019). Within CNS injury astrocytes

become reactive and in mild cases undergo cellular hypertrophy of the cell body and processes. In severe astrogliosis astrocytes form elongated shapes, rapidly proliferate and from compact borders of the glial scar at injury site (Sofroniew, 2015). Within the lesion model however, astrocytes were the dominant cell type at the lesion border, but there was a lack of tight borders present. Plus, Ki67 staining did not display rapid proliferation at the lesion edge. The astrocytes within the model had projections directing into the lesion and were also not obscuring neuronal projections suggesting a lack of border. Whether the cells are hypertrophic may need future analysis with a control with no lesion so morphology can be compared as a preliminary study into the effects on astrocytes and if they mimic some vivo observations. The addition of neuronal projections is not usually seen in vivo. Yet, immature astrocytes derived from human glial restricted progenitors were implanted into a mouse SCI site offered support for axonal regeneration in vivo yet this regeneration was limited and did not result in completely abridged connections (Haas and Fischer, 2013). It may be possible that the infiltrating astrocytes are creating a more positive environment for neuronal projections as they may be mimicking more the findings of Haas and Fischer. Yet the amount of neuronal projection is still minimal with astrocytes being dominant. Further, neuronal projections also did not bridge over the lesion site.

Phase and SEM imaging have identified cells with microglia like morphology within the injury site itself. In vivo, microglia act as immune response cells through the activation from DAMPs released from injury trauma playing a key role in neuroinflammation also migrating into lesion sites (Tran, Warren, and Silver, 2018). This suggests the injury model shows similarities with vivo observations. The observations suggest the injury model may be suitable for primary studies into microglia responses in SCI. In addition, our current imaging analysis suggest the microglia internalise or interact with the PODs. Why they are interacting and if this suggests the PODs are causing an immune response should be investigated. Other studies have looked at the microglia interactions with biomaterials. With biomaterials potentially having effects on neuroinflammation such as recorded by: Cornelison et al., 2022, Tsui et al., 2018 and Sharaf et al., 2020. This model may be a simplistic model for observations and experimentation in future research.

SEM showed promising results of cell and POD interactions with no cell death observations made from these interactions suggesting they have no toxicity effects on NSC cultures. Furthermore, cells interacting with PODs could maybe indicate potential internalization or BDNF intake. Yet, seen as POD interaction occurs with both empty and BDNF loaded PODs maybe there is another factor on the PODs causing this effect. Importantly though this effect or interaction is nontoxic which may be a positive for future applications of PODs mediated growth factor delivery. PODs were visible under SEM in the multicellular cultures in lesion models, indicating they are visible in SEM imaging

techniques and can withstand sample preparation. This will be useful for future exploration of PODs interactions with neural cells.

From visual observation, all conditions showed projections into the lesion. PODs at these concentrations seemed to have no influence on projection outgrowth. Increasing the concentration of PODs with BDNF to varying levels would help determine if there is a desirable concentration to induce effects in projection outgrowth. Increasing the concentration of PODs would also help with future EM work making them easier to find in SEM and TEM. Further analysis into length and lesion width would be desirable. However, due to the charging within the lesions in this experiment this would need to be achieved with an optimised SEM technique or via light microscopy.

Ultrastructural cell morphology is visible with SEM imaging, fig 16. As these structures are linked to internalisation and cell activity, such as filopodia and circular ruffles, future investigations could examine whether PODs do undergo internalisation into the cell. In addition, if PODs BDNF have any effects on cell membrane activation and if this is altered by cell location to the lesion. TEM alongside this may display if these cell surface structures linked to internalisation and activation is linked to the internalisation of PODs. Further, this may then be correlated with any internal cellular changes.

Fluorescence microscopy indicated that increase presentation of ki67 within the injury model when exposed to PODs containing BDNF than the control injury models, with the highest values noted at 72 hours. Using SEM, cell proliferation morphology was only observed in 72Hr PODs BDNF and not witnessed in any other conditions. Potentially this supports the fluorescence findings and indicated that over the longer time period (compared to 24 hours) there is a positive impact on replication close to the lesion in BDNF PODs conditions compared to controls. Further quantitative analysis would need to perform under SEM to corroborate this point. The cell type of the cells replicating could not be determined. However, Nakajima et al, 2009 reported that BDNF induced proliferation of oligodendrocytes. In addition, in a paper by Chen et al, 2013 they stated that BDNF can potentially promote proliferation in NSCs via the Tropomyosin receptor kinase B (TrkB) receptor triggering the Wnt/β-catenin signalling pathway. Here, the blocking of the Wnt pathway with 1WR1 blocker inhibited the proliferation and differentiation under BDNF influence (Chen et al., 2013). However, other studies have indicated the increased proliferation of NG2+ OPCs can have a detrimental effect on regeneration so this may not have a positive outcome for regeneration (O'Shea, Burda and Sofroniew, 2017). Whether this is the way the PODs BDNF are affecting the proliferation remains to be examined. However, this indicated that the PODs BDNF may have some regenerative effects on multicellular cultures.

SEM can be used to image a lesion model of multicellular monolayer along with being used to identify the drug delivery system, PODs, within the culture. One issue that arose was the charging in the lesions on the majority of samples that prevented imaging within the lesion. Only two samples did not experience charging and images of potential microglia were taken. DAG was used to try help mitigate this effect however it was not enough. In future using carbon coating may be a good alternative making all areas conductive, but this also reduces the resolution available so would depend on what resolution would be required.

Ultrastructural imaging via TEM is possible but due to time constraints and need for specialized techniques it was difficult to achieve anything quantifiable between conditions within this thesis. TEM imaging did display ultra structures within the cells that were identifiable such as mitochondria, endoplasmic reticulum, and micro fibres. This suggests TEM can produce imaging of multicellular injury models and with more time and skill can produce something for comparable analysis. In addition, TEM images from this thesis have shown the possibility of observing the cytoskeleton within cells. Within stem cell and tissue engineering the rearrangement of the cytoskeleton is an important aspect in determining cell lineage, gene expression and cell adhesion. Being able to image the cytoskeleton and observe any effects that a biomaterial may have would help research in determining the potential negative or positive effects biomaterials may have on cells and pushing cells towards a specific differentiation path (Ambriz, Lanerolle and Ambrosio, 2018). Therefore, TEM can have a potential use in cytoskeleton research in tissue engineering. Furthermore, imaging via SEM was also achievable but requires optimization due to the charging experienced in the samples. Yet, images and qualitative analysis to some degree is achievable.

TEM does fall short at its lack of ability to generate a highly detailed overview of an area without grid bars obstructing images. One way to combat this is via using another EM technique such as array tomography that uses serial block face imaging techniques (SBF). Optimization using SBF imaging would offer a wider overview of the lesion region. In addition, can offer the same ultrastructural imaging needed like with TEM but with no obstructions from grid bars. Yet the imaging is not as high resolution as TEM but still a high magnification to visualise the ultrastructural organelles within a cell. In addition, POD structures have been proven to be visible in SEM and TEM imaging. SBF would allow us to have an overview of the lesion but also how that might correlate with POD internalisation by cells.

In addition, sectioning experience would reduce damaged sample for more TEM sections and would produce speedier results that were lacking in this thesis, to generate images from other conditions. Therefore, more experience and exploration into other EM techniques would lead into better

enhancement of analysing the ultrastructure of multicellular injury models. Initial imaging shows that EM is promising as a method and can have research benefits in observations of the multicellular injury model and in cellular interactions with biomaterials in tissue engineering.

In summary, although the model does not match the ratio of glial cells: neurones as in vivo models it was still a useful tool and produced novel preliminary results that can be further investigated and potentially translated into in vivo. Both EM, phase and fluorescence worked complementary to each other indicating how a correlative response of multiple microscopy techniques can create the best outcome and observations in research. The EM techniques did provide important information however improvement in the techniques would be a benefit. Attempting SBF SEM imaging may allow for a broader 3D imaging of the lesion site. Thus, may be useful in determining the internalisation of PODs. In addition, immunogold labelling may also be a beneficial technique in identifying a cell type within TEM potentially in the analysis of the microglia in internalisation of PODs or neurons and their filaments. Fluorescence to identify which cells are undergoing proliferation that were identified within fluorescence and SEM could help determine if the proliferation is advantageous or a hinderance in the regeneration and what cells PODs BDNF are affecting and potentially further research into why.

Combined Discussion

5.1 Key findings

Experiment 1:

- JANUS fibres increased neuronal projection length significantly when compared to collagen, independently of magnetic stimulus, indicating the presence of the fibre itself may have affected neuronal outgrowth positively via another means not accounted for.
- Other parameters, cell differentiation proportions and cell membrane activity showed no significant difference between groups.
- Cells did not display toxicity towards hydrogels, indicating a level of biocompatibility and potential for vivo use.
- All hydrogels could be imaged using SEM along with the cells, producing high resolution images. Yet protocols will have to be optimised to reduce shrinkage of the sample.
- SEM can used as a quantitative and qualitative research tool, being more effective as quantifying ultrastructure's whilst fluorescence was opted for quantifying cell types.
- SEM was valuable in quantifying and observing ultrastructure's and hydrogels. Whilst fluorescence was useful in the quantification of cell types. Both provided information of morphological observations.

Experiment 2:

- Gross morphological observations were made on the progression of the lesion site using EM, with astrocytes producing broad projections, some neurones following suit, and microglia infiltrating the lesion itself. Both SEM and fluorescence imaging enforced findings from one another.
- The presence of PODs BDNF increased proliferation within the injury model. As to the cell type effected, this remains to be determined.
- SEM imaging was able to capture POD-cell interactions. This was alongside cell membrane ultrastructure, including astrocyte and neuronal like cell projections into the lesion site.
- Observations of cell replication in the PODs BDNF 72Hr condition were made but not in any other condition.
- SEM fell short due to the charging experienced within the lesion itself and is something to investigate reducing going forward.
- TEM was able to produce images of the multicellular injury model with ultrastructure's being clearly visualised. In addition, POD internalisation in PODs empty 72 hour condition was observed. However, more skill in sectioning and adaptation of the method is required to develop results of all conditions.

5.2 Future EM avenues for research

Cryo-SEM samples are only required to be fixed before imaging (mostly for safety reasons samples can also go in live or unfixed). After this samples are plunged into liquid ethane or nitrogen, sublimated, and imaged still in a frozen state. This works at an advantage by reducing the potential damage or artifacts that can be produced from staining and shrinkage that occurs with dehydration critical point drying and sample techniques in traditional SEM. One drawback to cryo-SEM is that water will remain within the sample obscuring any structures under it. Observations of the filaments within the hydrogel and cells interactions may be obscured or more difficult to interpret. With that any cell surface structures or internal ultrastructure's will be difficult to discern. In addition, samples cannot be reimaged once removed from the SEM. Removing the water within the sample would make for better observation but will require less shrinkage than what occurs under critical point drying. One such method would be freeze drying and fracturing. With the slow sublimation of water, shrinkage may be significantly reduced than with critical point drying. For observations at the surface of the gel looking at cell/hydrogel interactions this would be ideal. However, freeze drying has a penetration depth of approximately a millimetre. To make observations with fracturing inside the gel the gel size would have to be reduced or other methods would have to be explored.

One such method is serial block face imaging. This follows a similar method to TEM with fixation, staining, dehydration with a series of ethanol, resin embedding and sectioning. However, imaging can be done via SEM using backscattered electrons. The same samples can be used if desired for TEM potentially saving on cost and resources. The SEM imaging can provide more information without the obscuring of grid bars. The sectioning can also be done in series with the ability to generate a 3D image using volume EM techniques. The imaging can be timely and costly, but intracellular structures can be observed. One drawback is tomography of the cell surface, and hydrogels is not possible but freeze drying would be an ideal method to attempt for this. This method may also be ideal for researching the possibility of internalisation of PODs along with observing ultracellular structures. TEM produces a higher resolution, so for imaging of neurofilaments or actin TEM would be the best option. Preparing the samples for block face imaging would provide the opportunity for both forms of imaging. In addition, using a longer osmication and *en bloc* staining with uranyl acetate before embedding would mitigate the need for a post stain, therefore reducing the presence of artefacts from lead precipitation on the grid (Karin Muller, 2019).

Optimization of EM techniques to the sample are vital for producing the best images possible. Requiring a deep understanding of the sample but also what you wish to observe within it. For samples that have not been imaged before this can be a research area within itself. Electron microscopy techniques vary between groups and sample types. In addition, the techniques available

can be limited to the instrumentation you have readily available. Collaboration across groups and institutions could bridge this gap allowing people to explore more techniques within EM to produce the most effective images.

Being able to use florescence and EM within imaging is important as they can overcome each other's limitations. Fluorescence offers targeting of proteins or cell types. Whilst EM offers the high resolution to observe targeted structures. Correlative light electron microscopy (CLEM) combines both modalities to fluorescently tag specific proteins to image with Light microscopy techniques then with the same sample visualise the subcellular structure using EM. These images can be superimposed and used to target the region and observe its structure (Perkovic et al., 2014). Traditionally TEM is used with samples being sectioned and placed on grids before light microscopy or EM. However, other techniques such as SBF are possible and offer a more 3D approach. Yet, the fluorescence usually requires infection or genetic engineering as is the case with Russell et al., 2017 where mycobacterium tuberculosis expressing EGFP (green fluorescence protein) was used. In addition, studies tend to use only one fluorescence at a time therefore multi targeted imaging may be limited or may be interesting to explore for future research (Russell et al., 2017). Within the drug delivery model, targeting proliferation tags with TEM imaging may offer some insights as to the structure of the cells proliferating and whether there is a difference to proliferation within the PODs BDNF to the controls. In addition, potentially finding a target on PODs or introducing them with a fluorescence tag with SBF or TEM imaging may offer information missing on how cells interact with PODs or if they become internalised and potentially what that might be doing to the cellular structure and function.

Volume EM (Vem) is a new technique whereby samples are sectioned to generate a series of which either TEM or SEM can be used to image. The series of images can then be integrated using software to generate a 3D rendering of the volume of sample. This has been conducted at either the cellular or tissue level. Originally, the technique was derived to understand the architecture and connections within the nervous system but has since been used in other tissues such as sensory organs, infected tissue and even plants. One technique involves SBF-SEM, using backscattered electrons to generate an image with TEM like qualities. Other imaging techniques could be used in parallel with X-ray microscopy, which can add smaller scale information, and Fluorescence Microscopy, that can add localised targeted information. Both can add information lacking in EM to build a full picture or the structure and its meanings within research. One drawback would be the huge data collected and the storage and integration that would be required (Collinson et al., 2023). Vem needs specialisation and multidiscipline approaches to reach the final results. This offers a potential though for varying groups and disciplines to work together and produce 3D rendering of structures not yet produced. VCLEM is

a technique that has been adapted for using Vem. Fluorescence can help find specific areas to target with ROI but also images from fluorescence and EM can be superimposed to generate a structure and function results (Paddie et al., 2022). This is a potential for tissue engineering as Vem and VCLEM are newer techniques with little research using such imaging techniques has been done in tissue engineering and as both techniques can be used in larger tissue imaging or down to cell-cell interactions. Hydrogel structures and cell-biomaterial interactions have potential in results. Using Vem with other imaging modalities could produce new and exciting data within tissue engineering and is something investigate in future research.

5.3 Conclusion

Biomaterials have displayed alterations to cell behaviour within these experiments. With JANUS fibres increasing projection length and PODs increasing proliferation within a lesion model. The mechanisms of both findings are still uncertain. Future studies into the mechanisms of the findings may shed some light into how biomaterials may affect cellular functions. EM would be useful with enhancements to help in such research in observing the internalised ultrastructure's on cells. Further research into other EM techniques for both biomaterials used may provide more effective imaging with reduction in artifacts and better analysis. Focusing in on serial block face, freeze drying and cryo SEM. In addition, combining EM and fluorescence is an under-explored yet potentially impactful avenue for tissue engineering research. Using a mutilating technique such as CLEM on biomaterials may offer a deeper understanding combining the ability to target proteins and cells with observing their ultrastructure. Yet, as shown in this experiment the type of EM for each type of biomaterial must be optimised and trailed. This optimisation and development of a technique would be advantageous to the world of imaging in tissue engineering for SCI injury, with EM and Fluorescence being both equally important.

Acknowledgments

I would like to thank Dr Christopher Adams, Prof Dave Furness, Simon Holborn, and Anthea Mutepfa for their support and input within producing this thesis. Furthermore, an acknowledgement to Anthea Mutepfa for.

Dr Andrew and Dr Ferguson (University of Florida) designed, fabricated and characterised the magnetic fibres used in Experimental Chapter 1 and kindly supplied them free of charge. They were also involved in experimental design discussions. I designed the specific experiments needed to address the aims. I subsequently carried out all the cellular experimental work described.

For Chapter 2, Anthea Mutepfa (Keele University) is establishing a model of traumatic injury using the neural stem cell model outlined. She established these cultures, and I subsequently took over to conduct the experiments for my thesis. I informed the design of the experiments, then conducted all the technical aspects from cell maintenance, fixation and electron microscopy processing. In addition, Anthea provided the fluorescence images for experiment two that helped with analysis and supported EM findings.

References

Ahuja, Christopher S., et al. "Traumatic Spinal Cord Injury." *Nature Reviews Disease Primers*, vol. 3, no. 1, 27 Apr. 2017, www.nature.com/articles/nrdp201718, https://doi.org/10.1038/nrdp.2017.18.

Alaa Emad Eldeeb, et al. "Biomaterials for Tissue Engineering Applications and Current Updates in the Field: A Comprehensive Review." *AAPS PharmSciTech*, vol. 23, no. 7, 26 Sept. 2022, www.ncbi.nlm.nih.gov/pmc/articles/PMC9512992/, https://doi.org/10.1208/s12249-022-02419-1.

Alizadeh, Arsalan, et al. "Traumatic Spinal Cord Injury: An Overview of Pathophysiology, Models and Acute Injury Mechanisms." *Frontiers in Neurology*, vol. 10, no. 282, 22 Mar. 2019, www.ncbi.nlm.nih.gov/pmc/articles/PMC6439316/, https://doi.org/10.3389/fneur.2019.00282.

Amar, Arun Paul, and Michael L. Levy. "Pathogenesis and Pharmacological Strategies for Mitigating Secondary Damage in Acute Spinal Cord Injury." *Neurosurgery*, vol. 44, no. 5, May 1999, pp. 1027–1039, https://doi.org/10.1097/00006123-199905000-00052.

Ambriz, X., et al. "The Mechanobiology of the Actin Cytoskeleton in Stem Cells during Differentiation and Interaction with Biomaterials." *Stem Cells International*, vol. 2018, no. PMC6196919, 8 Oct. 2018, pp. 1–11, https://doi.org/10.1155/2018/2891957.

Anderson, Mark A, et al. "Astrocyte Scar Formation Aids Central Nervous System Axon Regeneration." *Nature*, vol. 532, no. 7598, 2016, pp. 195–200, www.ncbi.nlm.nih.gov/pubmed/27027288, https://doi.org/10.1038/nature17623.

Anjum, Anam, et al. “Spinal Cord Injury: Pathophysiology, Multimolecular Interactions, and Underlying Recovery Mechanisms.” *International Journal of Molecular Sciences*, vol. 21, no. 20, 13 Oct. 2020, p. 7533, www.ncbi.nlm.nih.gov/pmc/articles/PMC7589539/, https://doi.org/10.3390/ijms21207533.

Ankeny, Daniel P., et al. “Spinal Cord Injury Triggers Systemic Autoimmunity: Evidence for Chronic B Lymphocyte Activation and Lupus-like Autoantibody Synthesis.” *Journal of Neurochemistry*, vol. 99, no. 4, Nov. 2006, pp. 1073–1087, https://doi.org/10.1111/j.1471-4159.2006.04147.x.

Antal Nógrádi, and Gerta Vrbová. “Anatomy and Physiology of the Spinal Cord.” *Nih.gov*, Landes Bioscience, 2013, www.ncbi.nlm.nih.gov/books/NBK6229/.

Bartanusz, Viktor, et al. “The Blood-Spinal Cord Barrier: Morphology and Clinical Implications.” *Annals of Neurology*, vol. 70, no. 2, 14 June 2011, pp. 194–206, https://doi.org/10.1002/ana.22421. Accessed 21 Nov. 2019.

Bozzola, John J, and Lonnie Dee Russell. *Electron Microscopy : Principles and Techniques for Biologists*. Sudbury, Mass., Jones And Bartlett, 1999.

Bradl, Monika, and Hans Lassmann. “Oligodendrocytes: Biology and Pathology.” *Acta Neuropathologica*, vol. 119, no. 1, 22 Oct. 2009, pp. 37–53, www.ncbi.nlm.nih.gov/pmc/articles/PMC2799635/, https://doi.org/10.1007/s00401-009-0601-5.

Brambilla, Roberta, et al. “Inhibition of Astroglial Nuclear Factor KappaB Reduces Inflammation and Improves Functional Recovery after Spinal Cord Injury.” *The Journal of Experimental Medicine*, vol. 202, no. 1, 4 July 2005, pp. 145–156, pubmed.ncbi.nlm.nih.gov/15998793/, https://doi.org/10.1084/jem.20041918.

Bregman, Barbara S., et al. “Neurotrophic Factors Increase Axonal Growth after Spinal Cord Injury and Transplantation in the Adult Rat.” *Experimental Neurology*, vol. 148, no. 2, Dec. 1997, pp. 475–494, https://doi.org/10.1006/exnr.1997.6705.

Brennan, Faith H., and Phillip G. Popovich. “Emerging Targets for Reprograming the Immune Response to Promote Repair and Recovery of Function after Spinal Cord Injury.” *Current Opinion in Neurology*, vol. 31, no. 3, June 2018, pp. 334–344, https://doi.org/10.1097/wco.0000000000000550. Accessed 11 May 2022.

Britannica. “Spinal Cord | Anatomy | Britannica.” *Encyclopædia Britannica*, 2019, www.britannica.com/science/spinal-cord. Accessed 7 Mar. 2024.

Cekanaviciute, Egle, and Marion S. Buckwalter. “Astrocytes: Integrative Regulators of Neuroinflammation in Stroke and Other Neurological Diseases.” *Neurotherapeutics*, vol. 13, no. 4, 1 Oct. 2016, pp. 685–701, www.ncbi.nlm.nih.gov/pmc/articles/PMC5081110/, https://doi.org/10.1007/s13311-016-0477-8. Accessed 12 Feb. 2020.

Chang, Hsiang-Tsun, et al. “An Engineered Three-Dimensional Stem Cell Niche in the Inner Ear by Applying a Nanofibrillar Cellulose Hydrogel with a Sustained-Release Neurotrophic Factor Delivery System.” *Acta Biomaterialia*, vol. 108, 1 May 2020, pp. 111–127, www.sciencedirect.com/science/article/pii/S1742706120301392?casa_token=QcCZpiTwshsAAAAA:3THByCCQk88EUzeudmHgPp9EitZ3hM_irOBXyaj6oBrNPbGbc30XaX7mZ9AeI4twobzAHUrDUEI, https://doi.org/10.1016/j.actbio.2020.03.007. Accessed 28 Dec. 2021.

Chen, Ai, et al. “The Neuroprotective Roles of BDNF in Hypoxic Ischemic Brain Injury (Review).” *Biomedical Reports*, vol. 1, no. 2, 1 Mar. 2013, pp. 167–176, www.spandidos-publications.com/br/1/2/167#, https://doi.org/10.3892/br.2012.48. Accessed 18 Aug. 2022.

Chen, Keyi, et al. “Biomaterial-Based Regenerative Therapeutic Strategies for Spinal Cord Injury.” *NPG Asia Materials*, vol. 16, no. 1, 19 Jan. 2024, https://doi.org/10.1038/s41427-023-00526-4. Accessed 22 Mar. 2024.

Chen, Wenci, et al. “The Mechanism of AMPA Receptor Subunit GluR1 in Electroacupuncture Treatment of Acute Spinal Cord Injury in Rats.” *Brain Research*, vol. 1783, 1 May 2022, pp. 147848–147848, https://doi.org/10.1016/j.brainres.2022.147848. Accessed 22 Mar. 2024.

Cheng, Hong, et al. “Electrical Stimulation Promotes Stem Cell Neural Differentiation in Tissue Engineering.” *Stem Cells International*, vol. 2021, 20 Apr. 2021, pp. 1–14, downloads.hindawi.com/journals/sci/2021/6697574.pdf, https://doi.org/10.1155/2021/6697574.

Choi, Sung-Wook, et al. “Three-Dimensional Scaffolds for Tissue Engineering: The Importance of Uniformity in Pore Size and Structure.” *Langmuir*, vol. 26, no. 24, 21 Dec. 2010, pp. 19001–19006, https://doi.org/10.1021/la104206h. Accessed 30 May 2019.

Chu, Tianci, et al. “Astrocyte Transplantation for Spinal Cord Injury: Current Status and Perspective.” *Brain Research Bulletin*, vol. 107, Aug. 2014, pp. 18–30, https://doi.org/10.1016/j.brainresbull.2014.05.003. Accessed 13 June 2022.

Collinson, Lucy M, et al. “Volume EM: A Quiet Revolution Takes Shape.” *Nature Methods*, vol. 20, no. 6, 19 Apr. 2023, pp. 777–782, https://doi.org/10.1038/s41592-023-01861-8. Accessed 31 July 2023.

Cornelissen, Tom. “The Effect of Genetic Background and Immunophenotype on Microglial Response to AD Pathology.” *Frontiers of Immunology*, vol. 18, no. S4, 1 Dec. 2022, https://doi.org/10.1002/alz.069045. Accessed 31 July 2023.

Diaz, Eric, and Humberto Morales. “Spinal Cord Anatomy and Clinical Syndromes.” *Seminars in Ultrasound, CT and MRI*, vol. 37, no. 5, Oct. 2016, pp. 360–371, https://doi.org/10.1053/j.sult.2016.05.002.

Dimatteo, Robert, et al. “In Situ Forming Injectable Hydrogels for Drug Delivery and Wound Repair.” *Advanced Drug Delivery Reviews*, vol. 127, Mar. 2018, pp. 167–184, https://doi.org/10.1016/j.addr.2018.03.007.

Du, Yangzhou, et al. “Astroglia-Mediated Effects of Uric Acid to Protect Spinal Cord Neurons from Glutamate Toxicity.” *Glia*, vol. 55, no. 5, 2007, pp. 463–472, https://doi.org/10.1002/glia.20472. Accessed 18 Feb. 2020.

England, Marjorie A, and Jennifer Wakely. *Color Atlas of the Brain & Spinal Cord*. Mosby Incorporated, 1991.

Esmaeili, Elaheh, et al. “Magnetoelectric Nanocomposite Scaffold for High Yield Differentiation of Mesenchymal Stem Cells to Neural-like Cells.” *Journal of Cellular Physiology*, vol. 234, no. 8, 5 Jan. 2019, pp. 13617–13628, https://doi.org/10.1002/jcp.28040. Accessed 17 Aug. 2023.

Estomih Mtui, et al. *FitzGerald Neuroanatomía Clínica Y Neurociencia*. Barcelona, Elsevier, 2016.

Fan, Baoyou, et al. “Microenvironment Imbalance of Spinal Cord Injury.” *Cell Transplantation*, vol. 27, no. 6, June 2018, pp. 853–866, www.ncbi.nlm.nih.gov/pmc/articles/PMC6050904/, https://doi.org/10.1177/0963689718755778.

Fernandes, Alinda R, et al. “Early Membrane Responses to Magnetic Particles Are Predictors of Particle Uptake in Neural Stem Cells.” *Particle & Particle Systems Characterisation* , vol. 32, no. 6, 29 Jan. 2015, pp. 661–667, https://doi.org/10.1002/ppsc.201400231. Accessed 3 Aug. 2023.

Fletcher, Jessica, et al. “Brain-Derived Neurotrophic Factor in Central Nervous System Myelination: A New Mechanism to Promote Myelin Plasticity and Repair.” *International Journal of Molecular Sciences*, vol. 19, no. 12, 19 Dec. 2018, p. 4131, https://doi.org/10.3390/ijms19124131. Accessed 2 Dec. 2021.

Gallop, J.L. “Filopodia and Their Links with Membrane Traffic and Cell Adhesion.” *Seminars in Cell & Developmental Biology*, vol. 102, June 2020, pp. 81–89, https://doi.org/10.1016/j.semcdb.2019.11.017.

Ghosh, Sumit, et al. “Viral Vector Systems for Gene Therapy: A Comprehensive Literature Review of Progress and Biosafety Challenges.” *Applied Biosafety*, vol. 25, no. 1, 24 Jan. 2020, pp. 7–18, https://doi.org/10.1177/1535676019899502.

Goldstein, Joseph L., et al. “Coated Pits, Coated Vesicles, and Receptor-Mediated Endocytosis.” *Nature*, vol. 279, no. 5715, 1 June 1979, pp. 679–685, www.nature.com/articles/279679a0, https://doi.org/10.1038/279679a0.

Haas, Christopher, and Itzhak Fischer. “Human Astrocytes Derived from Glial Restricted Progenitors Support Regeneration of the Injured Spinal Cord.” *Journal of Neurotrauma*, vol. 30, no. 12, 15 June 2013, pp. 1035–1052, https://doi.org/10.1089/neu.2013.2915. Accessed 10 Apr. 2019.

Han, Seung-Wan, et al. “Functions and Dysfunctions of Oligodendrocytes in Neurodegenerative Diseases.” *Frontiers*, vol. 16, 20 Dec. 2022, https://doi.org/10.3389/fncel.2022.1083159. Accessed 31 July 2023.

Hao, Jian, et al. “Mechanisms Underlying the Promotion of Functional Recovery by Deferoxamine after Spinal Cord Injury in Rats.” *Neural Regeneration Research*, vol. 12, no. 6, 1 June 2017, pp. 959–968, www.ncbi.nlm.nih.gov/pmc/articles/PMC5514872/, https://doi.org/10.4103/1673-5374.208591. Accessed 13 Mar. 2022.

Hermenegildo, B., et al. “Hydrogel-Based Magnetoelectric Microenvironments for Tissue Stimulation.” *Colloids and Surfaces B: Biointerfaces*, vol. 181, Sept. 2019, pp. 1041–1047, www.sciencedirect.com/science/article/pii/S0927776519304278?via%3Dihub, https://doi.org/10.1016/j.colsurfb.2019.06.023. Accessed 29 Aug. 2019.

Hicks, Anna U., et al. “Transplantation of Human Embryonic Stem Cell-Derived Neural Precursor Cells and Enriched Environment after Cortical Stroke in Rats: Cell Survival and Functional Recovery.” *European Journal of Neuroscience*, vol. 29, no. 3, Feb. 2009, pp. 562–574, https://doi.org/10.1111/j.1460-9568.2008.06599.x. Accessed 20 Apr. 2021.

Hoon, Jing-Ling, et al. “Functions and Regulation of Circular Dorsal Ruffles.” *Molecular and Cellular Biology*, vol. 32, no. 21, 1 Nov. 2012, pp. 4246–4257, https://doi.org/10.1128/mcb.00551-12. Accessed 5 Apr. 2023.

Hu, Xiao, et al. “Spinal Cord Injury: Molecular Mechanisms and Therapeutic Interventions.” *Signal Transduction and Targeted Therapy*, vol. 8, no. 1, 26 June 2023, https://doi.org/10.1038/s41392-023-01477-6. Accessed 13 Aug. 2023.

Huang, Lei, et al. “Iron Metabolism and Ferroptosis in Peripheral Nerve Injury.” *Oxidative Medicine and Cellular Longevity*, vol. 2022, 2 Dec. 2022, pp. 1–14, https://doi.org/10.1155/2022/5918218. Accessed 21 Nov. 2023.

Hussein, Rowan K., et al. “Role of Chondroitin Sulfation Following Spinal Cord Injury.” *Frontiers in Cellular Neuroscience*, vol. 14, 5 Aug. 2020, https://doi.org/10.3389/fncel.2020.00208. Accessed 21 Apr. 2021.

Jeffries, Marisa, and Veronica Tom. “Peripheral Immune Dysfunction: A Problem of Central Importance after Spinal Cord Injury.” *Biology*, vol. 10, no. 9, 17 Sept. 2021, p. 928, https://doi.org/10.3390/biology10090928.

Jones, T. Bucky. “Lymphocytes and Autoimmunity after Spinal Cord Injury.” *Experimental Neurology*, vol. 258, Aug. 2014, pp. 78–90, https://doi.org/10.1016/j.expneurol.2014.03.003. Accessed 18 Sept. 2019.

Kuhn, Sarah, et al. “Oligodendrocytes in Development, Myelin Generation and Beyond.” *Cells*, vol. 8, no. 11, 12 Nov. 2019, p. 1424, www.ncbi.nlm.nih.gov/pmc/articles/PMC6912544/, https://doi.org/10.3390/cells8111424.

Lee, Hong J., et al. “Human Neural Stem Cells Genetically Modified to Overexpress Brain-Derived Neurotrophic Factor Promote Functional Recovery and Neuroprotection in a Mouse Stroke

Model." *Journal of Neuroscience Research*, vol. 88, no. 15, 3 Sept. 2010, pp. 3282–3294, https://doi.org/10.1002/jnr.22474. Accessed 1 Apr. 2020.

Levi, Allan D., et al. "Clinical Outcomes from a Multi-Center Study of Human Neural Stem Cell Transplantation in Chronic Cervical Spinal Cord Injury." *Journal of Neurotrauma*, vol. 36, no. 6, 19 Mar. 2019, pp. 891–902, https://doi.org/10.1089/neu.2018.5843.

Liu, Xiangyu, et al. "Inflammatory Response to Spinal Cord Injury and Its Treatment." *World Neurosurgery*, vol. 155, 1 Nov. 2021, pp. 19–31, www.sciencedirect.com/science/article/pii/S1878875021011670, https://doi.org/10.1016/j.wneu.2021.07.148. Accessed 18 Nov. 2022.

Lööv, Camilla, et al. "Engulfing Astrocytes Protect Neurons from Contact-Induced Apoptosis Following Injury." *PLoS ONE*, vol. 7, no. 3, 26 Mar. 2012, p. e33090, https://doi.org/10.1371/journal.pone.0033090.

---. "Identification of Injury Specific Proteins in a Cell Culture Model of Traumatic Brain Injury." *PLOS ONE*, vol. 8, no. 2, 7 Feb. 2013, pp. e55983–e55983, https://doi.org/10.1371/journal.pone.0055983. Accessed 30 Oct. 2023.

McDaid, David, et al. "Understanding and Modelling the Economic Impact of Spinal Cord Injuries in the United Kingdom." *Spinal Cord*, vol. 57, no. 9, 13 May 2019, pp. 778–788, www.nature.com/articles/s41393-019-0285-1, https://doi.org/10.1038/s41393-019-0285-1.

Meek. Geoffrey A. *Practical Electron Microscopy for Biologists*. John Wiley & Sons, 1970.

Montague-Cardoso, Karli, and Marzia Malcangio. "Changes in Blood–Spinal Cord Barrier Permeability and Neuroimmune Interactions in the Underlying Mechanisms of Chronic Pain." *PAIN Reports*, vol. 6, no. 1, Jan. 2021, p. e879, https://doi.org/10.1097/pr9.0000000000000879. Accessed 31 Oct. 2021.

Nakajima, Hideaki, et al. “Distribution and Polarization of Microglia and Macrophages at Injured Sites and the Lumbar Enlargement after Spinal Cord Injury.” *Neuroscience Letters*, vol. 737, 1 Oct. 2020, pp. 135152–135152, https://doi.org/10.1016/j.neulet.2020.135152. Accessed 22 Mar. 2024.

---. “Targeted Retrograde Gene Delivery of Brain-Derived Neurotrophic Factor Suppresses Apoptosis of Neurons and Oligodendroglia after Spinal Cord Injury in Rats.” *Spine*, vol. 35, no. 5, Mar. 2010, pp. 497–504, https://doi.org/10.1097/brs.0b013e3181b8e89b. Accessed 12 Apr. 2022.

Niemczyk-Soczynska, Beata, et al. “Hydrogel, Electrospun and Composite Materials for Bone/Cartilage and Neural Tissue Engineering.” *Materials*, vol. 14, no. 22, 15 Nov. 2021, p. 6899, https://doi.org/10.3390/ma14226899. Accessed 11 Mar. 2022.

O’Shea, Timothy M., et al. “Cell Biology of Spinal Cord Injury and Repair.” *Journal of Clinical Investigation*, vol. 127, no. 9, 24 July 2017, pp. 3259–3270, https://doi.org/10.1172/jci90608.

Ohtake, Yosuke, and Shuxin Li. “Molecular Mechanisms of Scar-Sourced Axon Growth Inhibitors.” *Brain Research*, vol. 1619, Sept. 2015, pp. 22–35, https://doi.org/10.1016/j.brainres.2014.08.064. Accessed 9 Apr. 2021.

Osseward, Peter J, and Samuel L Pfaff. “Cell Type and Circuit Modules in the Spinal Cord.” *Current Opinion in Neurobiology*, vol. 56, June 2019, pp. 175–184, https://doi.org/10.1016/j.conb.2019.03.003.

Peddie, Christopher J, et al. “Volume Electron Microscopy.” *Primer*, vol. 2, no. 1, 7 July 2022, https://doi.org/10.1038/s43586-022-00131-9. Accessed 31 July 2023.

Pereira, Inês M., et al. “Filling the Gap: Neural Stem Cells as a Promising Therapy for Spinal Cord Injury.” *Pharmaceuticals*, vol. 12, no. 2, 29 Apr. 2019, www.ncbi.nlm.nih.gov/pmc/articles/PMC6631328/, https://doi.org/10.3390/ph12020065. Accessed 11 Apr. 2020.

Perez-Gianmarco, Lucila, and Maria Kukley. “Understanding the Role of the Glial Scar through the Depletion of Glial Cells after Spinal Cord Injury.” *Cells*, vol. 12, no. 14, 13 July 2023, pp. 1842–1842, https://doi.org/10.3390/cells12141842.

Perkovic, Mario, et al. “Correlative Light- and Electron Microscopy with Chemical Tags.” *Journal of Structural Biology*, vol. 186, no. 2, May 2014, pp. 205–213, www.sciencedirect.com/science/article/pii/S1047847714000719, https://doi.org/10.1016/j.jsb.2014.03.018. Accessed 4 Feb. 2020.

Quadri, Syed A., et al. “Recent Update on Basic Mechanisms of Spinal Cord Injury.” *Neurosurgical Review*, 11 July 2018, link.springer.com/article/10.1007/s10143-018-1008-3, https://doi.org/10.1007/s10143-018-1008-3.

Rahman, Md., et al. “Stem Cell Transplantation Therapy and Neurological Disorders: Current Status and Future Perspectives.” *Biology*, vol. 11, no. 1, 17 Jan. 2022, p. 147, https://doi.org/10.3390/biology11010147.

Rauti, Rossana, et al. “BDNF Impact on Synaptic Dynamics: Extra or Intracellular Long-Term Release Differently Regulates Cultured Hippocampal Synapses.” *Molecular Brain*, vol. 13, no. 1, 17 Mar. 2020, https://doi.org/10.1186/s13041-020-00582-9. Accessed 22 Aug. 2020.

Reddaway, Jack, et al. “Microglial Morphometric Analysis: So Many Options, so Little Consistency.” *Frontiers in Neuroinformatics*, vol. 17, 10 Aug. 2023, https://doi.org/10.3389/fninf.2023.1211188. Accessed 31 Oct. 2023.

Regan, R.F., and D.W. Choi. “Glutamate Neurotoxicity in Spinal Cord Cell Culture.” *Neuroscience*, vol. 43, no. 2-3, Jan. 1991, pp. 585–591, https://doi.org/10.1016/0306-4522(91)90317-h.

Russell, Matthew B, et al. “3D Correlative Light and Electron Microscopy of Cultured Cells Using Serial Blockface Scanning Electron Microscopy.” *Journal of Cell Science* , vol. 130, no. 1, 1 Jan. 2016, https://doi.org/10.1242/jcs.188433. Accessed 22 May 2023.

S. Amelinckx, et al. *Electron Microscopy*. John Wiley & Sons, 26 Sept. 2008.

Schmidt, C. E., et al. "Stimulation of Neurite Outgrowth Using an Electrically Conducting Polymer." *Proceedings of the National Academy of Sciences*, vol. 94, no. 17, 19 Aug. 1997, pp. 8948–8953, https://doi.org/10.1073/pnas.94.17.8948.

Siebert, Justin R., et al. "Chondroitin Sulfate Proteoglycans in the Nervous System: Inhibitors to Repair." *BioMed Research International*, vol. 2014, 2014, www.ncbi.nlm.nih.gov/pmc/articles/PMC4182688/, https://doi.org/10.1155/2014/845323.

Silvestro, Serena, et al. "Stem Cells Therapy for Spinal Cord Injury: An Overview of Clinical Trials." *International Journal of Molecular Sciences*, vol. 21, no. 2, 19 Jan. 2020, p. 659, https://doi.org/10.3390/ijms21020659. Accessed 7 June 2020.

Snell, Richard S. *Clinical Neuroanatomy*. 7th ed., Philadelphia, Wolters Kluwer Health/Lippincott Williams & Wilkins, 2010.

Sterner, Robert C., and Rosalie M. Sterner. "Immune Response Following Traumatic Spinal Cord Injury: Pathophysiology and Therapies." *Frontiers in Immunology*, vol. 13, 6 Jan. 2023, https://doi.org/10.3389/fimmu.2022.1084101.

Stys, PK, et al. "Ionic Mechanisms of Anoxic Injury in Mammalian CNS White Matter: Role of Na+ Channels and Na(+)-Ca2+ Exchanger." *The Journal of Neuroscience*, vol. 12, no. 2, 1 Feb. 1992, pp. 430–439, https://doi.org/10.1523/jneurosci.12-02-00430.1992.

Svitlana Kopyl, et al. "Magnetoelectric Effect: Principles and Applications in Biology and Medicine– a Review." *Elsiver*, vol. 12, 1 Sept. 2021, pp. 100149–100149, https://doi.org/10.1016/j.mtbio.2021.100149. Accessed 31 July 2023.

Tom, Veronica J, et al. "Exogenous BDNF Enhances the Integration of Chronically Injured Axons That Regenerate through a Peripheral Nerve Grafted into a Chondroitinase-Treated Spinal Cord Injury

Site." *Experimental Neurology*, vol. 239, 1 Jan. 2013, pp. 91–100, https://doi.org/10.1016/j.expneurol.2012.09.011. Accessed 3 Oct. 2023.

Tran, Amanda Phuong, et al. "The Biology of Regeneration Failure and Success after Spinal Cord Injury." *Physiological Reviews*, vol. 98, no. 2, Apr. 2018, pp. 881–917, https://doi.org/10.1152/physrev.00017.2017.

Tsui, C.K, et al. "Biomaterials and Glia: Progress on Designs to Modulate Neuroinflammation." *Acta Biomaterialia*, vol. 83, 1 Jan. 2019, pp. 13–28, https://doi.org/10.1016/j.actbio.2018.11.008. Accessed 26 Apr. 2023.

Venkatesh, Humsa S., et al. "Electrical and Synaptic Integration of Glioma into Neural Circuits." *Nature*, vol. 573, no. 7775, 1 Sept. 2019, pp. 539–545, www.nature.com/articles/s41586-019-1563-y, https://doi.org/10.1038/s41586-019-1563-y.

Vielreicher, M., et al. "Taking a Deep Look: Modern Microscopy Technologies to Optimize the Design and Functionality of Biocompatible Scaffolds for Tissue Engineering in Regenerative Medicine." *Journal of the Royal Society Interface*, vol. 10, no. 86, 6 Sept. 2013, p. 20130263, https://doi.org/10.1098/rsif.2013.0263.

Wake, Hiroaki, et al. "Functions of Microglia in the Central Nervous System--beyond the Immune Response." *Neuron Glia Biology*, vol. 7, no. 1, 2011, pp. 47–53, www.ncbi.nlm.nih.gov/pubmed/22613055, https://doi.org/10.1017/S1740925X12000063.

Wang, Jing, et al. "Robust Myelination of Regenerated Axons Induced by Combined Manipulations of GPR17 and Microglia." *Neuron*, vol. 108, no. 5, Dec. 2020, pp. 876-886.e4, https://doi.org/10.1016/j.neuron.2020.09.016. Accessed 13 Jan. 2021.

White, Robin E, and Lyn B Jakeman. "Don't Fence Me In: Harnessing the Beneficial Roles of Astrocytes for Spinal Cord Repair." *Restorative Neurology and Neuroscience*, vol. 26, no. 2-3, 2008, pp. 197–214, www.ncbi.nlm.nih.gov/pmc/articles/PMC2825119/. Accessed 10 Apr. 2019.

Willerth, Stephanie M., and Shelly E. Sakiyama-Elbert. “Approaches to Neural Tissue Engineering Using Scaffolds for Drug Delivery.” *Advanced Drug Delivery Reviews*, vol. 59, no. 4-5, May 2007, pp. 325–338, https://doi.org/10.1016/j.addr.2007.03.014. Accessed 13 May 2020.

Yin, Liang-wei, et al. “Neural Stem Cells Over-Expressing Brain-Derived Neurotrophic Factor Promote Neuronal Survival and Cytoskeletal Protein Expression in Traumatic Brain Injury Sites.” *Neural Regeneration Research*, vol. 12, no. 3, 2017, p. 433, https://doi.org/10.4103/1673-5374.202947. Accessed 20 Mar. 2020.

Zamanian, J. L., et al. “Genomic Analysis of Reactive Astrogliosis.” *Journal of Neuroscience*, vol. 32, no. 18, 2 May 2012, pp. 6391–6410, https://doi.org/10.1523/jneurosci.6221-11.2012.